UNIVERSITY
OF OSLO

Master's thesis

Transport in the one-dimensional spin-S XXZ model

João Guilherme Carvalho Inácio

Computational Science: Physics
60 ECTS study points

Department of Physics
Faculty of Mathematics and Natural Sciences

Spring 2023

Abstract

The Stochastic Series Expansion (SSE) method with the Directed Loop updates allows for efficient simulation of quantum spin lattice systems at finite temperatures. Here we develop a new approach for sampling response functions in the SSE framework to calculate transport properties in the linear regime. This procedure is based on an imaginary time representation of the SSE configurations. It allows us to bypass the calculation of hypergeometric functions present in existing approaches, and to write a sampling algorithm with linear complexity. As so, we are able to perform accurate calculations for the DC spin conductivity, in the low temperature regime, for spin-S XXZ chains. Calculations for the heat conductivity and the spin-Seebeck coefficient are possible but have large standard deviations. We are able to reproduce results from Bosonization for the spin conductivity in spin-1/2 XXZ chains. We extend these calculations to spin-1 and spin-3/2 XXZ chains, and found different types behaviours of the conductivity between integer and half-integer spin chains. Furthermore, an extrapolation to the large spin limit is also performed, showing good agreement with the spin conductivity in classical spin systems.

Acknowledgements

My appreciation to Prof. Olav Syljuåsen for his supervision and all of the insightful discussions we have had during the last year. I thank everyone who has been by my side during these last two years. Their friendship and companionship is highly appreciated. I also thank Mira for her care and unconditional support. Gostaria de expressar a minha mais profunda gratidão à minha família, especialmente à minha mãe, pelo seu carinho e apoio.

Contents

1 Introduction **1**

2 Magnetic Interactions and Spin Models **3**

2.1 Magnetic Interactions 3

2.1.1 Phase Transitions 4

2.2 The spin-S XXZ Model 5

2.2.1 Ground State Phase Diagram 6

2.2.2 Symmetries and Currents 8

3 Stochastic Series Expansion **11**

3.1 Series Expansion of the Partition Function 11

3.2 Expressions for Expectation Values 13

3.3 Sampling Sub-Routines 15

3.3.1 Diagonal Updates 16

3.3.2 Directed Loop Updates 17

3.3.3 A Monte Carlo Cycle 22

3.4 SSE Applied to the spin-S XXZ Model 23

3.4.1 Observables 24

3.4.2 Code Verification 25

3.4.3 Finite Size Effects 26

4 Magnetic Transport in the Linear Regime **29**

4.1 Linear Response Theory 29

4.1.1 The Kubo Formula 30

4.1.2 Generalized Susceptibility 32

4.2 Magnetic Transport 33

4.3 Transport Coefficients 35

4.3.1 Local gradient perturbations 36

4.3.2 Kinetic Coefficients as Response Functions 37

5 Transport in the SSE formalism **39**
5.1 Sampling $L_{ij}(\omega_M)$ with MC . . . 39
5.2 Imaginary Time Representation of SSE . . . 40
5.2.1 Expressions for Expectation Values . . . 41
5.3 Expressions for $L_{ij}(\omega_M)$ in the Imaginary Time Representation of SSE . . . 43
5.3.1 Expression for L_{SS} . . . 44
5.3.2 Expression for L_{HH} . . . 45
5.3.3 Expressions for L_{SH} and L_{HS} . . . 47
5.4 Code Verification . . . 47

6 Results and Discussion **51**
6.1 Initial Considerations . . . 51
6.1.1 Dependence on $x - y$ . . . 52
6.1.2 Finite Size Effects . . . 52
6.1.3 Extrapolations to $\omega = 0$ . . . 54
6.2 Spin-1/2 XY Chain . . . 55
6.2.1 Spin-S XY Chains . . . 57
6.3 Spin-1/2 XXZ chain . . . 58
6.3.1 Spin-S XXZ Chain . . . 60
6.3.2 Adding Easy-Axis Anisotropy . . . 61
6.4 Dependence on the Spin Number S . . . 63

7 Conclusion **65**

A Equivalence of Equations (4.15) and (5.1) **67**

B Proof of Integral Identities Used in Chapter 5 **69**
B.1 Identity for L_{SS} . . . 69
B.2 Identity for L_{HH} . . . 70
B.3 Identity for L_{SH} and L_{HS} . . . 71

List of Figures

2.1 Ground state phase diagram of the $S = 1/2$ XXZ chain as a function of magnetic anisotropy Δ and applied magnetic field h. Figure taken from [40]. 6

2.2 Ground state phase diagram of the $S = 1$ XXZ chain as a function of magnetic anisotropy $\Delta(J_z)$ and easy-axis anisotropy D. Figure taken from [40]. 7

3.1 **(a)** Operator sequence for a four-site system with $n = 4$. Each column of the figure represents one site and the states on each site are labelled by an integer. The operators are shown as black rectangles. A propagated state can be read as a row of encircled states. **(b)** The same operator sequence shown in (a) but in the vertex representation. All of the operators have become four-legged vertices. Each leg carries the information about the state and is connected to another leg in another vertex through the dashed lines. 18

3.2 Updating vertex with weight W_1 with a $+1$ update on the entrance leg (lower left leg). The conservation law is such that the sum of the states below equals the sum of the states above. 20

3.3 Updating vertex with weight W_2 with the entrance leg as the lower right leg. The update is such, that by exiting through the lower left leg, we recuperate vertex with weight W_1. 20

3.4 **(a)** Mean energy per particle as a function of uniaxial anisotropy, for $h = 0$. The value of the coupling constant is set to $J = 3/(S(S + 1))$ so that the energy scale is the same for each spin value. **(b)** Mean magnetization per particle as a function of applied magnetic field, for $\Delta = 1$. The system size is $N = 6$, with PBC, and the temperature is $\beta = 128$. Three different spin values are shown $S \in \{1/2, 1, 3/2\}$. ED results are show in black lines. SSE calculations were done with 10 bins, each with 10^4 MCS. Statistical errors are smaller than the size of the symbols. 25

3.5 **(a)** Mean energy per particle as a function of temperature and system size L. **(b)** Uniform susceptibility as a function of temperature and system size L. Insets show the behaviour at low temperatures. SSE calculations were performed for a spin-1/2 Heisenberg chain, with 20 bins, each with 10^5 MCS. Statistical errors may be smaller than the size of the symbols. . . 27

4.1 Schematic representation of the perturbation in the magnetic field. The dotted line represents a global gradient while the dashed line represents a local gradient given in the form of a step discontinuity. 35

5.1 Operator sequence for a four-site system with $n = 4$. Each column of the figure represents one site and the states on each site are labelled by an integer. The operators are shown as black rectangles. On the right hand side of the graphical representation o the operator string, the assigned times to the Hamiltonian operators and the propagated states are labelled. The times $\tau_0 = 0$ and $\tau_{n+1} = \beta$ are assigned to the first and last states in the expansion, respectively. 41

5.2 **(a)** Spin kinetic coefficient L_{SS} as a function of the Matsubara frequencies ω_M, for the XY chain. **(b)** Heat kinetic coefficient L_{HH} as a function of the Matsubara frequencies ω_M, for the Heisenberg model. **(c)** Off-diagonal coefficient L_{SH} as a function of the Matsubara frequencies ω_M, for the XY chain in a magnetic field $h = 0.5$. We present calculations for a system of $L = 6$ spin-1/2 particles, with OBC, at inverse temperature $\beta = 32$ and for two different values of x with $y = 2$. ED calculations are presented in the black lines. SSE calculations were performed with 20 bins and 10^7 MCS. Statistical errors may be smaller than the size of the symbols. 48

5.3 **(a)** Spin kinetic coefficient L_{SS} as a function of the Matsubara frequencies ω_M, for the XY chain. **(b)** Heat kinetic coefficient L_{HH} as a function of the Matsubara frequencies ω_M, for the Heisenberg model. **(c)** Off-diagonal coefficient L_{SH} as a function of the Matsubara frequencies ω_M, for the XY chain in a magnetic field $h = 1$. We present calculations for a system of $L = 256$ spin-1/2 particles, with OBC, at inverse temperature $\beta = 128$ and for two different values of x with $y = 127$. SSE calculations were performed with 100 bins and 10^5 MCS. Statistical errors are sometimes smaller than the size of the symbols. 49

6.1 Spin kinetic coefficient L_{SS} as a function of the Matsubara frequencies and of spatial separation between the site of perturbation y and of measurement of the current x. The presented results are for the XY chain with $L = 256$ at inverse temperature $\beta = 128$. SSE calculations were performed with 20 bins and 10^5 MCS. Statistical errors are smaller than the size of the symbols. 52

6.2 Spin kinetic coefficient L_{SS} as a function of the Matsubara frequencies ω_M and the system size L, for the **(a)** XY chain and the **(b)** isotropic Heisenberg chain at inverse temperature $\beta = 128$, with $x = y$. SSE calculations were performed with 100 bins and 10^5 MCS. Statistical errors are smaller than the size of the symbols. 53

6.3 Extrapolation of the spin kinetic coefficient L_{SS} to $\omega = 0$, from the first 10 Matsubara frequencies and two set of values for x and y. The dots are the results from the MC calculation and the black lines are a 4^{th} order polynomial fit to the MC data. Inset shows the behaviour of the fitted lines from the bootstrap procedure near the extrapolation point $\omega_M = 0$. The presented results are for the XY chain with $L = 512$ at inverse temperature $\beta = 128$. SSE calculations were performed with 100 bins and 10^5 MCS. Statistical errors may be smaller than the size of the symbols. 54

6.4 Spin conductivity **(a)** and spin-Seebeck coefficient **(b)** as a function of the applied magnetic field, for the spin-1/2 XY chain with $L = 512$. The black dashed line is the solution in the thermodynamic limit, at inverse temperature $\beta = 128$, given by the JW transformation for both the spin conductivity and spin-Seebeck coefficient. The MC calculations were done with 10^5 MCS and 25 bins. Statistical errors are sometimes smaller than the size of the symbols. 56

6.5 Spin conductivity as a function of the applied magnetic field, for the **(a)** spin-1 and the **(b)** spin-3/2 XY chains with $L = 512$. The MC calculations were done with 10^5 MCS and 25 bins. Statistical errors are sometimes smaller than the size of the symbols. 57

6.6 Spin conductivity as a function of the anisotropy parameter Δ for the spin-1/2 XXZ chain $L = 512$, with $h = 0$. The black dashed line shows the conductivity of the Luttinger liquid model by Apel and Rice [17]. The MC calculations were performed with 10^5 MCS and 25 bins. Statistical errors are smaller than the size of the symbols. 59

6.7 Spin conductivity as a function of the anisotropy parameter Δ for the **(a)** spin-1 and **(b)** spin-3/2 XXZ chains $L = 512$, with $h = 0$. The MC calculations were performed with 10^5 MCS and 25 bins. Statistical errors are sometimes smaller than the size of the symbols. 61

6.8 Spin conductivity as a function of the easy-axis anisotropy D for the **(a)** spin-1 and **(b)** spin-3/2 for the XXZ chains with $L = 512$ at inverse temperature $\beta = 128$. Results for different values of Δ are presented. The MC calculations were performed with 10^5 MCS and 25 bins. Statistical errors are sometimes smaller than the size of the symbols. 62

6.9 Dependence of the DC spin conductivity of spin-S XXZ chains on the spin number S. Results are presented for the Heisenberg ($\Delta = 1$) and XY ($\Delta = 0$) chains at the inverse temperature $\beta = 128$. The MC calculations were performed with 10^5 MCS and 25 bins. Statistical errors are sometimes smaller than the size of the symbols. 63

6.10 Spin conductivity of spin-S XXZ chains as a function of $1/S$, for half-integer S. Results are presented for the Heisenberg ($\Delta = 1$) and XY ($\Delta = 0$) chains at the inverse temperature $\beta = 128$. The black lines are second order polynomial fits to the MC calculated points. 64

Chapter 1

Introduction

The field of low-dimensionality magnetism has developed into an active area of solid-state physics. Its origins can be traced back to 1925 when Ernst Ising investigated a one-dimensional (1D) version of a spin model [1], now known as the Ising model, as a means of explaining paramagnetic-ferromagnetic phase transitions, and to 1932 when Hans Bethe wrote his seminal paper [2] describing the Bethe ansatz (BA) method to find the exact ground state of the antiferromagnetic Heisenberg model, for the 1D case. In the 1970s, it became clear that 1D models could also be relevant to real materials [3] and, later in the 1980s, significant discoveries on fundamental properties of antiferromagnetic chains [4, 5, 6] increased interest in the field. In short, low-dimensional systems offer a unique opportunity to study ground and excited states of quantum models, possible new phases of matter, and the interplay between quantum and thermal fluctuations.

Since the 1990s, much of the research efforts on 1D systems have been devoted to studying the dynamical and transport properties. These efforts first began with the seminal work of Castella et al. [7], when they showed that integrable models[1], such as the spin-1/2 XXZ or Hubbard chains, exhibit ideal conducting behaviour. Subsequently, many studies were developed relating integrability to transport properties [8, 9, 10]. It was shown that integrable systems exhibit ballistic transport, i.e. a transport regime in which particles or excitations propagate without scattering. Although integrable models are fully solvable by the BA, the accurate calculation of their transport properties has always been a major challenge [11].

It is important to stress that the field was not only driven by theoretical questions but also by experiments [12, 13, 14], which showed that 1D quantum magnets show a large contribution from magnetic excitations to the thermal conductivity. Research about transport in 1D systems is especially important in the field of spintronics [15] and has seen many applications in quantum computing and in mesoscopic devices [16].

[1]Models that have an infinite number of conserved quantities and can be solved exactly either analytically by fermionization or via the BA.

The basic approaches to calculate transport properties of 1D models are either by Bosonization [17, 18, 19], which is only valid for the low temperature regime, or through exact diagonalization (ED) techniques. Although ED allows us to calculate practically any observable or correlation function in equilibrium, it can only be performed for small systems. To circumvent this, Monte Carlo (MC) methods, like the Stochastic Series Expansion (SSE) [20, 21], offer a good alternative as they provide essentially exact results for equilibrium thermodynamics on large systems. MC calculations of transport coefficients have been carried out for some models [10, 22, 23, 24, 25].

Many studies for the spin-1/2 XXZ chain have been carried out using ED and MC approaches [25, 22, 8, 26, 27, 28]. It is known that the thermal and spin conductivities are divergent at zero frequency and thus transport is ballistic [9]. At low temperatures, for gapless phases, it is known that the heat conductivity is proportional to the temperature and there is a finite spin conductivity coefficient. For gapped phases, the spin conductivity is zero in the low temperature limit, as magnetic excitations require a finite amount of energy. Appling a magnetic field breaks the spin-reversal symmetry and gives rise to magnetothermal effects, which are captured by the spin-Seebeck coefficient. Studies in this regime are more scarce [29, 30, 24]. For $S > 1/2$, studies focus more on the high temperature limit transport or on the real time spin dynamics [31, 32, 33].

This work has two main goals. The first one is to develop a more computationally efficient method for computing transport coefficients in the SSE framework based on the imaginary time representation of the SSE configurations. The second goal is to apply the developed sampling method to spin-S XXZ chains. Primarily, we aim to uncover possible differences between transport in $S = 1/2, 1, 3/2$ chains and try to get an estimate of the transport properties in the large S limit. Secondly, we wish to expand the knowledge of magnetothermal properties of $S = 1/2, 1, 3/2$ chains.

We begin this work with a discussion about magnetic interactions, modelled by the Heisenberg exchange, and the different ground states of the spin-S XXZ chain, with emphasis on differences between integer and half-integer spin chains, in Chapter 2. In Chapter 3, we present the SSE method with the Directed Loop updates. The necessary background in linear response theory and magnetic transport is presented in Chapter 4, alongside the procedure of the measurement of the transport coefficients in the XXZ chain. In Chapter 5 the derivation formulas to sample the transport coefficients is presented using the new sampling approach in the imaginary time representation of SSE. In Chapter 6, we present the results for the transport coefficients obtained with SSE. Chapter 7 is the conclusion.

Chapter 2

Magnetic Interactions and Spin Models

In this Chapter, the basic properties of magnetic interactions are explored through the Heisenberg exchange. The ground states of different phases, low-level excitations and phase transitions are discussed. The spin-S XXZ model is introduced along with a short discussion of the ground state properties for different parameters with emphasis on the spin gap for integer spin values. Symmetries of the model are discussed and associated currents are derived.

2.1 Magnetic Interactions

Magnetism is a phenomena that can only be described correctly by a quantum mechanical approach [34]. Magnetic moments are caused by the motion of electrons around the nucleus, orbital angular momenta, and by the intrinsic angular momenta of the electron, called spin. Due to the Pauli exclusion principle, which states that each electronic orbit can be occupied by only two electrons of opposite spin, in a large fraction of elements, the magnetic moment of electrons cancels out. However, in some elements such as transition metal atoms (iron, cobalt and nickel, for example), due to partially filled shells and a weak spin-orbit coupling, a magnetic moment arises from the spin of the electrons. In other elements, such as rare earth elements, the spin-orbit coupling is not weak and must be taken into account and the magnetic moments arise then as combinations of orbital angular momenta and spin. Interactions between the atomic moments in insulators happen when the partially filled shells in neighbouring atoms partially overlap. In 1928, Werner Heisenberg, proposed a simple model for the magnetic interactions [35]. In it, he considered only the isotropic spin-spin interaction,

$$H = J\boldsymbol{S}_i \cdot \boldsymbol{S}_j$$

known as Heisenberg exchange. Here $\boldsymbol{S}_i$ and $\boldsymbol{S}_j$ are the spin operators and J is referred to as the exchange integral/constant. For $J < 0$, alignment of spins is favoured. This

is known as a ferromagnetic interaction. Conversely, if $J > 0$, anti-alignment of spins is favoured. This is called an antiferromagnetic interaction.

A ferromagnetic interaction allows for all of the spins to be aligned in the same direction. Thus the state $|\uparrow\uparrow \ldots\rangle$ or $|\downarrow\downarrow \ldots\rangle$ will have maximum ferromagnetic ordering. For an antiferromagnetic system, the states $|\uparrow\downarrow\uparrow\downarrow \ldots\rangle$ and $|\downarrow\uparrow\downarrow\uparrow \ldots\rangle$ will have maximum antiferromagnetic ordering. This state is called the Néel state. Writing the exchange interaction as $H = -J\left[S_i^z S_j^z + \frac{1}{2}\left(S_i^+ S_j^- + S_i^- S_j^+\right)\right]$ [1], we can see that the ferromagnetic state is an eigenstate of the interaction while the Néel state is not. When acting on the perfect Néel state, the raising and lowering operators flip pairs of spins causing local deformities. Thus, fully antiferromagnetic ordering is destroyed by quantum fluctuations, whereas a ferromagnetic state is a ground state even in the presence of off-diagonal interactions. The amount of ordering in the true ground state of an antiferromagnetic system depends strongly on the details of the lattice and of the considered interaction types.

Low-energy excitations in a ferromagnetic system are superpositions of single overturned spins, i.e. a magnon, or domains of completely flipped spin, since the cost of their interactions lies at the boundary between the two domains. Ferromagnetic magnons have $S = 1$. As they can be thought of as a collectively oscillation of spins with $q \rightarrowtail 0$, they require no minimum amount of energy, meaning that ferromagnetic systems are gapless systems. In contrast, low-energy excitations in an antiferromagnetic ground state are two domain walls. Acting with a single S^- operator on one of the Néel states will create a so-called antiferromagnetic magnon, where three spins will be ferromagnetically aligned. By repeated action of the Hamiltonian, this state will decay into two domain walls where we have two $S = 1/2$ quasi-particles, known as spinons. Antiferromagnetic excitations are also gapless.

2.1.1 Phase Transitions

The temperature at which a phase transition occurs is called the critical temperature, denoted by T_c. The transition is characterized by a non-analytic change in the order parameter, which is non-zero in the ordered phase $T < T_c$ and zero in the disordered phase $T > T_c$. Phase transitions can be further divided into first-order and continuous. First-order phase transitions are characterised by the exchange of heat and by the existence of a coexistence of phases. Continuous phase transitions are often associated with the breaking of the system's symmetry[2]. Transitions that occur at zero temperature, by varying some non-thermal parameter, are called quantum phase transitions.

The Mermin–Wagner theorem [37] states that a continuous symmetry of a quantum

[1] Here the spin ladder operators S^+ and S^- are defined as $S^+ = S^x + iS^y$ and $S^- = S^x - iS^y$.

[2] Transitions like the Kosterlitz–Thouless transition in the 2D XY model [36], are continuous phase transitions which do not break symmetry.

system, with short-range interactions, can not be broken at $T \geq 0$ in one dimension neither at $T > 0$ in two dimensions. So, in a 1D Heisenberg system, with short-range interactions, there is no magnetic ordering, therefore we can expect no phase transition. In higher dimensions, we can expect phase transitions at $T = 0$ in 2D systems and $T \geq 0$ in 3D systems.

Ferromagnetic and antiferromagnetic phase transitions are measured by different order parameters. Since a ferromagnetic interaction favours alignment of spins a good order parameter to measure ferromagnetic ordering is the magnetization m. Antiferromagnetic interactions favours anti-alignment of neighbouring spin, and thus we use the staggered magnetization m_s as it measures sublattice magnetization. The formulas for m and m_s read

$$m = \frac{1}{N}\sum_{i=1}^{N} S_i^z, \qquad m_s = \frac{1}{N}\sum_{i=1}^{N}(-1)^i S_i^z.$$

As we can see, they are maximum for the respective ground states, i.e. equal to ± 1. Another noteworthy aspect is the behaviour of the magnetic fluctuations or magnetic susceptibility, χ. It is defined as the response of the magnetization to an applied magnetic field. For a ferromagnetic system, the magnetic susceptibility diverges as $T \to T_c$. On the other hand, for an antiferromagnetic system, it is maximum at $T = T_c$, and goes to a constant at $T = 0$.

2.2 The spin-S XXZ Model

The XXZ model is a generalization of the Heisenberg exchange, and belongs to a more general class of spin Hamiltonians, called the XYZ model. The spin-S XXZ model describes the neighbour-neighbour interactions of a 1D chain of N localized spin-S particles, through the following Hamiltonian,

$$H = J\sum_{i=1}^{N}\left(S_i^x S_{i+1}^x + S_i^y S_{i+1}^y + \Delta S_i^z S_{i+1}^z\right) - h\sum_{i=1}^{N} S_i^z,$$

where the Δ parameter sets an uniaxial anisotropy along the z-axis and h is an optional applied magnetic filed along the z-axis. S_i^α are the local spin operators in the $\alpha = x, y, z$ direction (we choose $\hbar = 1$). Using the ladder operators, S^+ and S^-, the Hamiltonian becomes

$$H = J\sum_{i=1}^{N}\left[\frac{1}{2}\left(S_i^+ S_{i+1}^- + S_i^- S_{i+1}^+\right) + \Delta S_i^z S_{i+1}^z\right] - h\sum_{i=1}^{N} S_i^z. \tag{2.1}$$

Note that setting $\Delta = 1$ and $h = 0$, we recover the Heisenberg model. Putting $\Delta = 0$, we have the XY model. For $S = 1/2$ this model is interesting as it can be mapped to a chain of free fermions, through the Jordan-Wigner (JW) transformation, and solved exactly

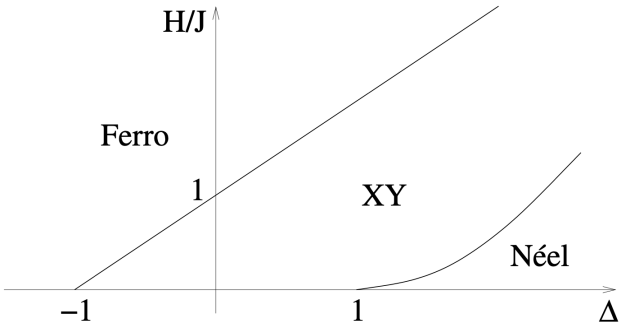

Figure 2.1: Ground state phase diagram of the $S = 1/2$ XXZ chain as a function of magnetic anisotropy Δ and applied magnetic field h. Figure taken from [40].

[38, 39]. The ferromagnetic ($J < 0$) and antiferromagnetic ($J > 0$) phases of the model can be related through some symmetries. By performing a rotation around the z-axis of every-other spin, followed by setting $\Delta \to -\Delta$, we can map the ferromagnetic case to the antiferromagnetic one, and vice-versa. Without loss of generality, we can set $J > 0$ and let the value of Δ dictate the phase of the system. In the antiferromagnetic case, the choice of boundary conditions and number of spins can also affect some properties of the model. By choosing periodic boundary conditions (PBC), if N is odd, we have a frustrated system. To illustrate this, consider the simplest case $N = 3$, for $S = 1/2$. For the first and second spins, we can choose them to be antiparallel, $|\uparrow\downarrow .\rangle$ or $|\downarrow\uparrow .\rangle$. In either case, choosing the third one to be up or down, will result in degenerate states with two possible orientations. When using open boundary conditions (OBC), we do not encounter frustration, for any N, as the interaction energy between the last and first spin is not taken into account. Frustration is never encountered for the ferromagnetic phase, in this model.

2.2.1 Ground State Phase Diagram

Figure 2.1 shows the ground state diagram of the spin-1/2 XXZ chain. As can be seen, sufficiently strong magnetic fields can cause the ground state of the system to lose its properties and turn in to an XY or ferromagnetic ground state. The field at which this transition occurs is called the critical or saturation field h_c. For the boundary of the XY and ferromagnetic phases $h_{c_1}(\Delta) = J(1 + \Delta)$. For the boundary between the antiferromagnetic and XY phases, the critical field is given in terms of the triplet gap energy $h_{c_2} = E_g(\Delta)$ [40]. For $|\Delta| \leq 1$, the model is gapless, i.e. there is no minimum required energy for a magnetic excitation. If the applied field is bigger than the saturation field h_{c_1}, there will be a gap in the excitation spectrum. For $|\Delta| > 1$, the system is gapped.

The ground state behaviour of antiferromagnetic chains with integer spin and half-integer spin is very different. In the 1980s, Haldane discovered that the ground state of

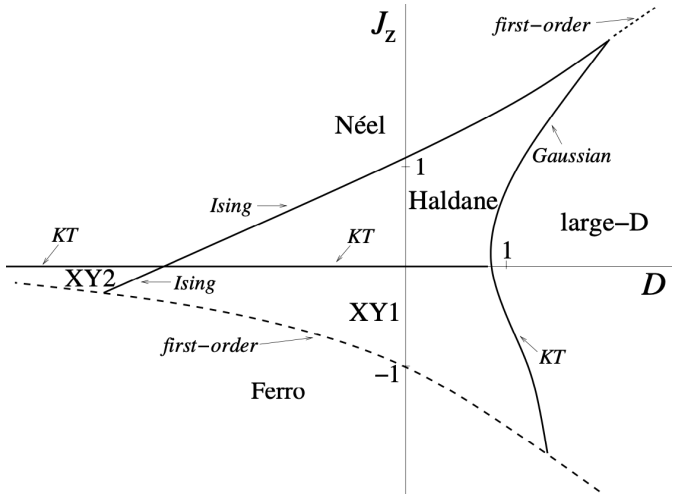

Figure 2.2: Ground state phase diagram of the $S = 1$ XXZ chain as a function of magnetic anisotropy $\Delta(J_z)$ and easy-axis anisotropy D. Figure taken from [40].

integer spin chains is gapped for a range of Δ values [5, 6]. This gives rise to the Haldane phase, which is a symmetry protected topological phase only detectable by the non-local string order parameter [41]. It is characterized by the presence of two free spin-1/2 (for a spin-1 chain) particles at the edges of the chain. The Haldane phase is a gapped phase [42]. This gap decreases exponentially as the spin number is increased. Furthermore, this phase is only realized for limited range of $\Delta > 0$ values. For $S = 1$, the Haldane phase was found to exist for the interval $\Delta \approx 0$ to $\Delta \approx 1.2$ [43].

For $S > 1/2$ it becomes interesting to add an uniaxial single-ion or easy-axis anisotropy term to the Hamiltonian,

$$H_D = D \sum_{i=1}^{N} (S_i^z)^2, \tag{2.2}$$

where D is called the easy-axis anisotropy. Depending on the sign of D, different spin projections will be energetically favourable. If $D < 0$, ordering along the z-axis is preferred, so states with $S^z = \pm S$ are energetically favourable, and if $D > 0$ states with $S^z = 0$ are preferred. The ground state phase diagram for the spin-S XXZ chain with easy-axis anisotropy was studied in [44, 41] using Bosonization. For the $S = 1$ case, the ground state phase diagram was computed numerically in [45, 43], as shown in Figure 2.2. We can interpret spin-1 chains as diluted spin-1/2 chains [41]. The site is empty if $S^z = 0$, or occupied by a spin-1/2 particle if $S^z = \pm 1$. Then the Néel phase can be interpreted as a AF spin-ordered solid, i.e. a phase which is characterized with long-range correlation of particle positions, and their spin have long-range antiferromagnetic order. The Haldane phase corresponds to the AF spin-ordered fluid phase, where there is antiferromagnetic order but no order in position of particles. The antiferromagnetic order vanishes for the XY1 gapless phase, which is described as spin-disordered fluid. The gapless XY2 phase

is described as a spin-disordered solid, where order in the position of particles is restored. The large-D phase can be characterized as a gas of bound pairs of particles with opposite spin. Some studies for $S = 2$ using density matrix renormalization group (DMRG) show that the Haldane phase is reduced, in favour of the XY1 phase, to a smaller range of Δ values [46, 47].

2.2.2 Symmetries and Currents

When studying dynamical properties of systems, we are often interested in the transport of conserved quantities. More specifically, we are interested in quantities Q that are conserved, that is $[Q, H] = 0$ and can be expressed as a sum of local quantities around a site i, $Q = \sum_i q_i$. If Q is not conserved, we can not necessarily speak of transport as Q is not transported from one place to another. Instead it is created and destroyed at different sites.

The XXZ model has many symmetries [48]. The most interesting ones from the point of view of transport are the invariance under time translations, which states that the total energy must be conserved $[e^{iHt}, H] = 0$, or that $[H, H] = 0$, and the invariance under the rotations along the z-axis, which conserves the total magnetization or spin $[S^z, H] = 0$. From this, the quantities of interest are H and $m = \sum_i S_i^z$. The Hamiltonian is associated with thermal or energy transport and the magnetization to spin transport.

Before deriving the current expressions, it is useful to define the local Hamiltonian operators h_i, such that $H = \sum_{i=1}^{N} h_i$ with

$$h_i = J\left[\frac{1}{2}\left(S_i^+ S_{i+1}^- + S_i^- S_{i+1}^+\right) + \Delta S_i^z S_{i+1}^z\right] - hS_i^z.$$

The definition of a local current density j_i^Q, associated with a conserved quantity Q, is given by the continuity equation and the time evolution equation for an operator in the Heisenberg picture,

$$\frac{\partial q_i}{\partial t} = -\nabla \cdot j_i^Q, \qquad \frac{\partial q_i}{\partial t} = i[H, q_i],$$

respectively. Since we consider a 1D chain, only one of the spatial derivatives, in the continuity equation, gives a non-zero result. If we consider the sites of the chain to be along the x-axis, and choose a lattice spacing equal to unity ($a = 1$), the spacial derivative may be written as $\nabla \cdot j_i^Q = j_i^Q - j_{i-1}^Q$. Therefore, by combining the two equations, the local current density is be defined as

$$j_i^Q - j_{i-1}^Q = i[q_i, H]. \tag{2.3}$$

Positive transport along the chain is defined as transporting the conserved quantity Q in the positive x direction. We can further define the total current $J^{(Q)}$ as

$$J^Q = \sum_i j_i^Q.$$

The conservation of the total magnetization gives rise to a spin current density J^S. So $Q = m$ and $q_i = S_i^z$. Using Equation (2.3), we see that S_i^z does not necessarily commute with the local Hamiltonian operators at sites $i-1$ and i,

$$j_i^S - j_{i-1}^S = i\left([S_i^z, h_{i-1}] + [S_i^z, h_i]\right).$$

The local current density at site i can be given by $j_i^S = i[S_i^z, h_i]$[3], so

$$j_i^S = i\frac{J}{2}\left(S_i^+ S_{i+1}^- - S_i^- S_{i+1}^+\right).$$

The total spin current density is then given as

$$J^S = i\frac{J}{2}\sum_i \left(S_i^+ S_{i+1}^- - S_i^- S_{i+1}^+\right). \tag{2.4}$$

By the form of j_i^S, we notice that the spin current measures the difference between magnetic excitations (magnons) moving to the left and right along the chain.

The conservation of the total energy generates a heat or energy current density J^H. So $Q = H$ and $q_i = h_i$. This quantity will not commute with the local Hamiltonian operators at sites $i-1$ and $i+1$,

$$j_i^H - j_{i-1}^H = i\left([h_i, h_{i-1}] + [h_i, h_{i+1}]\right).$$

The local heat current density at site i can be written as $j_i^H = i[h_i, h_{i+1}]$, such that

$$j_i^H = i\frac{J^2}{2}S_{i+1}^z\left(S_i^- S_{i+2}^+ - S_i^+ S_{i+2}^-\right) + J\Delta\left(S_i^z j_{i+1}^S + j_i^S S_{i+2}^z\right) - h j_i^S.$$

It is important to note that the heat current density is comprised of an energy and a spin contribution $j_i^H = j_i^E - h j_i^S$. In finite magnetic fields, the spin current couples to the energy current and there is a contribution to the heat current due to spin transport. The total thermal current density becomes

$$J^H = \sum_i \left[i\frac{J^2}{2}S_{i+1}^z\left(S_i^- S_{i+2}^+ - S_i^+ S_{i+2}^-\right) + J\Delta\left(S_i^z j_{i+1}^S + j_i^S S_{i+2}^z\right) - h j_i^S\right]. \tag{2.5}$$

These are the currents that govern the transport of heat and spin in the XXZ chain. In Chapter 4, we will use these currents to compute the transport coefficients associated with each current.

[3]This definition is not unique. We can always add a divergence free quantity or observable, like a constant.

Chapter 3

Stochastic Series Expansion

In this Chapter we will present an overview of the Stochastic Series Expansion method, i.e. the basic set up of the series expansion formalism, how to derive expressions for expectation values and sampling routines, diagonal updates and the directed loop updates. Towards the end of the Chapter, the method will be applied to the spin-S XXZ model, where comparisons with exact diagonalisation results, for small systems, are presented along side with a brief discussion of finite size effects.

3.1 Series Expansion of the Partition Function

The Stochastic Series Expansion (SSE) method is a Monte Carlo (MC) algorithm to simulate quantum lattice models. The main idea is to perform a high-temperature series expansion of the partition function Z. The first iteration was developed by Handscomb in the early 1960s to solve the $S = 1/2$ Heisenberg ferromagnet [49, 50]. He noticed that the Heisenberg exchange interaction between two spins, $H_{ij} = \boldsymbol{S}_i \cdot \boldsymbol{S}_j$, is a permutation operator, and traces of powers of these operators can be easily evaluated analytically. Using the Metropolis MC method [51], these traces can be sampled efficiently and various thermodynamic expectation values can be estimated. This method however, is very limited as it suffers of sign problems for the Heisenberg antiferromagnet, as the traces are a mixed product of positive and negative terms. This was eventually solved on bipartite lattices [52], but the formulation of the method performed worse than the path-integral based methods [53]. Although path-integral based approaches still had sign problems for some systems (namely fermionic and frustrated systems), the community was fast to dismiss series expansion methods due to their worse overall performance.

In the early 1990s, Sandvik and Kurkijärvi [20] realized that the traces could also be sampled in an imaginary time expansion, by introducing some convenient basis. This gave arise to the Stochastic Series Expansion method. Despite of sign problems still being present, this method does not suffer errors originated from the Suzuki–Trotter expansion

and time discretisation. It is in fact an exact method and any errors are due to the limited amount of samples or poor design of the random number generator used. In the later decade, the method gained recognition by the scientific community and many improvements were proposed, namely the general Directed Loop update sampling scheme by Sandvik and Syljuåsen [21, 54].

The starting point for the SSE method is the power series expansion of the partition function

$$Z = \mathrm{Tr}\{e^{-\beta H}\} = \sum_{\alpha} \sum_{n=0}^{\infty} \frac{(-\beta)^n}{n!} \langle \alpha | H^n | \alpha \rangle ,$$

where the trace is written as a sum over the diagonal elements in a complete basis $\{|\alpha\rangle\}$. Decomposing the Hamiltonian into bond operators, such as $H = \sum_a \sum_b H_{a,b}$, where a is the type of the operator and b is the bond at which it acts at, we can then represent the powers of the Hamiltonian H^n as a sum the string operator S_n. The operator string encodes the bond and type of the Hamiltonian operator that acts on the system at propagation step p

$$S_n = l_1, l_2, \ldots, l_n = [a_1, b_1], [a_2, b_2], \ldots, [a_n, b_n]$$

Here $a_i \in \{1, 2\}$ denotes the type of the operator (diagonal/off-diagonal) and $b_i \in \{1, \ldots, N_b\}$. We can then write the partition function as

$$Z = \sum_{\alpha} \sum_{n=0}^{\infty} \sum_{S_n} \frac{(-\beta)^n}{n!} \langle \alpha | \prod_{i=1}^{n} H_{l_i} | \alpha \rangle .$$

We can now think of the operator string as a propagation of the state $|\alpha\rangle$ in imaginary time indexed by $p = \{0, \ldots, n\}$, where $|\alpha\rangle = |\alpha(0)\rangle = |\alpha(n)\rangle$. So the propagated state by the p first operators is given by

$$|\alpha(p)\rangle = \prod_{i=1}^{p} H_{l_i} |\alpha\rangle .$$

Defining a weight function $W(\alpha, S_n)$ as

$$W(\alpha, S_n) = \frac{(-\beta)^n}{n!} \langle \alpha | \prod_{i=1}^{n} H_{l_i} | \alpha \rangle , \tag{3.1}$$

and using importance sampling methods we can sample the $\{\alpha, S_n\}$ space. One may notice that the weight function is cyclically permutable, meaning that $W(\alpha, S_n) = W(\alpha(p), S_n(p))$, where $S_n(p)$ is the index sequence $l_{p+1}, \ldots, l_n, l_1, \ldots, l_p$.

This kind of sampling is only possible however if W is a positive definite weight, such that we do not encounter sign problems [55]. Therefore we can write the bond decomposition of the Hamiltonian with an explicit negative sign $H = -\sum_b H_b$, making

sure, at the same time that $H_b \geq 0$. For negative diagonal terms we can add a suitable constant to the Hamiltonian guaranteeing that $H_{1,b} \geq 0$. Signs appearing from the off-diagonal part of the Hamiltonian are often difficult to avoid, limiting the class of methods that can be explored by these types of methods.

3.2 Expressions for Expectation Values

Having developed a framework where we can represent quantum lattice models as a power series expansion of the partition function, we now need a way to sample physical quantities. Unlike classical Monte Carlo methods, getting expectation values for thermodynamic properties is more challenging in the SSE, as the quantities we want to measure might not commute with the Hamiltonian operator. We will start by writing the thermal average of an operator A

$$\langle A \rangle = \frac{1}{Z} \mathrm{Tr}\{A e^{-\beta H}\}.$$

In the SSE framework we can write this as

$$\langle A \rangle = \frac{1}{Z} \sum_{\alpha} \sum_{n=0}^{\infty} \sum_{S_n} \frac{(-\beta)^n}{n!} \langle \alpha | \prod_{i=1}^{n} H_{l_i} A | \alpha \rangle .$$

Using the defined weights $W(\alpha, S_n)$, in Equation (3.1), our objective is now to find a function $A(\alpha, S_n)$, from which the average can be estimated using importance sampling in the $\{\alpha, S_n\}$ space

$$\langle A \rangle = \frac{\sum_{\alpha} \sum_{n=0}^{\infty} \sum_{S_n} A(\alpha, S_n) W(\alpha, S_n)}{\sum_{\alpha} \sum_{n=0}^{\infty} \sum_{S_n} W(\alpha, S_n)} \equiv \langle A(\alpha, S_n) \rangle_W .$$

Here $\langle . \rangle_W$ represents the average over the SSE configurations.

Since the operator string S_n is cyclically permutable, we can evaluate the average of $A(\alpha, S_n)$ over all of the states in the imaginary time propagation

$$\langle A \rangle = \left\langle \frac{1}{n} \sum_{p=0}^{n-1} A(\alpha(p), S_n(p)) \right\rangle_W . \tag{3.2}$$

Using the averaged A improves the statistics of the simulation. Furthermore, it will allow for some formal simplifications, as we will see.

We can divide the class of possible operators A into diagonal and off-diagonal operators in the chosen basis for the SSE computations. In most cases, if A is diagonal, finding $A(\alpha, S_n)$ proves to be an easy task. Let us consider the case where

$$A | \alpha(p) \rangle = a(p) | \alpha(p) \rangle .$$

Then we clearly have that $A(\alpha, S_n) = a(0)$, and then,

$$\langle A \rangle = \left\langle \frac{1}{n} \sum_{p=0}^{n-1} a(p) \right\rangle_W . \tag{3.3}$$

If A is off-diagonal the situation is generally more complicated. It is however possible in most cases to decompose A in to sums and products of Hamiltonian operators. For the case where $A = H_k$,

$$\langle A \rangle = \langle H_k \rangle = \frac{1}{Z} \sum_{\alpha} \sum_{n=0}^{\infty} \sum_{S_n} \frac{(-\beta)^n}{n!} \langle \alpha | \prod_{i=1}^{n} H_{l_i} H_k | \alpha \rangle .$$

This can be thought of sequences of operators of length $n+1$ which have H_k as H_{l_0}, so clearly, $A(\alpha, S_n) = -n/\beta \delta_{l_0,k}$, and

$$\langle H_k \rangle = \left\langle \frac{-1}{\beta} \sum_{p=0}^{n-1} \delta_{l_p,k} \right\rangle_W = \frac{-\langle N(k) \rangle_W}{\beta},$$

where $N(k)$ is the number of Hamiltonian operators H_k in the operator string S_n. The energy of the system E is then given as

$$E = \langle H \rangle = \frac{-\langle n \rangle_W}{\beta}, \tag{3.4}$$

and the specific heat C is

$$C = \langle n^2 \rangle_W - \langle n \rangle_W^2 - \langle n \rangle_W .$$

For a product of m operators we get

$$\langle A \rangle = \left\langle \prod_{i=1}^{m} H_{k_i} \right\rangle = \frac{1}{(-\beta)^m} \left\langle \frac{(n-1)!}{(n-m)!} N(k_1, \ldots, k_m) \right\rangle_W ,$$

where $N(k_1, \ldots, k_m)$ denotes the number of ordered subsequences $k_1, \ldots, k_m$ in S_n.

Let us now consider an imaginary time dependent product of two operators $A_2(\tau)A_1(0) = e^{\tau H} A_2 e^{-\tau H} A_1$. Taylor-expanding the exponentials, the ensemble average is

$$\langle A_2(\tau)A_1(0) \rangle = \frac{1}{Z} \sum_{\alpha} \sum_{n=0}^{\infty} \sum_{m=0}^{\infty} \frac{(\tau - \beta)^n (-\tau)^m}{n! m!} \langle \alpha | H^n A_2 H^m A_1 | \alpha \rangle .$$

Changing to a summation over string of operators and summing over all of the positions of A_2 in the operator string,

$$\langle A_2(\tau)A_1(0) \rangle = \frac{1}{Z} \sum_{\alpha} \sum_{n=0}^{\infty} \sum_{m=0}^{n} \sum_{S_n} \frac{(\tau - \beta)^{n-m} (-\tau)^m}{(n-m)! m!} \langle \alpha | \prod_{i=m+1}^{n} H_{l_i} A_2 \prod_{i=1}^{m} H_{l_i} A_1 | \alpha \rangle . \tag{3.5}$$

If A_1 and A_2 are diagonal operators,

$$\langle A_2(\tau)A_1(0)\rangle = \left\langle \sum_{p=0}^{n-1}\sum_{m=0}^{n} \frac{(\beta-\tau)^{n-m}\tau^m}{\beta^n}\frac{(n-1)!}{(n-m)!m!}a_2(p+m)a_1(p)\right\rangle_W ,$$

where the states $|\alpha(p)\rangle$ are periodic, i.e. $|\alpha(p+n)\rangle = |\alpha(p)\rangle$. For $A_1 = H_{k_1}$ and $A_2 = H_{k_2}$,

$$\langle H_{k_2}(\tau)H_{k_1}(0)\rangle = \left\langle \sum_{m=0}^{n-2} \frac{(\beta-\tau)^{n-2-m}\tau^m}{\beta^n}\frac{(n-1)!}{(n-2-m)!m!}N(k_1,k_2;m)\right\rangle_W ,$$

where $N(k_1, k_2; m)$ is the number of times the indices k_1 and k_2 appear in the operator string with m operators in-between.

Integrating the imaginary time correlation function from 0 to β gives a Kubo integral. In the diagonal case

$$\int_0^\beta d\tau\, \langle A_2(\tau)A_1(0)\rangle = \left\langle \frac{\beta}{n(n+1)}\left(\sum_{p=0}^{n-1}a_1(p)\sum_{p=0}^{n-1}a_2(p) + \sum_{p=0}^{n-1}a_1(p)a_2(p)\right)\right\rangle_W .$$

For the Hamiltonian terms product,

$$\int_0^\beta d\tau\, \langle H_{k_2}(\tau)H_{k_1}(0)\rangle = \frac{1}{\beta}\langle N(k_1)N(k_2)\rangle_W .$$

Having derived the equations according to [56], we can now measure any kind of operator in the SSE method, provided that off-diagonal ones can be decomposed into a sum or product of Hamiltonian operators. Derivations of other operators sich as the spin-stiffness ρ_s can be found in [57].

3.3 Sampling Sub-Routines

The most important part of any MC method is the way the configuration is updated. Here we present two methods for sampling the SSE configurational space $\{\alpha, S_n\}$. One is the diagonal updates, where we insert or remove a diagonal operator in S_n. The other is the Directed Loop updates.

To sample the $\{\alpha, S_n\}$ space, it is useful to truncate the series expansion at a maximum power $n = M$ and insert $M - n$ identity operators, $H_{0,0} = 1$, in the operator sequence such that all indices in the operator string have a corresponding operator. We can then write the partition function as

$$Z = \sum_\alpha \sum_{S_M} \frac{\beta^n(M-n)!}{M!}\langle\alpha|\prod_{i=1}^{M} H_{l_i}|\alpha\rangle , \tag{3.6}$$

where n is now the number of bond operators, i.e. the number of elements in S_M for which $H_{l_i} \neq H_{0,0}$. From the last section, we know that $\langle n\rangle = \beta N_b|E_b|$, where E_b is the energy

per bond, and that the width of this distribution is approximately $\langle n \rangle^{1/2}$. Thus, M can be chosen so that n never reaches the cut-off during the simulation, avoiding truncation errors. We do this by gradually adjusting M during the simulation such that $M = an_{max}$, where $a > 1$ and n_{max} is the maximum n reached by the simulation. In practice, $a \approx 1.33$.

It is also useful to define bond states at propagation time p as $\left|\alpha_{b_p}(p)\right\rangle$.

3.3.1 Diagonal Updates

This type of update was introduced in the first version of the SSE method. It is very effective since, in all systems, we can add a constant to the diagonal elements of the Hamiltonian, ensuring that they are positive. As so, there are no restrictions on the number or the positions of these operators in order to ensure a positive definite configurational weight. We can therefore insert/remove diagonal operators from the operator string, without any practical problems, ensuring detailed balance. This type of update allows us to sample different values of n, since we either increase it by 1 (insertion) or decrease it by 1 (removal).

The detailed balance equation reads as

$$W(s)P(s \to s') = W(s')P(s' \to s), \tag{3.7}$$

where $W(s)$ is the weight of the configuration s and $P(s \to s')$ is the probability of transitioning from the configuration s to s'. By taking the Metropolis choice, we can write the probability of changing configuration as

$$P(s \to s') = \max\left\{\frac{W(s')}{W(s)}, 1\right\}.$$

Choosing $W(s)$ as in Equation (3.6), we then have

$$\frac{W(\alpha', S'_M)}{W(\alpha, S_M)} = \beta^{n-n'} \frac{(M-n')! \left\langle\alpha'\right| \prod_{i=1}^{M} H_{l'_i} \left|\alpha'\right\rangle}{(M-n)! \left\langle\alpha\right| \prod_{i=1}^{M} H_{l_i} \left|\alpha\right\rangle}$$

For the insertion of a diagonal operator at propagation time p in bond b, $[0,0]_p \to [1,b]_p$, the operators strings only differ at $l_p = [0,0]_p$ and $l'_p = [1,b]_p$, and $n' = n+1$. Then the probability is given as

$$P([0,0]_p \to [1,b]_p) = \frac{N_b \beta \left\langle\alpha_{b_p}(p)\right| H_{1,b} \left|\alpha_{b_p}(p)\right\rangle}{M-n}.$$

Here we multiplied the expression by the number of bonds N_b, since we have to randomly choose a bond b to insert the operator out of N_b bonds. Similarly, for the removal of a diagonal operator, $[1,b]_p \to [0,0]_p$, we have

$$P([1,b]_p \to [0,0]_p) = \frac{M-n+1}{N_b \beta \left\langle\alpha_{b_p}(p)\right| H_{1,b} \left|\alpha_{b_p}(p)\right\rangle}.$$

These are the equations governing the diagonal updates sub-routine. In practice, we apply this update for every propagation time p where we encounter an identity $H_{0,0}$ or a diagonal $H_{1,b}$ operator.

3.3.2 Directed Loop Updates

The Directed Loop updates was developed in [21] and further generalized in [54]. Unlike the diagonal update, where we change the expansion order n, in the directed loop update, we focus on sampling configurations where off-diagonal operators are changed, at fixed n. The directed loop is a non-local update which allows for better sampling at lower temperatures avoiding the low temperature slowdown, which allows for more accurate simulations in these regimes. For this update, we disregard the identity operators introduced before and work again with the operator string S_n.

Before describing the algorithm, we need to introduce the graphical and vertex representations of an SSE configuration. An SSE configuration is described by an initial state $|\alpha\rangle$ and an operator string S_n, which propagates the initial state. In Figure 3.1a, we have represented the propagation of a four site system where the initial state is represented in the bottom row and the propagation is portrayed above. Here, the state of each particle is labelled by an integer value. This is the graphical representation of the SSE configuration. We can recast this representation into a picture where each operator is depicted as a four-legged vertex, Figure 3.1b. Each leg now contains the information of the state and is connected to two other legs, one at the same vertex and another at another vertex. We can map this onto a linked list, also known as the vertex list, where the connections between the every leg on every vertex are encoded.

In general, a vertex has N_{legs} which depend in the given interaction. For example, for a two-body interaction a vertex will have 4 legs. All of the vertices for a given system can be constructed by all of the non-zero entries in the Hamiltonian one bond operator, $\langle\alpha_b(p)| H_b |\alpha_b(p-1)\rangle$. The value of this entry is the weight $W(v)$ of the vertex. With this, our original weight, Equation (3.1), can be described as the product of all of the vertex weights. Since n is constant, we can ignore the combinatorial prefactor in Equation (3.1).

With the vertex representation mapped onto a linked list, loop update can be started. First, we randomly select an initial entrance leg e_1 in the s^0 configuration, which has some state $s^0(e_1) = s_0$. Then we propose a new state s_u for this leg. An exit leg is chosen, according to some probability table, given the entrance leg, vertex type and proposed state. This probability table will be given by the solutions of the directed loop equations. With this, we determine the new state of the exit leg and progress in the linked list to the leg which the exit leg links to. Then, to not create impossible configurations, we require that the new state at the new entrance leg is the same state as the new state at the exit leg. Using the probability table, we again choose a new exit leg, given the state

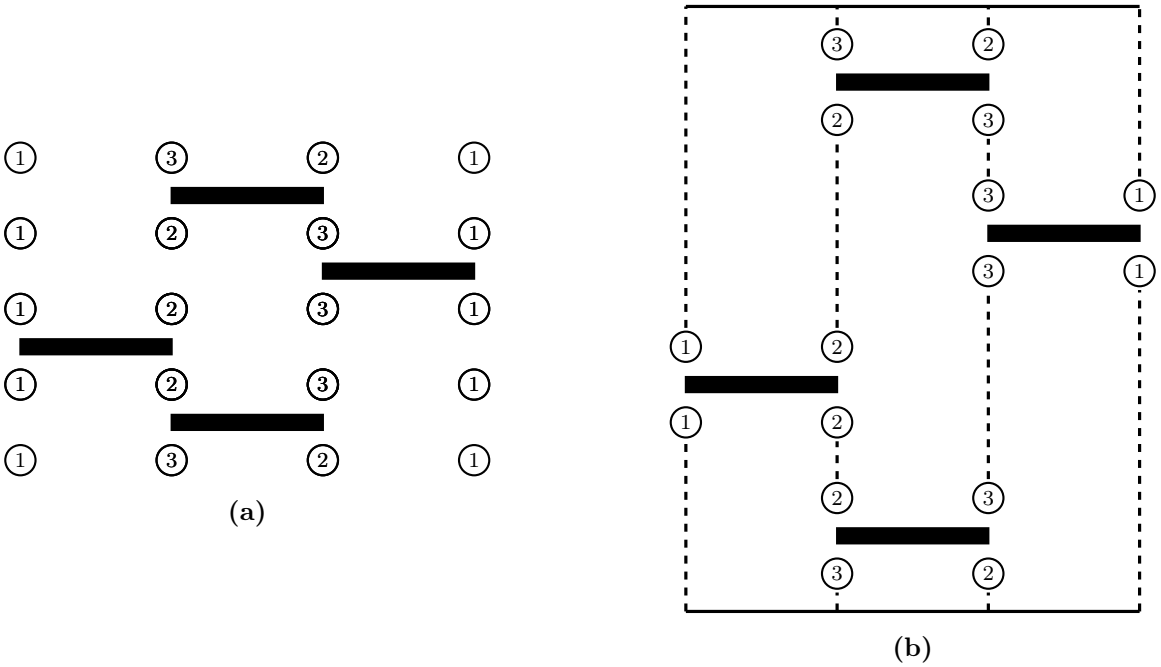

Figure 3.1: (a) Operator sequence for a four-site system with $n = 4$. Each column of the figure represents one site and the states on each site are labelled by an integer. The operators are shown as black rectangles. A propagated state can be read as a row of encircled states. **(b)** The same operator sequence shown in (a) but in the vertex representation. All of the operators have become four-legged vertices. Each leg carries the information about the state and is connected to another leg in another vertex through the dashed lines.

of entrance leg, and update its value. This process repeats until we close the loop, i.e. until one of the exit legs connects to the initial entrance leg e_1 through the vertex list.

Let us now take a look at the equations governing the directed loop update. We start with the general equation for the detailed balance, Equation (3.7). For the loop update, the probability of changing the configuration $s \equiv s^0$ to $s' \equiv s^n$, after n steps, can be written as

$$P(s \to s') = \sum_{\text{all paths}} R(s^0, e_1) P_s(s^0(e_1) = s_0 \to s_u) \\ P(s^0, e_1 \to s^1, x_1) P(s^1, e_2 \to s^2, x_2) \dots P(s^{n-1}, e_n \to s^n, x_n),$$

where $R(s^0, e_1)$ is the probability for choosing the vertex leg e_1 as the initial entrance leg in the s^0 configuration and $P_s(s^0(e_1) = s_0 \to s_u)$ is the probability for choosing a specific new state s_u at the entrance leg. During the loop construction, we traverse the vertex list, so the entrance(exit) leg on the visited vertex i is denoted by $e_i(x_i)$. We also denote s^i as the full configuration after i changes and $s^i(e_i)$ as the state of leg e_i on the configuration s^i. Then, $P(s^{i-1}, e_i \to s^i, x_i)$ is the probability, given the full configuration s^{i-1} and the entrance leg e_i, to exit on leg x_i as we update the configuration, i.e. $s^{i-1}(x_{i-1}) = s^i(e_i)$. For

the reverse probability, we can change the states in reverse order. Thus, the probability for the reverse process, can be written as

$$P(s' \to s) = \sum_{\text{all paths}} R(s^n, x_n) P_s(s^n(x_n) \to s^{n-1}(x_n))$$
$$P(s^n, x_n \to s^{n-1}, e_n) P(s^{n-1}, x_{n-1} \to s^{n-2}, e_{n-1}) \dots P(s^1, x_1 \to s^0, e_1).$$

Requiring that detailed balance holds in the change of a single vertex, we have

$$W(s^{i-1}) P(s^{i-1}, e_i \to s^i, x_i) = W(s^i) P(s^i, x_i \to s^{i-1}, e_i). \tag{3.8}$$

Comparing this expression with the one for detailed balance for the whole process, it is required that must also hold

$$R(s^0, e_1) P_s(s^0(e_1) \to s^1(e_1)) = R(s^n, x_n) P_s(s^n(x_n) \to s^{n-1}(x_n)).$$

Since e_1 and x_n refer to different legs on the same link, the state changes P_s should be opposite of each other. So if $R(s^0, e_1)$ is chosen to be uniform, we have detailed balance. In addition to this, we should require that the path always exits a vertex

$$\sum_{x_i} \sum_{s^i(x_i)} P(s^{i-1}, e_i \to s^i, x_i) = 1, \tag{3.9}$$

where we sum over all possible exit legs and state changes on this leg.

Equation (3.8) involves a ratio between the weights of two configurations that differ only in one vertex. Since the full configuration weight is a product over the individual weights of every vertex, we can simplify Equation (3.8) to consider only the information corresponding to the updated vertex in step i. We define v as the state configuration of a single vertex, $W(v)$ as its weight and a as

$$P(v^{i-1}, e_i \to v^i, x_i) = \frac{a(v^{i-1}, e_i \to v^i, x_i)}{W(v^{i-1})},$$

such that, Equations (3.8) and (3.9) are expressed as

$$a(v^{i-1}, e_i \to v^i, x_i) = a(v^i, x_i \to v^{i-1}, e_i), \tag{3.10}$$

$$\sum_{x_i} \sum_{v^i(x_i)} a(v^{i-1}, e_i \to v^i, x_i) = W(v^{i-1}). \tag{3.11}$$

These are called the directed loop equations. Solving these for every vertex type, will give us the allowed transitions, i.e. which type of state changes on the entrance leg are possible, and their respective probabilities.

To solve the directed loop equations, we start by selecting a reference vertex and label its weight W_1. We choose an entrance leg on this vertex and label is as leg 1, and the rest

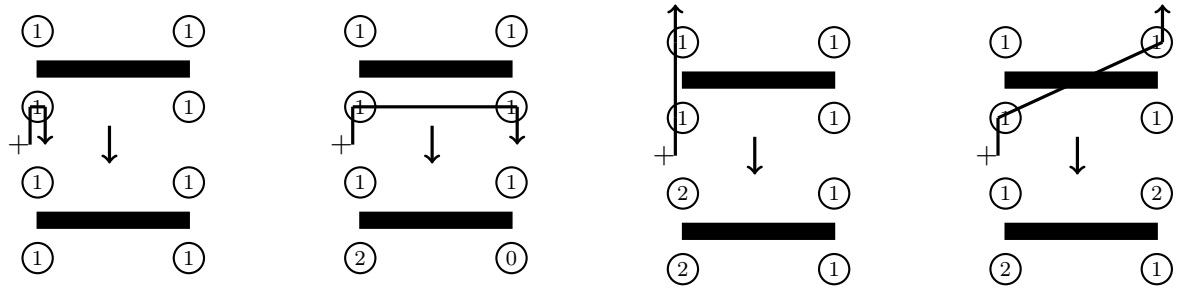

Figure 3.2: Updating vertex with weight W_1 with a +1 update on the entrance leg (lower left leg). The conservation law is such that the sum of the states below equals the sum of the states above.

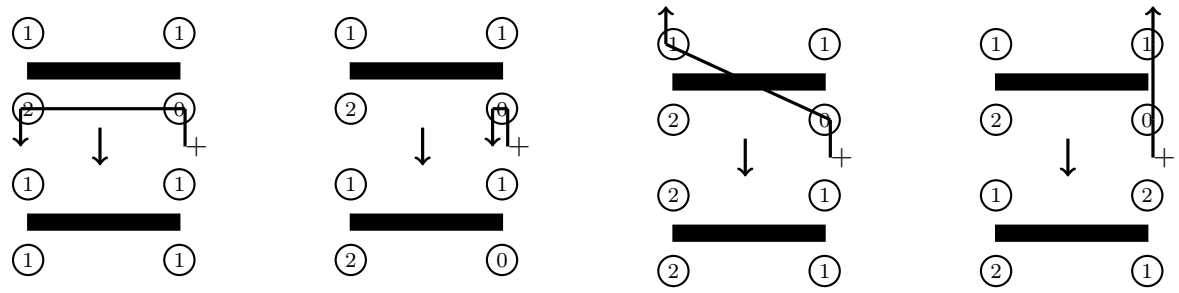

Figure 3.3: Updating vertex with weight W_2 with the entrance leg as the lower right leg. The update is such, that by exiting through the lower left leg, we recuperate vertex with weight W_1.

of the legs as $2, 3, \ldots, n = N_{legs}$. Then, we pick a specific way of changing the entrance leg. The system conservation laws will dictate how to update the configuration. In Figure 3.2 show an example is shown on how to update a vertex given an update +1 on the entrance leg, and a conservation law which states that the sum of state above must equals sum of state below. The equation

$$W_1 = a_{11} + a_{12} + \ldots + a_{1n}$$

determines the probability, when in the vertex with weight W_1, to exit on the different legs, given the specific update on the entrance leg, leg 1. Here a_{ij} denotes the probability to enter in leg i and exit in leg j on the vertex with weight W_i. The vertex generated by exiting at leg 2, updating vertex W_1, is labelled W_2 and its equation is

$$W_2 = a_{21} + a_{22} + \ldots + a_{2n}.$$

The update process in the vertex with weight W_2 is such that $a_{12} = a_{21}$. This means that by starting at W_2, entering through the second leg, exiting through the first leg and updating the vertex, we should get vertex W_1 back, such as depicted in Figure 3.3. So, the update process for vertex W_2 is given by the update process through which by entering through leg 2 and exiting through leg 1 we arrive at W_1. To get W_3, we start at vertex W_1 and exit through leg 3. Similarly we can also start at vertex W_2 and exit at leg 3. This

results in the same vertex as W_1 and W_2 only differ in legs 1 and 2, and by updating W_2 by exiting on leg 3 we are undoing the change in leg 2. Performing the same procedure for the rest of the n legs, we get the following linear system

$$\begin{bmatrix} a_{11} & a_{12} & \dots & a_{n1} \\ a_{12} & a_{22} & \dots & a_{n2} \\ \vdots & \vdots & \vdots & \vdots \\ a_{1n} & a_{2n} & \dots & a_{nn} \end{bmatrix} \begin{bmatrix} 1 \\ 1 \\ \vdots \\ 1 \end{bmatrix} = \begin{bmatrix} W_1 \\ W_2 \\ \vdots \\ W_n \end{bmatrix}. \tag{3.12}$$

The matrix on the left hand side is a real symmetric $n \times n$ matrix with non-negative entries which determine the probabilities for the loop update. The diagonal elements a_{ii} are determined by entering and exiting the vertex through the same leg, the so-called bounce process. In solving this linear system, one would like to minimize the bounce process, since it does not update the configuration, leading to a less efficient algorithm.

Although we present here a set of $n = N_{legs}$ equations, for many models, the number of equations is often reduced. This is due to some updates leading to non allowed vertices, as a consequence of the conservation law. In that case, all matrix entries concerning the disallowed vertex are set to zero, reducing the dimensionality of the matrix.

Due to the large number of unknown variables compared to the known quantities, there are many solutions for the directed loop equations [54]. An easy and general solution to the equation is the heat-bath solution [58, 21]. Here we set

$$a_{ij} = \frac{W_i W_j}{W_1 + W_2 + \ldots + W_n},$$

so,

$$P(i \to j) = \frac{W_j}{W_1 + W_2 + \ldots + W_n}.$$

This solution is general, works for every case, and it is easy to implement. However, as it does not treat bounce process any differently, it does not perform very well [21].

A more general approach is to solve the system for every n while minimizing the bounces. The system, Equation (3.12), contains $n(n+1)/2$ equations. Setting all of the diagonal elements (bounce probabilities) to zero, we have a system with $n(n-1)/2$ equations. For $n \leq 3$, the system has only one well defined solution. When $n > 3$, there are many solutions, and often we have to include bounces. In short, following [54], one

bounce-free solution to the system of equations for general n is given as

$$\begin{aligned}
a_{12} &= (W_1 + W_2 - W_3 - W_4)/2, \\
a_{13} &= (W_1 - W_2 + W_3 - W_4)/2, \\
a_{23} &= (-W_1 + W_2 + W_3 + W_4)/2, \\
a_{14} &= W_4 - W_5/2, \\
a_{15} &= (W_5 - W_6)/2, \ldots, \\
a_{1,n-1} &= (W_{n-1} - W_n)/2, \\
a_{1n} &= W_n/2, \\
a_{45} &= W_5/2, \\
a_{56} &= W_6/2, \\
a_{n-1,n} &= W_n/2.
\end{aligned}$$

Here we assume that $-W1 + W_2 + W_3 + \ldots + W_n \geq 0$ and $W_1 \geq W_2 \geq W_3 \geq \ldots \geq W_n$. When a bounce free solution is not possible, again, there are many approaches. One that generalizes to larger n, is to bounce off of the vertex with the largest weight W_1. For this, we set

$$\begin{aligned}
a_{11} &= W_1 - (W_2 + W_3 + \ldots + W_n), \\
a_{1,i} &= a_{i,1} = W_i, \ i = 2, \ldots, n.
\end{aligned}$$

3.3.3 A Monte Carlo Cycle

One Monte Carlo cycle/sweep (MCS) is defined by a sweep of diagonal updates in all positions of S_M where possible, followed by the construction of the vertex linked list, the construction of N_l loops and the eventual update of S_M. During the update of S_M, we can pick a random state for the particles which are untouched by any (non-identity) operator in S_M with a probability of $1/N_{states}$, while preserving ergodicity. If we are in the thermalisation phase of our simulation, we also adjust the expansion cut-off M by setting $M = a \times n$ (usually $1.2 \leq a \leq 1.5$) and the number of loops N_l. N_l is updated such that, in average, $2M$ (or $2\langle n \rangle$) vertices are visited during each MCS. For this we need to keep record of the number of vertices visited per MCS, disregarding bounces, since they do not update the configuration. If, however, the thermalisation process has ended, we are free to sample the desired thermodynamic quantities with the derived estimators. It is important to keep N_l fixed during the sampling part, so we do not create bias in our measurements [21].

3.4 SSE Applied to the spin-S XXZ Model

In Chapter 2, we discussed the spin-S XXZ model. We can rewrite the XXZ Hamiltonian as

$$H = -J \sum_{b=1}^{N_b} \left(H_{1,b} - H_{2,b} \right),$$

where $H_{1,b}$ and $H_{2,b}$ denote the diagonal and off-diagonal parts of the interaction at bond b. J is given in antiferromagnetic units $J > 0$ and

$$H_{1,b} = -\Delta S^z_{i(b)} S^z_{j(b)} + \frac{h}{2J} \left(S^z_{i(b)} + S^z_{j(b)} \right),$$
$$H_{2,b} = \frac{1}{2} \left(S^+_{i(b)} S^-_{j(b)} + S^-_{i(b)} S^+_{j(b)} \right).$$

Here bond b connects the spins on sites $i(b)$ and $j(b)$. It can be useful to define $H^+_{2,b}$ and $H^-_{2,b}$ as

$$H^+_{2,b} = \frac{1}{2} S^+_{i(b)} S^-_{j(b)}, \qquad H^-_{2,b} = \frac{1}{2} S^-_{i(b)} S^+_{j(b)}.$$

For the $S = 1/2$ case, these terms are equivalent, i.e. acting on the respective two-body state, they will have the same contribution to the Hamiltonian. However, for $S > 1/2$, they can have different contributions. This is useful for computing the winding numbers [57], for example.

The SSE method requires that $H_{a,b} \geq 0$, for $a = 1, 2$. For the diagonal part, we can simply add and subtract a constant C, such that $H_{1,b} \geq 0$. For a general spin number S it is easy to see that $C \geq |\Delta| S^2 + hS/J$. So,

$$C = C_0 + \epsilon, \qquad C_0 = |\Delta| S^2 + hS/J,$$

and $\epsilon \geq 0$ is a constant added so that certain bond operators have a value bigger than zero. Having a finite ϵ has shown to improve sampling in some cases [21]. For the spin-1/2 XXZ model, the minimum values for ϵ were thoroughly analysed in [21]. Adding this constant will raise the energy levels, so the only observable that changes is the energy. To restore the energies for the XXZ model, we need to add JCN_b to the energy expectation value defined previously. For the off-diagonal part, on bipartite lattices, we can rotate every other spin around the z-axis by an angle of π, changing the its sign. To show this, let us consider a bond b where the spin on site $i(b)$ is rotated. This will change the operators on site $i(b)$ as

$$S^z_{i(b)} \to e^{i\pi S^z_{i(b)}} S^z_{i(b)} e^{-i\pi S^z_{i(b)}} = S^z_{i(b)},$$
$$S^+_{i(b)} \to e^{i\pi S^z_{i(b)}} S^+_{i(b)} e^{-i\pi S^z_{i(b)}} = -S^+_{i(b)},$$
$$S^-_{i(b)} \to e^{i\pi S^z_{i(b)}} S^-_{i(b)} e^{-i\pi S^z_{i(b)}} = -S^-_{i(b)}.$$

Thus, we have shown that rotating one spin per bond will change the sign of the off-diagonal part of the Hamiltonian. Doing this only changes values of observables that depend on the values of the ladder operators. Using this trick, for bipartite lattices, the sign of Δ will dictate if we have a ferromagnetic (< 0) or antiferromagnetic (> 0) system.

Then, Hamiltonian simulated by the SSE method is given by,

$$H = -J \sum_{b=0}^{N_b} H_b$$

where $H_b = H_{1,b} + H_{2,b}$ and

$$H_{1,b} = C - \Delta S^z_{i(b)} S^z_{j(b)} + \frac{h}{2J}\left(S^z_{i(b)} + S^z_{j(b)}\right),$$
$$H_{2,b} = \frac{1}{2}\left(S^+_{i(b)} S^-_{j(b)} + S^-_{i(b)} S^+_{j(b)}\right).$$

It is assumed that $J = 1$ unless stated otherwise. Note that for OBC sites 1 and N will only have a contribution of $h/2J$ to the energy as the bond between them is removed.

3.4.1 Observables

The XXZ model is a physics rich model, thus there are many interesting observables we can measure [56, 57]. Here we define some of the basic ones for magnetic systems. These are magnetizations and susceptibilities.

The average magnetization per spin is given by

$$m = \frac{1}{N} \sum_{i=1}^{N} S^z_i.$$

The staggered magnetization m_s is defined by rotating one of the sub-lattices, on a bipartite lattice, around the x-axis by an angle of π, or equivalently by taking the Fourier transform of the magnetization at $q = \pi$. It reads

$$m_s = \frac{1}{N} \sum_{i=1}^{N} (-1)^i S^z_i.$$

A susceptibility is a linear response function of the form

$$\chi_{AB} = \left.\frac{\partial A(b)}{\partial b}\right|_{b=0}$$

where b is the prefactor of a field term B, added to the Hamiltonian and A is the operator whose response to this perturbation we want to measure. Such susceptibility is given by

$$\chi_{AB} = \int_0^\beta d\tau \left\langle A(\tau) B(0) \right\rangle - \beta \left\langle A \right\rangle \left\langle B \right\rangle.$$

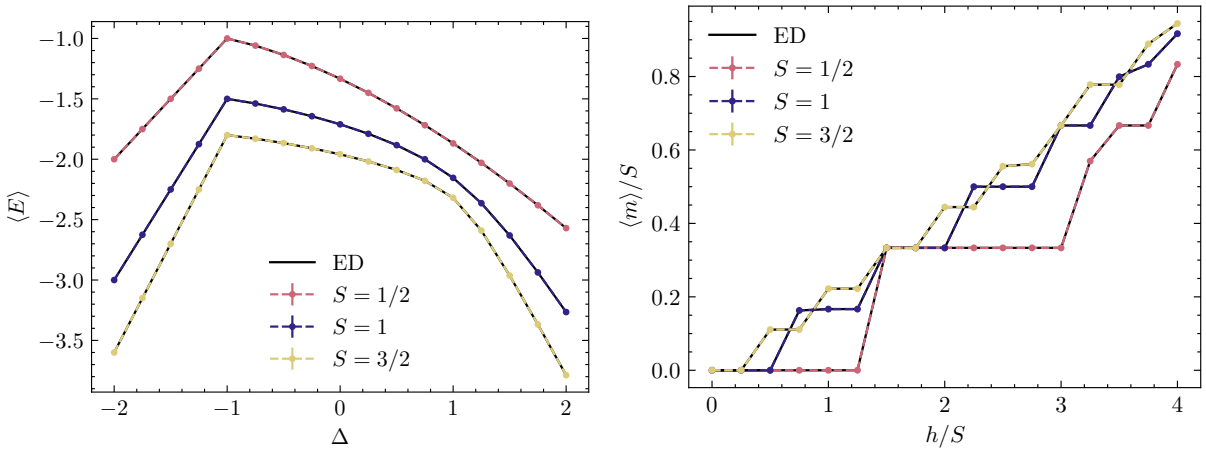

(a) **(b)**

Figure 3.4: **(a)** Mean energy per particle as a function of uniaxial anisotropy, for $h = 0$. The value of the coupling constant is set to $J = 3/(S(S+1))$ so that the energy scale is the same for each spin value. **(b)** Mean magnetization per particle as a function of applied magnetic field, for $\Delta = 1$. The system size is $N = 6$, with PBC, and the temperature is $\beta = 128$. Three different spin values are shown $S \in \{1/2, 1, 3/2\}$. ED results are show in black lines. SSE calculations were done with 10 bins, each with 10^4 MCS. Statistical errors are smaller than the size of the symbols.

The most common susceptibility is the magnetic susceptibility, where the perturbation is given by the Zeeman term $-bM$, and the measured quantity is the magnetization. Since the magnetization is a conserved quantity, we can write the magnetic susceptibility as

$$\chi = N\beta \left(\langle m^2 \rangle - \langle m \rangle^2 \right).$$

Another interesting susceptibility is the staggered susceptibility, where we measure the response of the staggered magnetization to an applied staggered magnetic field. Since the staggered magnetization is not conserved, we get

$$\chi_s = N \int_0^\beta d\tau \, \langle m_s(\tau) m_s(0) \rangle - N\beta \, \langle m_s \rangle \, \langle m_s \rangle .$$

All of these quantities can be sampled using the SSE method by applying the formulas derived in Section 3.2.

3.4.2 Code Verification

Any implementation of a MC method should always be verified by comparing results for small systems with exact diagonalization (ED) approaches. When implemented correctly, the SSE method should always be exact. This meas that the deviation between the average values computed by SSE and the exact values should be purely statistical

caused by the finite number of samples. As most of the time we do not have access to its exact value, we can measure the the standard error or the standard deviation of the mean of some quantity O by MC [59]. One approach of estimating the standard error is to use the binning method. Here we accumulate statistics for the mean value of O through performing N_b independent simulations, each with M MCS, and then we can compute its standard deviation. The averaged value of O over the N_b bins is

$$\langle O \rangle = \frac{1}{N_b} \sum_{i=1}^{N_b} \langle O \rangle_i .$$

The standard error can then be computed by

$$\sigma_O = \frac{1}{N_b} \sum_{i=1}^{N_b} (\langle O \rangle_i - \langle O \rangle)^2. \tag{3.13}$$

One could also use methods like bootstrap or blocking to estimate the standard error by performing just one simulation [59]. These approaches however require that we store the sampled values of O each MCS.

It is important to test the program for a different range of parameters and large systems. In this section we test the implementation for different S, Δ and h values, for a small system, and on the next section we show some finite size effects at lower temperatures for larger systems.

Computations of the energy and magnetization, per particle, for a system with 6 sites and PBC, are shown in Figure 3.4. The calculations are performed at an inverse temperature $\beta = 128$ such that we can approximate the ground state properties of the system. The chosen coupling constant is $J = 3/(S(S+1))$ so the energy scale is the same for all spin numbers. We can see that all of the computed quantities by SSE appear to coincide with the ED solution. Furthermore, for the ferromagnetic regime, Figure 3.4a, the approximated ground state energies are linear and follow the Ising ground state energy relation $E_{Ising} = J\Delta S^2$. Moreover, in Figure 3.4b, for higher spin numbers, the $m(h)$ curve is smoother, as a result of a higher number of degrees of freedom. We can thus conclude that our implementation of the SSE method is working as intended.

3.4.3 Finite Size Effects

When performing any type of thermodynamic simulations, all calculations are carried out for finite lattices where the effects of size need to be considered. When studying critical behaviour, i.e. phase transitions, or properties at very low temperatures, finite size effects come to have a big impact. The finite size of the system often result in discretization of the energy levels. This affects the distribution and spacing of the energy levels in the excitation spectrum, leading to finite size effects. Due to this discretization

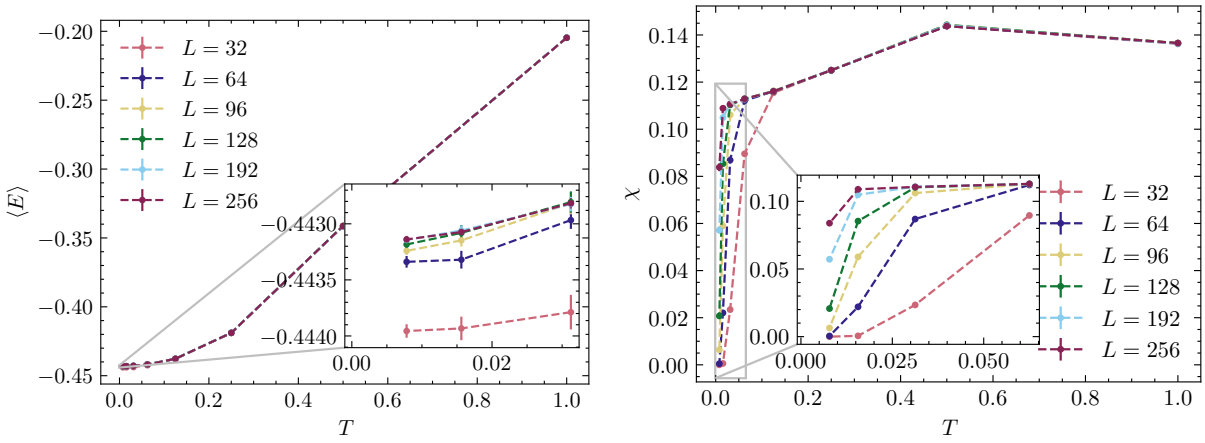

Figure 3.5: (a) Mean energy per particle as a function of temperature and system size L. **(b)** Uniform susceptibility as a function of temperature and system size L. Insets show the behaviour at low temperatures. SSE calculations were performed for a spin-1/2 Heisenberg chain, with 20 bins, each with 10^5 MCS. Statistical errors may be smaller than the size of the symbols.

of the energy levels, energy gaps may emerge in the excitation spectrum that are absent in the thermodynamic limit. The presence of such gaps can affect the system's physical properties. Since the excitation energy of thermal fluctuations is approximately β^{-1}, at low temperatures, the thermal energy might not be enough to excite the system, due to the presence of finite size gaps. So thermodynamic averages become skewed from the thermodynamic limit value or simply vanish as there are no reachable excitations. To minimize this, we can increase the system size, such that the gap between the energy levels becomes smaller. In general, we can determine the properties of the infinite size system from a finite size system at inverse temperature β if the gap between energy levels $\Delta E \approx L^{-1}$ is smaller than the available thermal energy $E_{th} \approx \beta^{-1}$. The precise finite size gap between energy levels will also depend on the Hamiltonian parameters Δ and h.

In Figure 3.5a, we can see the mean energy as function of temperature for different system sizes L. At higher temperatures, the different systems appear to behave similarly. However, at low temperatures $T < 0.2$, as seen in the inset, we start to see a deviation as the system size decreases. These are the finite size effects at low temperatures, as described earlier. For the case of the uniform susceptibility, it is known that it should approach its zero temperature value with an infinite slope. At zero temperature, from low-energy field theory, the uniform susceptibility should go to $\chi(0) = \frac{1}{J\pi^2}$ (≈ 0.101, for $J = 1$) [60]. As we can see in Figure 3.5b, this is not the case. Instead for smaller systems χ goes, exponentially, to zero for finite temperatures. This is due to excitation gaps caused by the finite size of the system. Note that it is possible to estimate the finite size gaps from the results in Figure 3.5b since the susceptibility goes to zero as the

finite size gap becomes smaller than T. Before the decay, the values follow a trend to the aforementioned value.

Chapter 4

Magnetic Transport in the Linear Regime

In this Chapter, we preset a general overview of linear response theory and define magnetic transport coefficients in terms of the kinetic matrix entries. We also present our approach to calculate the transport coefficients for the XXZ chain, using step perturbations in the chain. For Section 4.1 we will follow the book by Pottier [61].

4.1 Linear Response Theory

Linear response theory is a general framework, developed in the 1950s, that allow us to represent physical measurements in a mathematical way. All physical measurements of a macroscopic many-body system are, in practice, the measurement of the response of the system, to an applied force at position $\boldsymbol{r}$ and time t, at some other position $\boldsymbol{r}'$ at time later time $t' > t$. One can also measure the response of the whole system to an uniform perturbation, as it is the case of the magnetic susceptibility, for example. When this external force is small, it will take the system slightly out of equilibrium allowing us to measure its response in a linear regime, i.e. truncating a series expansion. We can relate the system's response to correlation functions of the unperturbed (or equilibrium) system through the Kubo formula.

Let us consider a system described by a Hamiltonian H in thermal equilibrium. The density operator ρ of the system is defined by

$$\rho = \frac{1}{Z} e^{-\beta H},$$

where $Z = \mathrm{Tr}\left(e^{-\beta H}\right)$ is the partition function. At some time t_0, we subject the system to an external field $a(t)$, $t > t_0$. The external perturbation is described by the Hamiltonian

$$H^{ext}(t) = -a(t)A. \tag{4.1}$$

Here A represents the conjugate physical observable to the field $a(t)$. It is now convenient to work in the interaction picture (Heisenberg's picture with respect to the unperturbed Hamiltonian H). Here the subscripts S and I denote the Schrödinger and interaction pictures, respectively. The states and operators are time dependent in the interaction representation,

$$|\psi_I(t)\rangle = e^{iHt} |\psi_S(t)\rangle ,$$
$$B_I(t) = e^{iHt} B_S e^{-iHt}.$$

The time evolution operator from time t_0 to t is given by

$$U(t, t_0) = T \exp\left(-i \int_{t_0}^{t} dt' H_I^{ext}(t')\right),$$

where T is the time ordering operator. The density operator in the interaction picture is

$$\rho_I(t) = e^{-iHt} \rho_S(t) e^{iHt},$$

and $\rho_I(t < t_0) = \rho$ is the density operator of the unperturbed system. Note that the result of measuring an observable is independent of the representation we are working in.

4.1.1 The Kubo Formula

Having introduced the form of the perturbation and the interaction picture, our objective now is to calculate the response of some observable B to the perturbation $H^{ext}(t)$. This is defined by the change in quantity B, from its equilibrium value, due to having a field $a(t)$ applied, $\delta \langle B(t)\rangle_a = \langle B(t)\rangle_a - \langle B\rangle$. We start by writing the thermal average of the quantity B as

$$\langle B(t)\rangle_a = \mathrm{Tr}\left(\rho_I(t) B_I(t)\right) = \mathrm{Tr}\left(U(t, t_0)\rho_I(t_0)U^\dagger(t, t_0) B_I(t)\right).$$

From now on, we assume that every time dependency is given in the interaction picture. Taylor expanding the time evolution operator and truncating the expansion at first order terms we have

$$\langle B(t)\rangle_a \approx \langle B\rangle + i \int_{t_0}^{t} dt' \ \mathrm{Tr}\left(\rho[H^{ext}(t'), B(t)]\right).$$

Taking the limit $t_0 \to -\infty$, the response of B to the field $a(t)$ is written as

$$\delta \langle B(t)\rangle_a = \int_{-\infty}^{\infty} dt' \ \tilde{\chi}_{BA}(t - t') a(t'), \tag{4.2}$$

where

$$\tilde{\chi}_{BA}(t) = i\Theta(t) \langle [B(t), A]\rangle ,$$

is the Kubo formula for the linear response function. The thermodynamical average is taken with respect to the equilibrium density operator ρ. This is the main result of linear response theory. The Kubo formula relates an integral of a correlation function of the system in equilibrium. The response function $\tilde{\chi}_{BA}$ is a general quantity which describes the time dependent response of quantity B to a field coupled to a quantity A, without specifying the form of the field $a(t)$. Furthermore, we can see that it obeys the causality principle. This is, letting $t = t - t_0$, where t_0 is the time for which we apply a perturbation, the response function of the system is zero for any $t < t_0$.

We can simplify the expression for the response function. We start by rewriting the commutator $\langle [B(t), A] \rangle = \mathrm{Tr}\left([A, \rho]B(t)\right)$

$$[A, e^{-\beta H}] = e^{-\beta H} \int_0^\beta d\lambda \; e^{\lambda H}[H, A]e^{-\lambda H}.$$

Using the time evolution equation $\dot{A} = i[H, A]$, the Kubo formula is given by

$$\tilde{\chi}_{BA}(t) = \Theta(t) \int_0^\beta d\lambda \left\langle e^{\lambda H}\dot{A}e^{-\lambda H}B(t) \right\rangle .$$

We define

$$\tilde{K}_{BA}(t) = \frac{1}{\beta} \int_0^\beta d\lambda \, \langle A(-i\lambda)B(t) \rangle$$

as the Kubo canonical correlation function, where $A(-i\lambda) = e^{\lambda H}Ae^{-\lambda H}$ is the time evolution of A in imaginary time $-i\lambda$. The response function of a system at thermal equilibrium, at temperature T, is expressed in terms of the canonical correlation function of B with $\dot{A}$,

$$\tilde{\chi}_{BA}(t) = \beta\Theta(t)\tilde{K}_{B\dot{A}}(t). \tag{4.3}$$

Equation (4.3) allows for a simpler evaluation of the response function without having to calculate the expectation value of a commutator.

For the case of a non-uniform perturbation,

$$H^{ext} = -\int d\boldsymbol{r} \; a(\boldsymbol{r}, t)A(\boldsymbol{r}),$$

the change in quantity B is given by

$$\delta \langle B(\boldsymbol{r}, t) \rangle_a = \int d\boldsymbol{r}' \int_{-\infty}^{\infty} dt' \; \tilde{\chi}_{BA}(\boldsymbol{r}, t; \boldsymbol{r}', t')a(\boldsymbol{r}', t').$$

The Kubo formula is

$$\tilde{\chi}_{BA}(\boldsymbol{r}, t; \boldsymbol{r}', t') = i\Theta(t - t') \left\langle [B(\boldsymbol{r}, t), A(\boldsymbol{r}', t')] \right\rangle .$$

Note that the response function depends both on the time and positions difference, not on their absolute values. As we can see, the response of a non-uniform perturbation is non-local but still obeys the causality principle.

4.1.2 Generalized Susceptibility

Usually, when measuring responses, it is convenient to measure the response of the system to a perturbation with a certain frequency ω. For example, in an optical experiment, it is useful to know the response of the system as a function of the frequency of the incident electromagnetic wave. Equation (4.2) defines a convolution between the response function $\tilde{\chi}_{BA}(t)$ and the driving field $a(t)$. So, using the Convolution Theorem, the Fourier transform of Equation (4.2) is

$$\delta \langle B(\omega) \rangle_a = \chi_{BA}(\omega) a(\omega),$$

where $\chi_{BA}(\omega)$ and $a(\omega)$ are the Fourier transforms of $\tilde{\chi}_{BA}(t)$ and $a(t)$, respectively. $\chi_{BA}(\omega)$ is called the generalized susceptibility

$$\chi_{BA}(\omega) = \int_0^\infty dt\ e^{i\omega t} \tilde{\chi}_{BA}(t). \tag{4.4}$$

The integral in Equation (4.4) may not converge. In that case, a generalized susceptibility may not exist as a function, however, it can exist as a distribution. This is, it is the limit of a convenient sequence of functions. By defining $z = \omega + i\epsilon$, with $\epsilon > 0$, the generalized susceptibility is defined

$$\chi_{BA}(\omega) = \lim_{\epsilon \to 0^+} \chi_{BA}(\omega + i\epsilon)$$

and

$$\chi_{BA}(z) = \int_0^\infty dt\ \tilde{\chi}_{BA}(t) e^{izt} \tag{4.5}$$

is the Fourier-Laplace transform of the response function. Due to the fact that the response function $\tilde{\chi}_{BA}(t)$ is causal, $\chi_{BA}(z)$ is analytic on the upper half of the complex plane.

Since $a(t)$ is a real field and A is a Hermitian operator, $\tilde{\chi}_{BA}$ must be a real quantity. Let us look at the properties of its Fourier transform $\chi_{BA}(\omega)$. We can write the generalized susceptibility as $\chi_{BA}(\omega) = \chi'_{BA}(\omega) + i\chi''_{BA}(\omega)$, where χ'_{BA} and χ''_{BA} denotes the real and imaginary parts of χ_{BA}, respectively. We can write the imaginary part as

$$\begin{aligned} \chi''(\omega) &= -\frac{i}{2}[\chi(\omega) - \chi^*(\omega)] \\ &= -\frac{i}{2} \int_{-\infty}^\infty dt\ e^{i\omega t} [\tilde{\chi}(t) - \tilde{\chi}(-t)]. \end{aligned}$$

We can see that $\chi''(\omega)$ is not invariant under time reversal $t \to -t$. Since the dynamics of microscopic systems are typically invariant under time reversal, $\chi''(\omega)$ must arise from dissipative processes. Thus it is usually called the dissipative part of the response function. It is also an odd function. The real part $\chi'(\omega)$ can be written as

$$\chi'(\omega) = \frac{1}{2} \int_{-\infty}^\infty dt\ e^{i\omega t} [\tilde{\chi}(t) + \tilde{\chi}(-t)].$$

It is invariant under time reversal and it is usually called the reactive part of the response function. It is also an even function.

4.2 Magnetic Transport

Spin transport occurs when the system is subjected to a gradient in the magnetic field ∇h, and heat transport is driven by a temperature gradient ∇T. These phenomena can be described by a system of equations relating the currents and driving fields, such as

$$\begin{pmatrix} J^S \\ J^H \end{pmatrix} = \begin{pmatrix} L_{SS} & L_{SH} \\ L_{HS} & L_{HH} \end{pmatrix} \begin{pmatrix} \nabla h \\ -\nabla T/T \end{pmatrix}.$$

This is called the phenomenological matrix, where all of the relations between the currents and the driving fields are encapsulated. The matrix entries L_{ij} are know as kinetic coefficients and they are related to the transport coefficients. The diagonal kinetic coefficients describe the spin and heat transport. The coefficients L_{SH} and L_{HS} describe the creation of a spin current due to a thermal gradient and of a heat current due to a magnetic field gradient, respectively. From nonequilibrium thermodynamics [61], we can derive the following relations

$$L_{ii} \geq 0, \qquad L_{ii}L_{jj} \geq \frac{1}{4}\left(L_{ij} + L_{ji}\right)^2.$$

Furthermore, if the driving fields obey time reversal symmetry, we can relate the off-diagonal terms through the Onsager reciprocity relations. For this case, the Onsager relation reads

$$L_{SH} = L_{HS}.$$

From Chapter 2, we know that the heat and spin currents are coupled in the presence of an applied uniform magnetic field. In the case where $h = 0$, the system obeys spin-reversal symmetry. So, as there is no preferred direction for the magnetization, the application of a temperature gradient will not cause a magnetic current, so the off-diagonal elements of the kinetic matrix will be zero [9]. For finite h, the spin-reversal symmetry is broken, and a temperature gradient will now cause a magnetization parallel to the field, and the off-diagonal entries can be non-zero [9, 62, 24]. These are related to the magnetothermal effects.

Transport coefficients are defined as proportionality constants between the currents and driving fields. One well known example is the Fourier's law of heat conduction. It relates the heat current to a gradient in temperature, in the absence of a spin current, by

$$J^H = -\kappa \nabla T, \tag{4.6}$$

where κ is the thermal conductivity coefficient. For the XXZ chain, we can define three other coefficients. Namely, the spin conductivity and the spin-Seebeck and Peltier effects.

The spin conductivity σ is the proportionality constant between the spin current and gradient in the magnetic field, in the absence of a temperature gradient,

$$J^S = \sigma \nabla h. \tag{4.7}$$

The spin-Seebeck effect η is associated to the creation of a spin current due to a temperature gradient. This spin current arises due to an increase in entropy resulting from an increase in temperature and results in an induced gradient in the magnetic field. The Seebeck effect is defined as the ratio between the temperature and field gradients, when the spin current is zero,

$$\nabla h = \eta \nabla T. \tag{4.8}$$

Similarly, the Peltier effect π is associated to the creation of a heat current due to a gradient in the magnetic field. It is defined as the ratio between the heat and spin currents, when the temperature gradient vanishes,

$$J^H = \pi J^S. \tag{4.9}$$

The spin-Seebeck and Peltier effects are also known as magnetothermal effects. Moreover, sometimes the spin-Seebeck coefficient is known as the thermomagnetic power of the material.

Relating the four transport coefficients to the kinetic matrix entries is a straight forward process. When $\nabla T = 0$,

$$J^S = L_{SS} \nabla h, \qquad J^H = L_{HS} \nabla h.$$

From Equations (4.7) and (4.9), we see that

$$\begin{aligned} \sigma &= L_{SS}, \\ \pi &= \frac{L_{HS}}{L_{SS}}. \end{aligned}$$

Furthermore, when $J^S = 0$,

$$\nabla h = \frac{1}{T} \frac{L_{SH}}{L_{SS}} \nabla T, \qquad J^H = L_{HS} \nabla h - \frac{1}{T} L_{HH} \nabla T.$$

Using Equations (4.6) and (4.8)

$$\begin{aligned} \eta &= \frac{1}{T} \frac{L_{SH}}{L_{SS}}, \\ \kappa &= \frac{1}{T} \left(L_{HH} - \frac{L_{SH} L_{HS}}{L_{SS}} \right). \end{aligned}$$

From the Onsager relation $\pi = T\eta$.

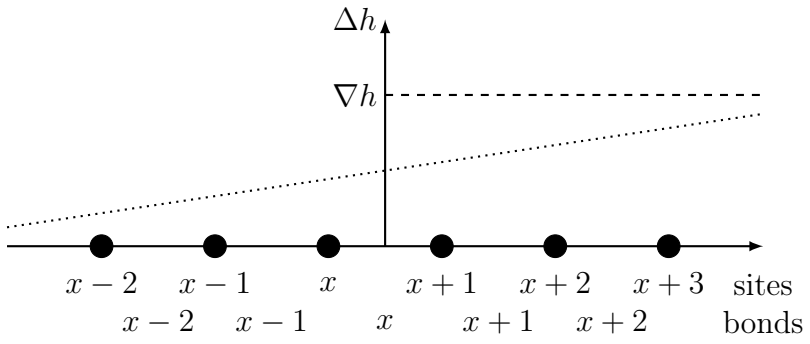

Figure 4.1: Schematic representation of the perturbation in the magnetic field. The dotted line represents a global gradient while the dashed line represents a local gradient given in the form of a step discontinuity.

4.3 Transport Coefficients

Having defined the transport coefficients in terms of the kinetic matrix entries, we are now interested on how to measure them in the XXZ chain using the linear response theory formalism. For this, we first need to define the driving fields in the form of perturbations to the unperturbed Hamiltonian coupled to a field. Let us begin by writing the Hamiltonian of the XXZ chain as $H = \sum_n H_{n,n+1}$, where

$$H_{n,n+1} = \frac{1}{2}\left(S_n^+ S_{n+1}^- + S_n^- S_{n+1}^+\right) + \Delta S_n^z S_{n+1}^z - h S_n^z.$$

In Chapter 2, we saw that there are two currents in this model, the spin current J^S, Equation (2.4), and the heat current J^H, Equation (2.5). The heat current can be written in therms of the energy current J^E and the spin current J^S, $J^H = J^E - hJ^S$. In the linear regime, these currents will couple to the driving forces, either a gradient in the magnetic field or a gradient in temperature. There are two main approaches to represent these. The most common approach is to define a gradient along each site of the chain, as shown in the dotted line in Figure 4.1. In this case, we measure the response of the whole system to the perturbation. An equivalent approach is to introduce a local gradient at some site y, as depicted in the dashed line in Figure 4.1. This way, we measure the response of the system at some site x due to the perturbation at site y. From the computational side, the first method involves the computation of a total current correlation function [24], which might be challenging to compute for a large system. Using the second approach, we calculate correlations functions of the local current densities and perturbation operators [22]. So, we will opt for the latter approach, as it is easier to compute with MC.

4.3.1 Local gradient perturbations

The local gradient perturbations have the form of a step discontinuity, Figure 4.1. Here we define the perturbation Hamiltonian $H_x^i = A_x^i F^i$, which introduces a perturbation at bond x with a perturbation observable A_x^i coupled to a driving field F^i; here $i \in \{S, H\}$. This approach was first presented by Kim Louis and Claudius Gros for the MC calculation of the spin conductivity of the spin-1/2 XXZ model [22].

We can write the local perturbation in the magnetic field at bond x by setting a site dependent magnetic field. This takes the form of a step function, which can be written as

$$h(n) = h + \Theta[n - (x+1)]\nabla h,$$

where $\Theta[n]$ is the discrete Heaviside step function[1]. We take the perturbation to lie in the middle of the bond x, which connects sites x and $x+1$, as shown in Figure 4.1 by the dashed line. Inserting this in the Hamiltonian, we get a perturbation of the form

$$A_x^S = \sum_{n>x} S_n^z, \tag{4.10}$$

with a driving field $F^S = \nabla h$. For the local gradient in temperature, the procedure is not so straight forward as the temperature is not a field that we can add to the Hamiltonian. Instead, we write a site dependent temperature of the form $\beta(n) = \beta + \Theta[n-(x+1)]\nabla\beta$. We take temperature gradient to lie on site $x+1$, so at the endpoint of bond x. This increases the temperature in bonds $x+1, x+2, \ldots$. Writing the Boltzmann factor as

$$\exp\left(-\sum_n \beta(n) H_n\right) = \exp\left(-\beta\left(H + \frac{\nabla\beta}{\beta}\sum_{n>x} H_{n,n+1}\right)\right),$$

we can clearly see that the perturbation is given by

$$A_x^H = \sum_{n>x} H_{n,n+1}, \tag{4.11}$$

with a driving force $F^H = \nabla\beta/\beta = -\nabla T/T$.

Before we derive the formulas to compute the kinetic coefficients in the linear response framework, it is useful to derive two relations between the time derivatives of the perturbations and the local current densities. From Chapter 2, we know that the local currents can be defined as

$$j_n^S = i[S_n^z, H_n], \qquad j_n^H = i[H_n, H_{n+1}].$$

We are now interested in relating these to the time derivatives of the local perturbations A_x^S and A_x^H. Let us start with the perturbation in the magnetic field. Using Heisenberg's

[1]Here we define $\Theta[n] = 0$ if $n < 0$, $\Theta[n] = 1/2$ if $n = 0$ and $\Theta[n] = 1$ if $n > 0$, with $n \in \mathbb{Z}$.

equation of motion for an operator, we have

$$\dot{A}_x^S = -i \sum_{n=x+1}^{N} [S_n^z, H] = -i \sum_{n=x+1}^{N} \left([S_n^z, H_n] + [S_n^z, H_{n-1}] \right).$$

Using the definitions of the currents, we get

$$\dot{A}_x^S = \sum_{n=x+1}^{N} \left(j_{n-1}^S - j_n^S \right).$$

Under OBC, ($j_N^S = 0$) we see that

$$\dot{A}_x^S = j_x^S. \tag{4.12}$$

Following the same procedure for the perturbation in the temperature, we arrive at

$$\dot{A}_x^H = j_x^H. \tag{4.13}$$

4.3.2 Kinetic Coefficients as Response Functions

In linear response theory, the kinetic coefficient L_{ij} is defined as the dynamical response of the local density current operator j_x^i at some site x to perturbation of the form F^j at some site y, with $i, j \in \{S, H\}$. In the Fourier space

$$j_x^i(\omega) = L_{ij}(\omega) F^j(\omega).$$

This way, the kinetic coefficient $L_{ij}(\omega)$ is the real part of the generalized susceptibility of the current operator j_x^i to the perturbation operator A_y^j. More generally, one can write the analytical continuation of $L_{ij}(\omega)$ to the upper part of the complex plane, $L_{ij}(z)$, with $\omega + i\epsilon = z$, $\mathrm{Im}\{z\} \geq 0$. The limit $(\omega)z \to 0$ is called the DC response regime, where we measure the response of the system due to a static field. So the kinetic coefficient L_{ij} in the DC regime is defined as

$$L_{ij} = \lim_{z \to 0} \mathrm{Re}\, i \int_0^\infty dt\ e^{izt} \left\langle [j_x^i(t), A_y^j] \right\rangle. \tag{4.14}$$

This is known as the Green-Kubo formula for the calculation of the kinetic coefficients. Here we are left with the freedom of taking $z \to 0$ by any path in the upper part of the complex plane.

By partial integration of Equation (4.14), and using the relations described in Equations (4.12) and (4.13), we arrive at

$$L_{ij}(z) = \mathrm{Re} \left\{ i \left(- \left\langle [A_x^i, A_y^j] \right\rangle - iz \int_0^\infty dt\ e^{izt} \left\langle [A_x^i(t), A_y^j] \right\rangle \right) \right\}.$$

Since A_x^i and A_y^j are always Hermitian operators, then we have $[A_x^i, A_y^j] = iO$, where O is also an Hermitian operator. With $i, j \in \{S, H\}$, we have four possible cases to evaluate the value of this commutator. We find that

$$\begin{aligned}
[A_x^S, A_y^S] &= 0, \\
[A_x^H, A_y^H] &= -ij^H_{\max(x,y)}, \\
[A_x^S, A_y^H] &= -ij^H_{y+1} \text{ if } x < y, \\
[A_x^S, A_y^H] &= ij^H_x \text{ if } x > y.
\end{aligned}$$

In any case, we are left with the expectation value of a local heat current. Since the total heat current J^H is conserved, then the flux of j_n^H at some site is 0 and $\left\langle j_n^H \right\rangle = 0$, for all n. Using the relation $\operatorname{Re} ab = \operatorname{Re} a \operatorname{Re} b - \operatorname{Im} a \operatorname{Im} b$, and restricting ourselves to $\operatorname{Re} z = 0$, we have

$$L_{ij}(z) = -\operatorname{Im} z \operatorname{Im} \left(\int_0^\infty dt \; e^{izt} \left\langle [A_x^i(t), A_y^j] \right\rangle \right). \tag{4.15}$$

According to its definition, the value of the kinetic coefficients might depend on the actual choice of x and y. However, in the limit $z \to 0$, it can be shown that the value of the coefficient is independent of this choice [22]. This way, Equation (4.15) allows us to compute the kinetic matrix entries by computing a real time correlation function of the perturbation operators A^i.

Chapter 5

Transport in the SSE formalism

In this Chapter, we focus on the computation of the kinetic coefficients and consequently the transport coefficients using the SSE MC method. We start by introducing a more MC friendly formula for L_{ij}, which is equivalent to Equation (4.15), at the Matsubara frequencies $\omega = \omega_M$, and discuss the known approaches to compute it with the SSE. Then, we present our new approach, where we use another MC sampling method to sample combinatorial factors from the series expansion. With this, we are able to derive a more efficient sampling scheme for L_{ij}.

5.1 Sampling $L_{ij}(\omega_M)$ with MC

Equation (4.15) allows for the calculations of the kinetic coefficients through an integral of a real time correlation function of the perturbation operators. Due to the ill-defined problem of the analytic continuation from imaginary time to real time, using this expression in a MC scheme would prove difficult. Instead, at the imaginary Matsubara frequencies $\omega_M = 2\pi M/\beta$, $M \in \mathbb{N}$, we can find an equivalent expression in imaginary time $\tau = -it$ ($\tau \in [0, \beta]$) [22]

$$L_{ij}(\omega_M) = \omega_M \operatorname{Re} \int_0^\beta d\tau \; e^{i\omega_M \tau} \left\langle A_x^i(\tau) A_y^j \right\rangle . \tag{5.1}$$

In Appendix A we show that Equations (4.15) and (5.1) are equivalent for $\omega = \omega_M$. As we are interested in the values of the transport coefficients as $\omega \to 0$, we are now left with the problem of extrapolating $L_{ij}(\omega)$ from the Matsubara frequencies ω_M to $\omega = 0$.

In the series expansion formalism, Equation (5.1) becomes

$$\begin{aligned} L_{ij}(\omega_M) = \frac{\omega_M}{Z} \sum_\alpha \sum_{n=0}^{\infty} \sum_{k=0}^{n} \operatorname{Re} \int_0^\beta d\tau \; e^{i\omega_M \tau} \frac{(\tau - \beta)^{n-k} (-\tau)^k}{(n-k)!k!} \times \\ \sum_{S_n} \langle \alpha | \prod_{i=k+1}^{n} H_{l_i} A_x^i \prod_{i=1}^{k} H_{l_i} A_y^j | \alpha \rangle . \end{aligned} \tag{5.2}$$

There are two main approaches to sample Equation (5.2) using the SSE method. One can simply sample $\left\langle A_x^i(\tau)A_y^j\right\rangle$ for an array of τ values, with $\tau \in [0,\beta]$, using Equation (3.5), as in [22]. Employing an integration method, like Simpson's method, on the sampled points the integral in Equation (5.1) can be calculated. To minimize truncation errors, we can sample the correlation function for a larger number of τ values. This approach is a $\mathcal{O}(n^2 * n_\tau)$ procedure, where n is the expansion order and n_τ is the number of τ values. As $n \approx N\beta$, performing this calculation for large systems at low temperatures, becomes very inefficient. Another approach is to solve the integral in Equation (5.2), such that we eliminate the τ dependence. We can either do this by approximating with a MC integration method or solve it analytically. The former introduces truncation errors and involves the computation of factorials. The latter, yields an expression [63]

$$\begin{aligned}\mathrm{Re}\int_0^\beta d\tau\; e^{i\omega_M\tau}(\tau-\beta)^{n-k}(-\tau)^k =& \beta^{n+1}\frac{\Gamma(k+1)\Gamma(n-k-1)}{\Gamma(n)}\times \\ & {}_2F_3\left(\frac{k+1}{2},\frac{k+2}{2};\frac{1}{2},\frac{n}{2},\frac{n+1}{2};-M^2\pi^2\right),\end{aligned}$$

where $\Gamma(n+1) = n!$ is the gamma function and ${}_2F_3$ is a hypergeometric function defined by

$${}_2F_3(a_1,a_2;b_1,b_2,b_3;z) = \sum_{n=0}^{\infty}\frac{(a_1)_n(a_2)_n}{(b_1)_n(b_2)_n(b_3)_n}\frac{z^n}{n!},$$

where $(a)_n$ denotes the rising factorial. This provides an exact expression for the computation of $L_{ij}(\omega_M)$, however it is still computationally expensive. Again, it scales as $\mathcal{O}(n^2)$, moreover for each iteration we have to compute ${}_2F_3$. So calculations for large systems at lower temperatures become inviable [63].

5.2 Imaginary Time Representation of SSE

Here we present the imaginary time representation of the SSE method. In this representation we substitute the combinatorial factors that come from the series expansion by products of integrals over imaginary times. This set of times is assigned to the Hamiltonian operators in the operator string. The series expansion of the partition function is given as

$$Z = \sum_\alpha\sum_{n=0}^{\infty}\frac{(-\beta)^n}{n!}\sum_{S_n}\langle\alpha|\prod_{i=1}^{n}H_{l_i}|\alpha\rangle\,.$$

Now, we assign an imaginary time $\tau_i \in (0,\beta)$ to each of the Hamiltonian operators H_{l_i} in the operator string S_n. Replacing the combinatorial weight $(-\beta)^n/n!$ as a product of imaginary time integrals, the partition function becomes

$$Z = \sum_\alpha\sum_{n=0}^{\infty}(-1)^n\int_0^\beta d\tau_n\ldots\int_0^{\tau_3}d\tau_2\int_0^{\tau_2}d\tau_1\sum_{S_n}\langle\alpha|\prod_{i=1}^{n}H_{l_i}|\alpha\rangle\,.$$

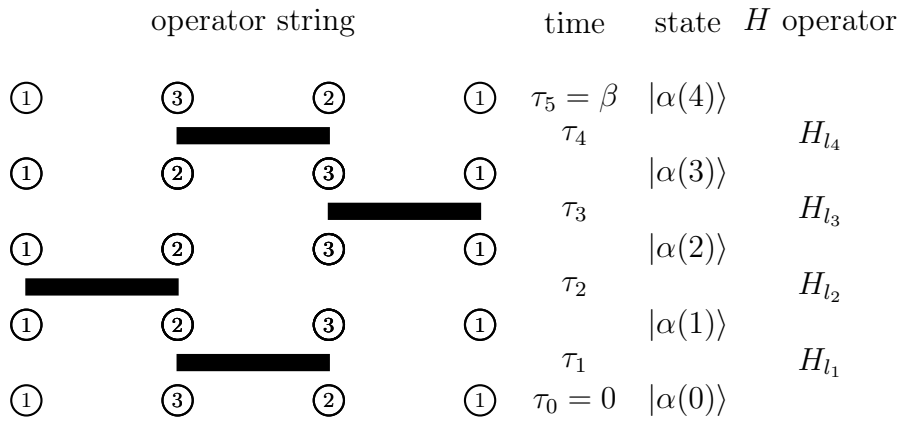

Figure 5.1: Operator sequence for a four-site system with $n = 4$. Each column of the figure represents one site and the states on each site are labelled by an integer. The operators are shown as black rectangles. On the right hand side of the graphical representation o the operator string, the assigned times to the Hamiltonian operators and the propagated states are labelled. The times $\tau_0 = 0$ and $\tau_{n+1} = \beta$ are assigned to the first and last states in the expansion, respectively.

The new configuration weight is defined as

$$W_\tau(\alpha, S_n, \{\tau\}) = (-1)^n \langle\alpha| \prod_{i=1}^{n} H_{l_i} |\alpha\rangle , \tag{5.3}$$

where $\{\tau\} = \{\tau_1, \ldots, \tau_n\}$ is the set of imaginary times assigned to each of the Hamiltonian operators in S_n. In Figure 5.1, we can see a graphical representation of one possible SSE configuration with weight W_τ. Here, $\tau_0 = 0$ and $\tau_{n+1} = \beta$ are the times of the first and last states in the propagation, $|\alpha(0)\rangle$ and $|\alpha(n)\rangle$ respectively. Moreover, it is important to note that the propagated state $|\alpha(k)\rangle$ only exists between the Hamiltonian operators H_{l_k} and $H_{l_{k+1}}$, respectively. Equivalently, it exists between the imaginary times τ_k and τ_{k+1}.

5.2.1 Expressions for Expectation Values

To derive expressions for operators in the configuration weight defined in Equation (5.3) we follow a similar procedure as in Section 3.2. Our objective is to find a function $A(\alpha, S_n, \{\tau\})$, such that

$$\langle A \rangle = \langle A(\alpha, S_n, \{\tau\}) \rangle_{W_\tau} = \frac{1}{Z} \sum_{\alpha} \sum_{n=0}^{\infty} \sum_{S_n} \int_0^\beta d\tau_n \ldots \int_0^{\tau_2} d\tau_1 A(\alpha, S_n, \{\tau\}) W_\tau(\alpha, S_n, \{\tau\}).$$

Then, A is sampled through randomly assigning imaginary times τ_i to each H_{l_i} in S_n and evaluating the expression for $A(\alpha, S_n, \{\tau\})$. In Chapter 3, we saw that, because S_n is cyclically permutable, we can average the propagated $A(\alpha(p), S_n(p))$ to get better

statistics. Equivalently, as $\tau \in [0, \beta]$, we can average the imaginary time evolution of the average value of A. So,

$$\langle A \rangle = \frac{1}{\beta} \int_0^\beta \langle A(\tau) \rangle \,. \tag{5.4}$$

Let us consider the case where A is a diagonal operator. In the series expansion and using Equation (5.4),

$$\langle A \rangle = \frac{1}{\beta} \left\langle \frac{n!}{\beta^n} \sum_{k=0}^{n} \int_0^\beta d\tau \frac{(\beta - \tau)^{n-k} \tau^k}{(n-k)!k!} A(k) \right\rangle_W , \tag{5.5}$$

where $A(k) = A\,|\alpha(k)\rangle$ is the value of the operator A after propagation step k. We now wish to rewrite the combinatorial factor as a product of imaginary time integrals. The combinatorial factor counts how many ways we can position $A(\tau)$ in the operator string given the expansion order n. This weight is then proportional to the times that the state $|\alpha(k)\rangle$ exists. So, τ is set to be some time between τ_k and τ_{k+1}. In integral form,

$$I = \int_0^\beta d\tau_n \ldots \int_0^{\tau_3} d\tau_2 \int_0^{\tau_2} d\tau_1 \left(\Theta(\tau - \tau_k) - \Theta(\tau - \tau_{k+1})\right),$$

where $\Theta(x)$ is the Heaviside step function. It is easy to prove this integral identity. We start by integrating until the τ_k integral,

$$I = \int_0^\beta \tau_n \ldots \int_0^{\tau_{k+1}} d\tau_k \frac{\tau_k^{k-1}}{(k-1)!} \left(\Theta(\tau - \tau_k) - \Theta(\tau - \tau_{k+1})\right).$$

Taking a closer look at the τ_k integral,

$$\int_0^{\tau_{k+1}} d\tau_k \frac{\tau_k^{k-1}}{(k-1)!} \left(\Theta(\tau - \tau_k) - \Theta(\tau - \tau_{k+1})\right)$$
$$= \underbrace{\int_0^{\tau_{k+1}} d\tau_k \frac{\tau_k^{k-1}}{(k-1)!} \Theta(\tau - \tau_k)}_{\tau \text{ can be either } > \text{ or } < \text{ than } \tau_{k+1}} - \Theta(\tau - \tau_{k+1}) \int_0^{\tau_{k+1}} d\tau_k \frac{\tau_k^{k-1}}{(k-1)!} = \Theta(\tau_{k+1} - \tau) \frac{\tau^k}{k!}.$$

Solving the rest of the integrals, we arrive at

$$I = \frac{(\beta - \tau)^{n-k} \tau^k}{(n-k)!k!}.$$

Inserting this identity in Equation (5.5) and integrating over τ,

$$\langle A \rangle = \frac{1}{\beta} \left\langle \sum_{k=0}^{n} (\tau_{k+1} - \tau_k) A(k) \right\rangle_{W_\tau} .$$

Now let us consider the case where $A = H_a$. Following the same procedure as in Chapter 3 and using Equation (5.4), we arrive at an expression

$$\langle H_a \rangle = -\frac{1}{\beta} \left\langle \frac{n!}{\beta^n} \sum_{k=0}^{n-1} \int_0^\beta d\tau \frac{(\beta - \tau)^{n-1-k} \tau^k}{(n-1-k)!k!} \delta_{l_{k+1},a} \right\rangle_W , \tag{5.6}$$

Since the Hamiltonian operators only exist at the time they are assigned to, we can replace the combinatorial factor by the following identity

$$I = \int_0^\beta d\tau_n \dots \int_0^{\tau_3} d\tau_2 \int_0^{\tau_2} d\tau_1 \delta(\tau - \tau_{k+1}).$$

To prove this, we start by integrating until the τ_{k+1} integral,

$$I = \int_0^\beta d\tau_n \dots \int_0^{\tau_{k+2}} d\tau_{k+1} \frac{\tau_{k+1}^k}{k!} \delta(\tau - \tau_{k+1}) = \frac{\tau^k}{k!} \int_0^\beta d\tau_n \dots \int_0^{\tau_{k+3}} d\tau_{k+2} \Theta(\tau_{k+2} - \tau') = \frac{(\beta - \tau)^{n-1-k} \tau^k}{(n-1-k)!k!}.$$

Here the Heaviside step function is introduce such that we assigned τ' to τ_{k+1}, and thus $\tau_{k+2} > \tau'$. Inserting this identity in Equation (5.6) and integrating over τ,

$$\langle H_a \rangle = -\frac{1}{\beta} \left\langle \sum_{k=1}^{n} \delta_{l_k,a} \right\rangle_{W_\tau}$$

Furthermore, one can derive expressions for imaginary time products of expectation values and their integrals can be derived. In this case, the integral identities would have to contain information about the imaginary times of the two operators. In the next section, we focus on deriving the formula for the kinetic coefficients using the framework developed here.

5.3 Expressions for $L_{ij}(\omega_M)$ in the Imaginary Time Representation of SSE

Using the formalism developed in the last section, we now derive the formulas to sample $L_{ij}(\omega_M)$ in the imaginary time representation of SSE. It is possible to write Equation (5.1) as

$$L_{ij}(\omega_M) = \omega_M \operatorname{Re} \sum_{a>x} \sum_{b>y} \int_0^\beta e^{i\omega_M \tau} \langle O_a(\tau) O_b \rangle ,$$

where O_a and O_b are spin operators S_a^z and/or Hamiltonian bond H_a operators. So, in general, we want to calculate an integral of the form

$$I = \int_0^\beta d\tau \; f(\tau) \langle O_a(\tau) O_b \rangle ,$$

with $f(\tau) = \operatorname{Re} e^{i\omega_M \tau}$. Using Equation (5.4), it is possible to write I as a sum of two parts,

$$I = \frac{1}{\beta} \int_0^\beta d\tau'' \int_0^\beta d\tau' \left(\langle O_a(\tau'') O_b(\tau') \rangle + \langle O_b(\tau'') O_a(\tau') \rangle \right) f(\tau'' - \tau') \Theta(\tau'' - \tau'). \quad (5.7)$$

Using this relation, now we may derive the formulas for L_{ij}, $i, j \in \{S, H\}$, using the formalism developed in the last section.

5.3.1 Expression for L_{SS}

For the spin kinetic coefficient L_{SS}, $O_a = S_a^z$ and $O_b = S_b^z$. Using Equation (5.7), in the SSE, I^{SS} can be sampled using

$$I^{SS} = \frac{1}{\beta}\left\langle \sum_{k=0}^{n}\sum_{l=0}^{n-k}\int_0^\beta d\tau''\int_0^\beta d\tau' C_{kl}(\tau'',\tau')\times \right. \\ \left. f(\tau''-\tau')\left[S_a^z(l+k)S_b^z(k)+S_b^z(l+k)S_a^z(k)\right]\right\rangle_W , \tag{5.8}$$

where

$$C_{kl}(\tau'',\tau') = \frac{(\beta-\tau'')^{n-k-l}(\tau''-\tau')^l\tau'^k}{(n-k-l)!k!l!}\Theta(\tau''-\tau')$$

is the combinatorial factors from the series expansion. Our objective now is to replace $C_{kl}(\tau'',\tau')$ with a product of n integrals over the imaginary times τ_i. As we have seen in the last section, diagonal operators are weighted by the time interval of which the state they act on exist. In this case, it mean that τ' is set to be between τ_k and τ_{k+1}, and τ'' is set to be between τ_{k+l} and τ_{k+l+1}. In integral form,

$$C_{kl}(\tau'',\tau') = \int_0^\beta d\tau_n \ldots \int_0^{\tau_2} d\tau_1(\Theta(\tau''-\tau_{k+l})-\Theta(\tau''-\tau_{k+l+1}))\times \\ (\Theta(\tau'-\tau_k)-\Theta(\tau'-\tau_{k+1}))\Theta(\tau''-\tau').$$

The proof can be found in Appendix B. Using this relation, the integrals in Equation (5.8), with $f(\tau) = \mathrm{Re}\, e^{i\omega_M\tau}$, follow

$$I_{k,l} = \mathrm{Re}\int_0^\beta d\tau''\int_0^\beta d\tau'(\Theta(\tau''-\tau_{k+l})-\Theta(\tau''-\tau_{k+l+1}))\times \\ (\Theta(\tau'-\tau_k)-\Theta(\tau'-\tau_{k+1}))\Theta(\tau''-\tau')e^{i\omega_M(\tau''-\tau')}.$$

There are now two cases we need to consider. First, the case where $l = 0$, in which we sample S_a^z and S_b^z at the same propagation step k, and the second case where $l \neq 0$. For $l = 0$,

$$I_{k,0} = \frac{1}{\omega_M^2}\left(1-\cos(\omega_M(\tau_{k+1}-\tau_k))\right).$$

For $l \neq 0$,

$$I_{k,l} = \mathrm{Re}\left(\frac{e^{i\omega_M\tau_{k+l+1}}-e^{i\omega_M\tau_{k+l}}}{i\omega_M}\frac{e^{-i\omega_M\tau_{k+1}}-e^{-i\omega_M\tau_k}}{-i\omega_M}\right).$$

Rewriting Equation (5.8),

$$I^{SS} = \frac{1}{\beta}\left\langle \sum_{k=0}^{n}\sum_{l=1}^{n-k}\left[\mathrm{Re}\left(\frac{e^{i\omega_M\tau_{k+l+1}}-e^{i\omega_M\tau_{k+l}}}{i\omega_M}\frac{e^{-i\omega_M\tau_{k+1}}-e^{-i\omega_M\tau_k}}{-i\omega_M}\right)\times \right.\right. \\ \left.\left.(S_a^z(l+k)S_b^z(k)+S_b^z(l+k)S_a^z(k))\right] + 2\sum_{k=0}^{n}\frac{1}{\omega_M^2}\left(1-\cos(\omega_M(\tau_{k+1}-\tau_k))\right)S_a^z(k)S_b^z(k)\right\rangle_{W_\tau}. \tag{5.9}$$

This equation allows us to sample $L_{SS}(\omega_M)$ using the weights W_τ. For this expression we only have to compute trigonometric functions which, from a computational standpoint, are inexpensive. However, this relation still scales as $\mathcal{O}(n^2)$, hindering the performance of computations at low temperatures. Let us define

$$K_a = \sum_{k=0}^{n} \frac{e^{i\omega_M \tau_{k+1}} - e^{i\omega_M \tau_k}}{i\omega_M} S_a^z(k). \tag{5.10}$$

Now we show that $\operatorname{Re} K_a K_b^*$ is an equivalent way of writing the summations in Equation (5.9).

$$\begin{aligned}
K_a K_b^* &= \sum_{k'=0}^{n}\sum_{k''=0}^{n} \underbrace{\frac{e^{i\omega_M \tau_{k'+1}} - e^{i\omega_M \tau_{k'}}}{i\omega_M} \frac{e^{-i\omega_M \tau_{k''+1}} - e^{-i\omega_M \tau_{k''}}}{-i\omega_M} S_a^z(k') S_b^z(k'')}_{=g_{ab}(k',k'')} \\
&= \underbrace{\sum_{k'=0}^{n}\sum_{k''=k'+1}^{n}}_{\text{let } k'=k \text{ and } k''=l} g_{ab}(k',k'') + \underbrace{\sum_{k''=0}^{n}\sum_{k'=k''+1}^{n}}_{\text{let } k'=l \text{ and } k''=k} g_{ab}(k',k'') + \sum_{k'=0}^{n}\sum_{k''=0}^{n} \delta_{k',k''} g_{ab}(k',k'') \\
&= \sum_{k=0}^{n}\sum_{l=1}^{n-k} \left(\frac{e^{i\omega_M \tau_{k+l+1}} - e^{i\omega_M \tau_{k+l}}}{i\omega_M} \frac{e^{-i\omega_M \tau_{k+1}} - e^{-i\omega_M \tau_k}}{-i\omega_M} \right) \left(S_a^z(l+k) S_b^z(k) + S_b^z(l+k) S_a^z(k)\right) \\
&\qquad + \sum_{k=0}^{n} \frac{2}{\omega_M^2} \left(1 - \cos(\omega_M(\tau_{k+1} - \tau_k))\right) S_a^z(k) S_b^z(k)
\end{aligned}$$

So, the expression for $L_{SS}(\omega_M)$ in the imaginary time representation of the SSE is given as

$$L_{SS}(\omega_M) = \frac{\omega_M}{\beta} \sum_{a>x} \sum_{b>y} \langle \operatorname{Re} K_a K_b^* \rangle_{W_\tau}, \tag{5.11}$$

with K_a defined in Equation (5.10). Therefore, by expressing the kinetic coefficient as the SSE average of $\operatorname{Re} K_a K_b^*$, the computational complexity of the algorithm is improved from $\mathcal{O}(n^2)$ to $\mathcal{O}(n)$. This enables faster sampling times large systems at low temperatures.

5.3.2 Expression for L_{HH}

Here we follow a similar procedure as for the spin kinetic coefficient L_{SS}. The heat kinetic coefficient L_{HH} involves the integral $I_{ab}^{HH} = \int_0^\beta d\tau f(\tau) \langle H_a(\tau) H_b \rangle$. In the SSE, this integral can be sampled by

$$\begin{aligned}
I^{HH} = \frac{1}{\beta} \Bigg\langle \sum_{k=0}^{n-2} \sum_{l=0}^{n-2-k} \int_0^\beta d\tau'' \int_0^\beta d\tau' C'_{kl}(\tau'', \tau') \times \\
f(\tau'' - \tau') \left[\delta_{l_{k+l+2},a} \delta_{l_{k+1},b} + \delta_{l_{k+1},a} \delta_{l_{k+l+2},b}\right] \Bigg\rangle_W,
\end{aligned} \tag{5.12}$$

with

$$C'_{kl}(\tau'', \tau') = \frac{(\beta - \tau'')^{n-2-k-l}(\tau'' - \tau')^l \tau'^k}{(n-2-k-l)!k!l!}\Theta(\tau'' - \tau'). \tag{5.13}$$

Using a similar approach as in Section 5.2, we can replace this combinatorial weight by setting τ' to τ_{k+1} and τ'' to τ_{k+l+2}, such that

$$C'_{kl}(\tau'', \tau') = \int_0^\beta d\tau_n \ldots \int_0^{\tau_2} d\tau_1 \delta(\tau'' - \tau_{k+l+2})\delta(\tau' - \tau_{k+1})\Theta(\tau'' - \tau').$$

The proof can again be found in Appendix B. Using this relation and $f(\tau) = \mathrm{Re}\, e^{i\omega_M \tau}$, the integrals in Equation (5.12), follow

$$\mathrm{Re}\int_0^\beta d\tau'' \int_0^\beta d\tau' \delta(\tau'' - \tau_{k+l+2})\delta(\tau' - \tau_{k+1})\Theta(\tau'' - \tau')e^{i\omega_M(\tau'' - \tau')} = \mathrm{Re}\, e^{i\omega_M(\tau_{k+l+2} - \tau_{k+1})}.$$

Defining $p = k + 1$ and $q = k + l + 2$ and inserting this result in Equation (5.12),

$$I_{SS} = \frac{1}{\beta}\left\langle \sum_{p=1}^{n-1}\sum_{q=1+p}^{n} \mathrm{Re}\, e^{i\omega_M(\tau_q - \tau_p)}\left[\delta_{l_q,a}\delta_{l_p,b} + \delta_{l_p,a}\delta_{l_q,b}\right]\right\rangle_{W_\tau}, \tag{5.14}$$

In the same manner as for L_{SS}, let us define

$$G_a = \sum_{p=1}^{n} e^{i\omega_M \tau_p}\delta_{l_p,a}. \tag{5.15}$$

Now we show that the summations in Equation (5.14) can be written as in terms of $\mathrm{Re}\, G_a G_b^*$.

$$G_a G_b^* = \sum_{p'=1}^{n}\sum_{p''=1}^{n} \underbrace{e^{i\omega_M(\tau_{p'} - \tau_{p''})}\delta_{l_{p'},a}\delta_{l_{p''},b}}_{=g'_{a,b}(p',p'')}$$

$$= \underbrace{\sum_{p'=1}^{n-1}\sum_{p''=p'+1}^{n}}_{\text{let } p'=p \text{ and } p''=q} g'_{a,b}(p', p'') + \underbrace{\sum_{p''=1}^{n-1}\sum_{p'=p''+1}^{n}}_{\text{let } p'=p \text{ and } p''=q} g'_{a,b}(p', p'') + \sum_{p'=1}^{n}\sum_{p''=1}^{n}\delta_{p',p''}g'_{a,b}(p', p'')$$

$$= \sum_{p=1}^{n-1}\sum_{q=1+p}^{n} e^{i\omega_M(\tau_q - \tau_p)}\left[\delta_{l_q,a}\delta_{l_p,b} + \delta_{l_p,a}\delta_{l_q,b}\right] + \sum_{p=1}^{n}\delta_{l_p,a}\delta_{l_p,b}$$

This way, the kinetic coefficient $L_{HH}(\omega_M)$ can be sampled in the imaginary time representation of the SSE by the expression

$$L_{HH}(\omega_M) = \frac{\omega_M}{\beta}\sum_{a>x}\sum_{b>y}\langle \mathrm{Re}\, G_a G_b^* - C_{ab}\rangle_{W_\tau} \qquad \text{and } n \geq 2, \tag{5.16}$$

where $C_{ab} = \sum_{p=1}^{n}\delta_{l_p,a}\delta_{l_p,b}$. Note again that this is an $\mathcal{O}(n)$ procedure.

5.3.3 Expressions for L_{SH} and L_{HS}

Similar expressions for $L_{SH}(\omega_M)$ and $L_{HS}(\omega_M)$ can be derived using the same procedures. Here we will not go through their full derivation, instead we go over the steps that differ from the derivations of L_{SS} and L_{HH}. Since now we do not have a correlation function of spin-spin or Hamiltonian-Hamiltonian operators, the imaginary times τ' and τ'' will either correspond to a spin operator or to a Hamiltonian operator. So the integral identity will involve a delta function and a Heaviside step function. The combinatorial factor in this case reads

$$C'''_{kl}(\tau', \tau'') = \frac{(\beta - \tau'')^{n-1-k-l}(\tau'' - \tau')^l \tau'^k}{(n-1-k-l)!k!l!}\Theta(\tau'' - \tau'). \tag{5.17}$$

Depending on whether τ' is assigned to the spin or the Hamiltonian operator, this combinatorial factor can be substituted by

$$\int_0^\beta d\tau_n \dots \int_0^{\tau_3} d\tau_2 \int_0^{\tau_2} d\tau_1 (\Theta(\tau'' - \tau_{k+l+1}) - \Theta(\tau'' - \tau_{k+l+2}))\delta(\tau' - \tau_{k+1})\Theta(\tau'' - \tau'),$$

or

$$\int_0^\beta d\tau_n \dots \int_0^{\tau_3} d\tau_2 \int_0^{\tau_2} d\tau_1 \delta(\tau'' - \tau_{k+l+1})(\Theta(\tau' - \tau_k) - \Theta(\tau' - \tau_{k+1}))\Theta(\tau'' - \tau').$$

In Appendix B, we show that both of these expressions are equivalent to Equation (5.17). Following the same procedure as for L_{SS} and L_{HH}, in the imaginary time representation of the SSE $L_{SH}(\omega_M)$ and $L_{HS}(\omega_M)$ can be sampled by

$$L_{SH}(\omega_M) = -\frac{\omega_M}{\beta} \sum_{a>x} \sum_{b>y} \langle \mathrm{Re}\, K_a G_b^* \rangle_{W_\tau}, \tag{5.18}$$

$$L_{HS}(\omega_M) = -\frac{\omega_M}{\beta} \sum_{a>x} \sum_{b>y} \langle \mathrm{Re}\, G_a K_b^* \rangle_{W_\tau},$$

where K_a and G_a are defined in Equations (5.10) and (5.15), respectively. Note that $n \geq 1$.

5.4 Code Verification

Having derived all of the equations to sample the kinetic coefficients using the imaginary time representation of SSE, we now validate our implementation of such equations and sampling procedure. For this, we compare the results from SSE simulations to ED results for three different systems, XY, Heisenberg and XY with $h = 0.5$, with $L = 6$ and OBC. In Figure 5.2, we see the kinetic coefficients L_{SS}, L_{HH} and L_{SH} for the first 30 Matsubara frequencies and two pairs of x and y values. These results are at inverse

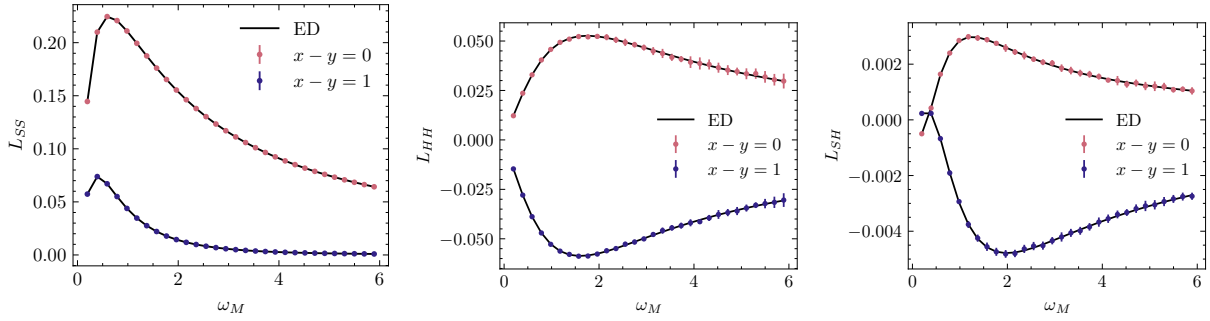

(a) **(b)** **(c)**

Figure 5.2: **(a)** Spin kinetic coefficient L_{SS} as a function of the Matsubara frequencies ω_M, for the XY chain. **(b)** Heat kinetic coefficient L_{HH} as a function of the Matsubara frequencies ω_M, for the Heisenberg model. **(c)** Off-diagonal coefficient L_{SH} as a function of the Matsubara frequencies ω_M, for the XY chain in a magnetic field $h = 0.5$. We present calculations for a system of $L = 6$ spin-1/2 particles, with OBC, at inverse temperature $\beta = 32$ and for two different values of x with $y = 2$. ED calculations are presented in the black lines. SSE calculations were performed with 20 bins and 10^7 MCS. Statistical errors may be smaller than the size of the symbols.

temperature $\beta = 32$. In general the SSE calculations agree with results from ED. One can notice that the standard deviations (given by the error bars) of L_{HH} and L_{SH}, Figures 5.2b and 5.2c, respectively, increase for larger Matsubara frequencies. However, the ED results are well within the confidence interval (approximately two standard deviation) of the SSE calculations, thus it is possible to conclude that the sampling method and implementation are working as intended.

As it is important to test the implementation for larger systems as well, here we present some results for chains with $L = 256$. We again consider the same systems, XY, Heisenberg and XY with $h = 1$. Figure 5.3 shows the calculated kinetic coefficients as a function of the Matsubara frequencies for two pairs of x and y. Calculations for L_{SS} remain still very accurate. Moreover, unfortunately, calculations for L_{HH} and L_{SH} have large standard deviations.

The standard error estimated through the binning procedure, Equation (3.13), can be written as [59]

$$\sigma_O = \frac{\sigma}{\sqrt{M}},$$

where σ is the standard deviation of the estimator for quantity O and M is the number of MCS in each bin. One possible reason for the large error bars in Figures 5.3b and 5.3c might be that of the estimators of L_{HH} and L_{SH}, have an inherently high standard deviation σ. This allied to the fact that their values are close to zero, will result in a high uncertainty. To mitigate this we could run calculations with a larger number of MCS. However, to reduce the error by a factor of 10, we would need to 100 times more MCS,

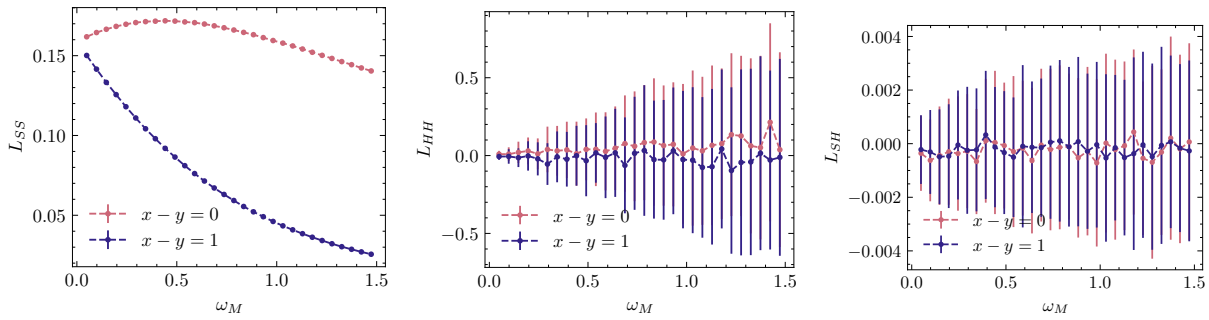

(a) **(b)** **(c)**

Figure 5.3: **(a)** Spin kinetic coefficient L_{SS} as a function of the Matsubara frequencies ω_M, for the XY chain. **(b)** Heat kinetic coefficient L_{HH} as a function of the Matsubara frequencies ω_M, for the Heisenberg model. **(c)** Off-diagonal coefficient L_{SH} as a function of the Matsubara frequencies ω_M, for the XY chain in a magnetic field $h = 1$. We present calculations for a system of $L = 256$ spin-1/2 particles, with OBC, at inverse temperature $\beta = 128$ and for two different values of x with $y = 127$. SSE calculations were performed with 100 bins and 10^5 MCS. Statistical errors are sometimes smaller than the size of the symbols.

which will increase the computation time hundredfold. As each of the calculations in Figure 5.3 took approximately 3h per bin on an AMD chip with 128 cores, we would need about 12 days of computation time per bin to reduce the error by a factor of 10. As this becomes very impractical to do for larger systems and especially for larger spin values, we will mostly focus on the behaviour of the spin kinetic coefficient (and thus the spin conductivity) for the rest of this work.

Chapter 6

Results and Discussion

In this Chapter, we present results for the transport coefficients, mainly the spin conductivity, calculated using the SSE method with imaginary time sampling, using Equation (5.1). The results are also discussed. We start by providing an overview of the practical aspects of extrapolating the kinetic coefficients to $\omega = 0$, such as finite size effects, dependence on the sites of measurement x and perturbation y, temperature dependence and the extrapolation procedure itself.

Afterwards, we present results for the XXZ chain. We start by introducing the Jordan Wigner transformation for the spin-1/2 XY chain through which we are able to obtain exact results for the spin conductivity and spin-Seebeck coefficient. We compare our MC calculations to the exact results and discuss results for larger spin values. Then, we introduce the Bosonization of the spin-1/2 XXZ chain and compare its results for the spin conductivity to our MC results. Calculations for larger spin values are also presented and discussed. Then we present results for spin-1 and spin-3/2 XXZ chains as a function of the easy-axis anisotropy. We end our discussion with an estimation of the spin conductivity in the large S limit.

6.1 Initial Considerations

Equation (5.2) allows us to calculate the kinetic coefficients through MC at Matsubara frequencies $\omega_M = 2\pi M/\beta$. With the calculated values of $L_{ij}(\omega_M)$ we want to perform an extrapolation to the DC regime, that is to $\omega = 0$. There are however, some pitfalls one can encounter when performing these extrapolations to the DC regime. As the spacing between the Matsubara frequencies scales linearly with temperature T, it becomes difficult to get reliable extrapolations to the zero frequency regime at higher temperatures, as due to the low density of Matsubara frequencies. So, this limits us to the low temperature regime. In this regime, finite size effects are more pronounced, as the energy of thermal excitations can become smaller than the minimal required energy for an excitation. It is

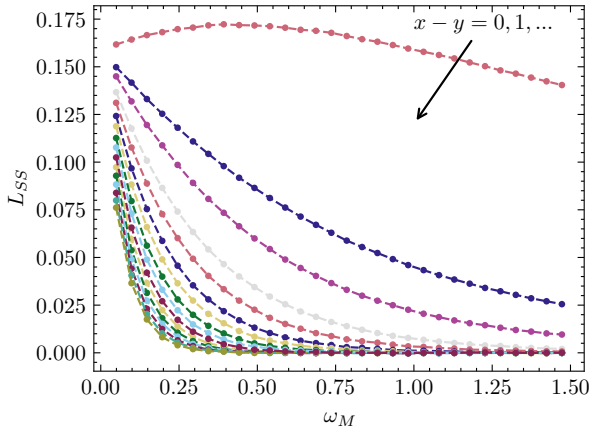

Figure 6.1: Spin kinetic coefficient L_{SS} as a function of the Matsubara frequencies and of spatial separation between the site of perturbation y and of measurement of the current x. The presented results are for the XY chain with $L = 256$ at inverse temperature $\beta = 128$. SSE calculations were performed with 20 bins and 10^5 MCS. Statistical errors are smaller than the size of the symbols.

thus crucial that we study a large enough system such that size effects are mitigated, for the given temperature and model parameters.

We will now discuss the finite size effects of the spin kinetic coefficient and its dependence on the sites of perturbation y and measurement of the current x. Afterwards, we will go through the procedure for performing a reliable extrapolation to $\omega = 0$ and evaluating its error from imperfect (with a standard deviation) MC data.

6.1.1 Dependence on $x - y$

The kinetic coefficient is defined as the linear response of the current operator at site x due to a perturbation at site y. As so, we are interested in measuring the current operator at sites $x \geq y$. Figure 6.1 shows the dependence of the spin kinetic coefficient L_{SS} on the difference between the perturbation and measurement sites $x - y$. Here, the perturbation site y to lies in the bond at the middle of the chain, $y = L/2 - 1$. We can see that the value of L_{SS} decreases exponentially for small small frequencies when the spatial separation between the perturbation and current measurement is increased. As so, we focus on measurements of the kinetic coefficients for $x - y \leq 1$ with $y = L/2 - 1$, for the rest of our discussion.

6.1.2 Finite Size Effects

Figure 6.2a shows the spin kinetic coefficient L_{SS}, for the first 30 Matsubara frequencies, as a function of the system size L, for the XY chain at $\beta = 128$. We see that the convergence with the system size L is fast. Moreover, for lower frequencies and small

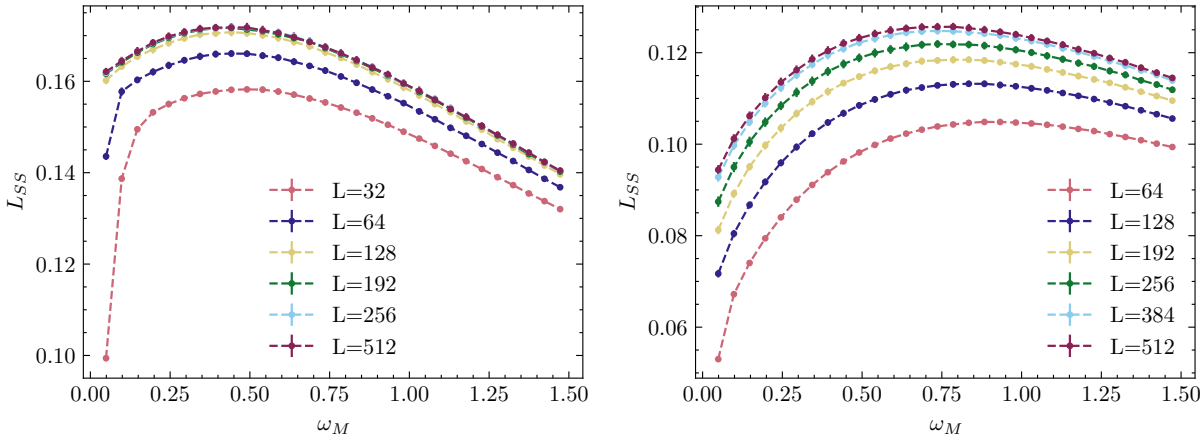

Figure 6.2: Spin kinetic coefficient L_{SS} as a function of the Matsubara frequencies ω_M and the system size L, for the **(a)** XY chain and the **(b)** isotropic Heisenberg chain at inverse temperature $\beta = 128$, with $x = y$. SSE calculations were performed with 100 bins and 10^5 MCS. Statistical errors are smaller than the size of the symbols.

system sizes L_{SS} approaches zero, as seen for the $L = 32,\ 64$ curves, for example. These curves start to approach zero for frequencies close to the finite energy gap between energy levels of the system, i.e. $\omega \approx \Delta E$ [23]. For the case of the XY chain, $\omega \approx -2\pi J/L$. From this relation, it is possible to set lower limit $L > J\beta$ on the system size needed to calculate L_{SS} at the first Matsubara frequency without any finite size effects. For the system presented in Figure 6.2a, we would need a chain with $L > 128$. So a system of $L = 192$, would be sufficient to reproduce the infinite size limit behaviour of the spin kinetic coefficient. As the gap in the finite size energy spectrum has proven to be proportional to the anisotropy parameter Δ [64], we investigate the finite size effects of the spin kinetic coefficient for the isotropic Heisenberg chain ($\Delta = 1$), as shown in Figure 6.2b. In this case, the convergence with L is slower. So, the system size we would need in order to perform calculations in the thermodynamic limit is larger than in the XY case. From Figure 6.2b it is possible to see that $L \gtrsim 512$.

As so it is possible to conclude that, in order to estimate the transport coefficients in the thermodynamic limit for a wide range of model parameters, we would need calculations of the kinetic coefficients for systems with $L \geq 512$. So, for the rest of this section, we compute the kinetic coefficients for systems with $L = 512$ at inverse temperatures $\beta = 64, 128$. From this we can gauge some possible (low) temperature dependence of the transport coefficients in the thermodynamic limit.

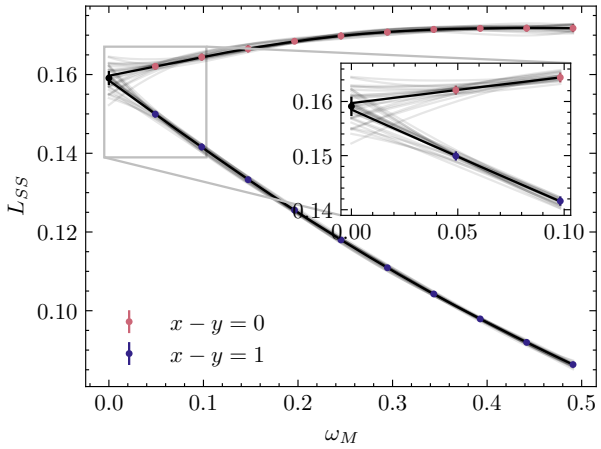

Figure 6.3: Extrapolation of the spin kinetic coefficient L_{SS} to $\omega = 0$, from the first 10 Matsubara frequencies and two set of values for x and y. The dots are the results from the MC calculation and the black lines are a 4^{th} order polynomial fit to the MC data. Inset shows the behaviour of the fitted lines from the bootstrap procedure near the extrapolation point $\omega_M = 0$. The presented results are for the XY chain with $L = 512$ at inverse temperature $\beta = 128$. SSE calculations were performed with 100 bins and 10^5 MCS. Statistical errors may be smaller than the size of the symbols.

6.1.3 Extrapolations to $\omega = 0$

Assuming that we have selected a combination of system size and temperature such that it finite size effects are minimized, performing the extrapolation to $\omega = 0$ becomes a simple task. The procedure we employ here is based on fitting a polynomial of degree p to the calculated values of $L_{ij}(\omega_M)$, for $x - y \leq 1$, and calculate the $\omega = 0$ point of the two fitted polynomials. As the MC data has error bars, i.e. a standard deviation, we must take it into account when performing these extrapolations. For this, we bootstrap the extrapolation procedure. For this, each bootstrap cycle we draw a new set of points for $L_{ij}(\omega_M)$ from a normal distribution using their MC mean and variance. This is shown in Figure 6.3. Here we see the polynomial fit of degree 4 to the first 10 Matsubara frequencies for L_{SS}. For illustrative purposes, we show 20 bootstrap cycles depicted in the grey lines.

As we can see in the inset of Figure 6.3, there seem to be some lines in the bootstrap which exhibit some oscillatory behaviour near the extrapolation point $\omega = 0$. This is known as Runge's phenomenon and happens we interpolating a set of equispaced points using a polynomial [65]. To minimize the impact of this effect in our estimation, instead of taking the mean of bootstrapped extrapolations, we take their median [23]. Another way of mitigating this effect is to fit the polynomial only to the first few Matsubara frequencies. As so, the rest of the presented results are obtained through a polynomial of degree 4 to the first 10 Matsubara frequencies.

6.2 Spin-1/2 XY Chain

It is important to consider the spin-1/2 XY chain in detail as it can be solved exactly through the JW transformation [38, 39]. The JW transformation maps the XXZ Hamiltonian to a Hamiltonian describing a systems of spinless fermions on a lattice. For this, we write the spin operators as

$$S_i^+ = c_i^\dagger e^{i\pi \sum_{n=1}^{i-1} c_n^\dagger c_n}, \qquad S_i^z = n_i - \frac{1}{2}.$$

Here $c_i^\dagger(c_i)$ creates(destroys) a fermion at site i and $n_i = c_i^\dagger c_i$ counts the number of fermions at site i. These obey the canonical commutation relations $\{c_i, c_i^\dagger\} = 1$ and $\{c_i, c_i\} = 0$. Due to the Pauli exclusion principle, each site can either be unoccupied or have one fermion. When a fermion is present at site i, $n_i = 1$, in the spin formalism it corresponds to having $S_i^z = 1/2$, and vice-versa. In the JW formalism, the XXZ Hamiltonian, Equation (2.1), reads

$$H = J\sum_{i=1}^{N}\left[\frac{1}{2}\left(c_i^\dagger c_{i+1} + c_i c_{i+1}^\dagger\right) + \Delta\left(c_i^\dagger c_i - \frac{1}{2}\right)\left(c_{i+1}^\dagger c_{i+1} - \frac{1}{2}\right)\right] - h\sum_{i=1}^{N}\left(c_i^\dagger c_i - \frac{1}{2}\right). \tag{6.1}$$

Here the magnetic field h is interpreted as the chemical potential μ. When $\Delta = 0$ (XY model), the fermionic chain becomes non-interacting and thus it is possible to solve it analytically. For PBC and letting $N \to \infty$, the full energy spectrum for $\Delta = 0$, in the Fourier space, is given by the dispersion relation

$$E(k) = J\cos(k) - h.$$

At zero temperature, the chemical potential is called the Fermi energy E_F, and all of the states with $E(k) \leq E_F$ are occupied. For strong fields, $h > J$, all of the fermion levels are occupied. For the case of $h < -J$, all of the fermionic levels are vacant. Note that $h = \pm J$ corresponds to the saturation field h_{c_1} defined in Chapter 2. In the JW formalism, the spin transport is interpreted as a transport of spinless charged particles due to a gradient in the electro-chemical potential $\nabla\mu$. If the fermion states are fully empty or fully occupied, we can expect this transport to be zero. The spin conductivity of the XY chain can then be exactly evaluated at any temperature and frequency. Following [22], the DC spin conductivity of the spin-1/2 XY model at inverse temperature β can be written as

$$\sigma_{\mathrm{JW}} = \frac{1}{4\pi}(\tanh(E(0)\beta/2) - \tanh(E(\pi)\beta/2)). \tag{6.2}$$

At zero temperature, the spin conductivity is $\sigma_{\mathrm{JW}} = \Theta(J-h)/(2\pi)$. As is expected, it vanishes for $h > J$, i.e. fully occupied fermion states. The spin-Seebeck coefficient can also be computed in the thermodynamic limit using the JW transformation. Following

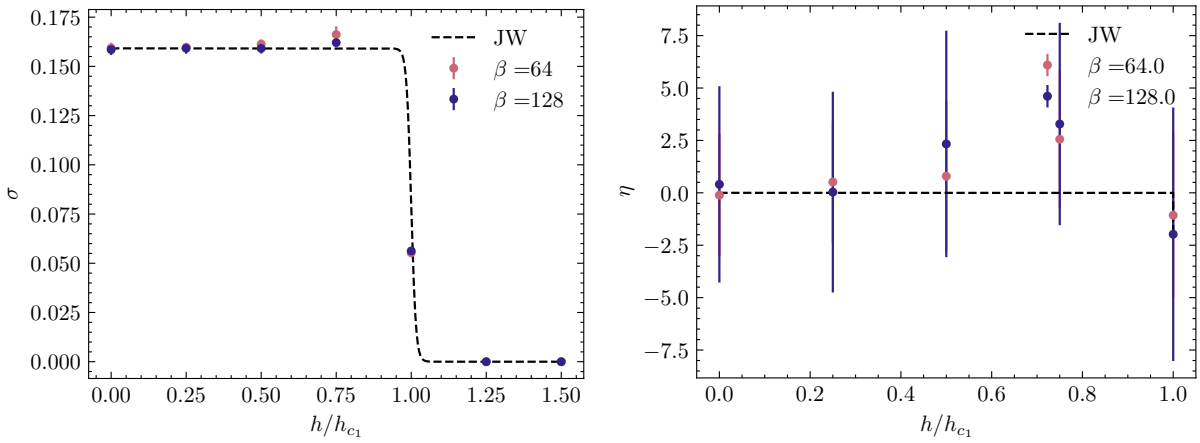

(a) **(b)**

Figure 6.4: Spin conductivity **(a)** and spin-Seebeck coefficient **(b)** as a function of the applied magnetic field, for the spin-1/2 XY chain with $L = 512$. The black dashed line is the solution in the thermodynamic limit, at inverse temperature $\beta = 128$, given by the JW transformation for both the spin conductivity and spin-Seebeck coefficient. The MC calculations were done with 10^5 MCS and 25 bins. Statistical errors are sometimes smaller than the size of the symbols.

[30], in the low temperature limit

$$\eta_{\mathrm{JW}} = \begin{cases} -\frac{\pi^2 h}{6(J^2-h^2)\beta} + \mathcal{O}(\beta^{-3}) \text{ for } h < h_{c_1} \\ -\frac{g(3)}{g(1)} + \mathcal{O}(\beta^{-1}) \text{ for } h = h_{c_1} \\ 2(J-h)\beta + \mathcal{O}(1) \text{ for } h > h_{c_1} \end{cases},$$

where $g(n) = (1 - 2^{1-n/2})\Gamma(1 + n/2)\zeta(n/2)$[1]. For $h = h_{c_1}$, the spin-Seebeck coefficient is $\eta_{\mathrm{JW}} \approx -1.897376$. The zero temperature limit of spin-Seebeck coefficient is $\eta_{\mathrm{JW}} = 0$ for $h < h_{c_1}$ and $\eta_{\mathrm{JW}} = -\infty$ for $h > h_{c_1}$.

The spin conductivity is related to the transport of magnetic excitations along the chain in the presence of an applied magnetic field gradient. In the low temperature regime, we can expect the conductivity for gapped phases to vanish, if the thermal energy is less than the energy of the gap. On the other hand, for gapless phases, as excitations do not have a minimum amount of required energy, we expect it to be finite.

In Figure 6.4a, we can see the magnetic field dependence of the spin conductivity for the spin-1/2 XY chain. SSE data and exact JW results are both presented. We see that for $h > h_{c_1}$, the spin conductivity is zero as predicted by Equation (6.2). One can also see that at $h/h_{c_1} = 0.75$, the MC calculated values deviate from the exact value. The same

[1]Note that $\Gamma(x)$ is the Gamma function and $\zeta(x)$ is the Riemann zeta function.

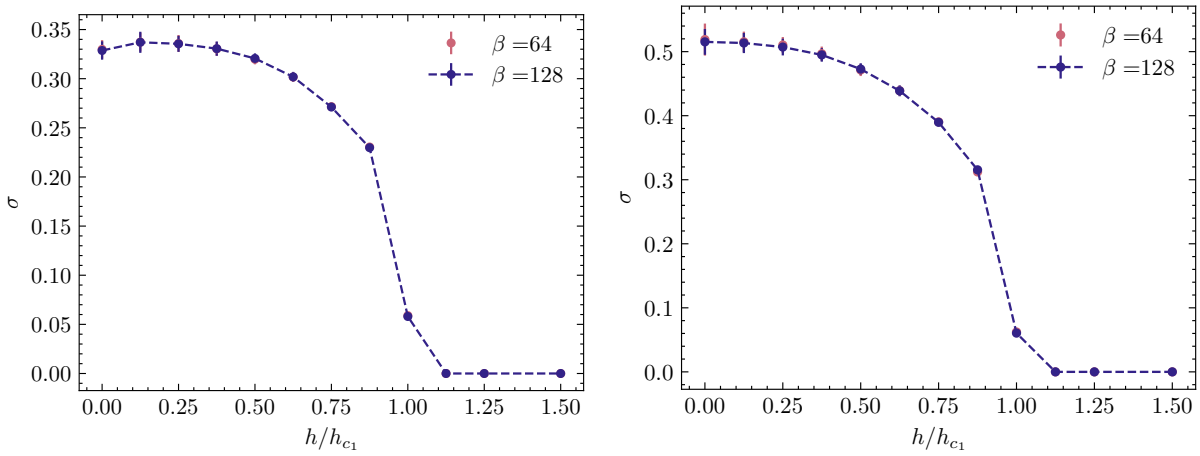

(a) **(b)**

Figure 6.5: Spin conductivity as a function of the applied magnetic field, for the **(a)** spin-1 and the **(b)** spin-3/2 XY chains with $L = 512$. The MC calculations were done with 10^5 MCS and 25 bins. Statistical errors are sometimes smaller than the size of the symbols.

can be seen, although not as pronounced, for the point $h/h_{c_1} = 0.5$. It is possible that this is caused by an effect of the extrapolation procedure to $\omega = 0$.

Figure 6.4b shows the spin-Seebeck coefficient for the spin-1/2 XY chain at different magnetic fields. Due to the bad scaling of the standard deviation of L_{SH} with the number of MCS, the error bars in the calculation of η are large. The low temperature results from the JW chain are within the confidence interval of the MC results. Furthermore, looking at the point $h = h_{c_1}$, the MC calculated spin-Seebeck coefficient is $\eta \approx -2 \pm 6$. From JW, $\eta_{\text{JW}} \approx -1.897376$. Although the values are close, the uncertainty in the MC value is too high to give any precise conclusions. Despite of this, it can be concluded that our approach of sampling the transport coefficients through SSE works well for the spin conductivity.

6.2.1 Spin-S XY Chains

Now we turn to the behaviour of the spin conductivity of spin-S XY chains with an applied magnetic field. For general spin-S, the saturation field h_{c_1} will also depend on the value of the spin number $h_{c_1}(S, \Delta) = 2JS(1 + \Delta)$. As in the spin-1/2 case, the ground state for the case of strong fields $h > h_{c_1}$ is also gapped. Therefore, at low temperatures, we expect that the spin conductivity will vanish there.

Figures 6.5a and 6.5b show the spin conductivity as a function of the applied magnetic field, for the spin-1 and spin-3/2 XY chains, respectively. We can observe that, for both spin values and in the case of strong fields $h > h_{c_1}$, the spin conductivity goes to zero as expected. In addition, the magnitude of the conductivity increases with the spin number.

This is due to a larger number of magnetic excitations being available to the system. For example, for a spin-1 system, there are 3 possible one particle excitations, with one of them even carrying $S = 2$ (from $|-1\rangle$ to $|+1\rangle$). Generally, the spin conductivity of spin-1 and spin-3/2 XY chains has a similar behaviour to the spin conductivity for the spin-1/2 XY chain. But unlike the spin-1/2 case, the way the conductivity vanishes at $h \to h_{c_1}$ for the spin-1 and spin-3/2 cases is different, as evidenced by the shape of the $\sigma(h)$ curves. This is possibly due to different scattering mechanisms, originating from the larger number of degrees of freedom.

Moreover, in spin-1 chains at the point $\Delta = 0, h = 0$ there is a quantum phase transition between the XY and Haldane phases. At this point, there are increased correlations in the system and so this might cause the spin conductivity to be lower than for small finite fields, as seen in Figure 6.5a.

6.3 Spin-1/2 XXZ chain

At low temperatures, the general behaviour of interacting 1D fermionic systems can be captured by the Luttinger liquid model [66]. This model assumes a linearized energy spectrum at the Fermi surface, i.e. at $k = \pm k_F$, which allows for well defined excitations near the Fermi surface. These excitations can be quantized and are of bosonic nature, allowing us to rewrite the Hamiltonian using bosonic field operators. In this representation, interactions, which usually are a product of four fermion operators, become quadratic and thus easy to diagonalize. It is possible to apply this technique to the spin-1/2 XXZ chain in order to derive a formula for the spin conductivity in the low temperature regime.

Following [66], the Luttinger liquid Hamiltonian in the bosonic language reads

$$H = \frac{1}{2\pi} \int dx \ \left(vK(\pi\Pi(x))^2 + \frac{v}{K}(\nabla\phi(x))^2 \right),$$

where $\phi(x)$ is a bosonic field, $\Pi(x)$ is the canonically conjugate momentum and they obey $[\phi(x), \Pi(x')] = i\delta(x - x')$. The quantities v and K are a velocity and a dimensionless parameter, respectively, which are model specific. Usually, K is known as the Luttinger liquid parameter. Generally, $K < 1$ for repulsive interactions and $K > 1$ for attractive ones. For the spin-1/2 XXZ chain, v and K are related through

$$vK = v_F = J\sin(k_F), \qquad \frac{v}{K} = v_F \left(1 + \frac{2\Delta}{\pi v_F} \left[1 - \cos(2k_F) \right] \right).$$

Note that these relations are only valid in the perturbative regime from the free fermions case, i.e. they are only valid for small anisotropies $|\Delta| \leq 1$. Since the spin-1/2 XXZ chain is exactly solvable via the BA, one can find exact expressions for v and K. For the case of zero magnetic field, the analytical solution reads

$$K = \frac{\pi}{2(\pi - \theta)}, \qquad v = J\frac{\pi}{2}\frac{\sqrt{1 - (\Delta/J)^2}}{\theta},$$

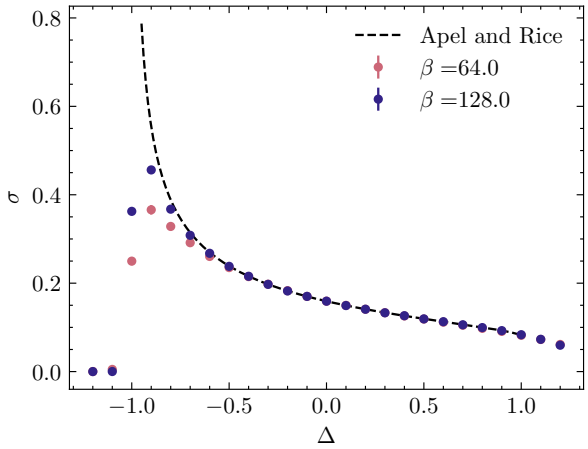

Figure 6.6: Spin conductivity as a function of the anisotropy parameter Δ for the spin-1/2 XXZ chain $L = 512$, with $h = 0$. The black dashed line shows the conductivity of the Luttinger liquid model by Apel and Rice [17]. The MC calculations were performed with 10^5 MCS and 25 bins. Statistical errors are smaller than the size of the symbols.

where $\theta = \arccos(\Delta/J)$. Using this formalism, Apel and Rice, in the 1980s, derived a general relation for the conductivity of the Luttinger liquid model [17]. It relates the conductivity to the Luttinger liquid parameter K, and reads

$$\sigma_{LL} = \frac{1}{2\pi} K.$$

The spin conductivity of the spin-1/2 XXZ chain, at low temperatures, is thus

$$\sigma_{LL} = \frac{1}{4(\pi - \theta)}.$$

This formula is only valid for the regime $|\Delta| \leq 1$, or $0 \leq \theta \leq \pi$. For the non-interacting case, i.e. $\Delta = 0$ or equivalently $\theta = \pi/2$, the spin conductivity of the Luttinger liquid has the same value as from the JW solution, $\sigma = 1/(2\pi)$. Furthermore, it is easy to see that as $\theta \to \pi$, the conductivity goes to infinity. This corresponds to the ferromagnetic Heisenberg point, i.e. $\Delta = -1$. Since the ground state of this phase is the maximally ordered ferromagnetic state, one excitation (one overturned spin) is allowed to propagate freely in the chain under the repeated action of the current operator, Equation (2.4), when a gradient in the magnetic field is applied. This suggests that the ferromagnetic Heisenberg point shows the behaviour of an ideal conducting state, i.e. ballistic transport. For the cases not covered by the Luttinger liquid solution, at large anisotropies, we would expect that, at low temperatures, the conductivity will vanish as they are gapped systems.

Figure 6.6 shows the spin conductivity for the spin-1/2 XXZ chain as a function of the anisotropy parameter calculated by SSE. The formula by Apel and Rice for the conductivity of the Luttinger liquid is also showed. We see that generally our MC approach is able to reproduce well the results from Bosonization. However, as we approach the

ferromagnetic Heisenberg point, the MC data slightly deviates from the Luttinger liquid solution. This is most likely due to finite size effects as when we decrease the temperature, the MC results approach the analytical solution. Furthermore, capturing the behaviour of the singularity of spin conductivity at the ferromagnetic Heisenberg point is a difficult task when performing numerical calculations for finite systems. Instead, a large temperature dependence is observed in the MC calculated values at this point, which we interpret as signs of a singularity. For values $|\Delta| > 1$, it is expected that at zero temperature the conductivity is zero. In our case, due to the finite temperature nature of our MC calculations and presumably by the existence of a very small energy gap, the conductivity for $\Delta > 1$ is non-zero. In the end, we can conclude that our MC approach works well for the calculation of the spin conductivity at different anisotropy strengths.

6.3.1 Spin-S XXZ Chain

Having checked that the MC sampling of the spin conductivity works for the spin-1/2 XXZ chain at different interaction strengths, we now turn to spin-1 and spin-3/2 chains. In the spin-1 chain, between $\Delta \approx 0$ and $\Delta \approx 1.2$, there exists a gapped phase, the Haldane phase. The gap energy E_g has been shown to depend on the value of Δ [67, 68]. In the low temperature regime, we expect that the conductivity vanishes when the gap energy E_g is higher than the available thermal energy. Exact calculations for E_g in the XY phase are scarce. General consensus is that at the antiferromagnetic point $E_g = 0.4105(2)$ [69], and that the E_g decreases exponentially as $\Delta \to 0$ [67, 68]. Following [68], the gap energies at $\Delta = 0.3$ and 0.4 are $E_g \approx 0.005$ and $E_g \approx 0.015$, respectively. So for the inverse temperature of $\beta = 128$ ($E_{th} \approx 0.008$), we expect the conductivity to vanish for some $\Delta \gtrsim 0.3$.

Figure 6.7a shows the spin conductivity for the spin-1 XXZ chain for various anisotropy strengths Δ. We see that for negative anisotropies, the spin conductivity of spin-1 chains has a similar behaviour to the conductivity of spin-1/2 chains. Furthermore, we can still identify traces of a possible divergence at $\Delta = -1$, due to the large temperature dependence of the conductivity at that point. However, for positive anisotropies, the behaviour of the conductivity for spin-1 differs from the spin-1/2 chains, as is expected by the existence of the Haldane gap. Moreover, we observe that the conductivity vanishes for $\Delta > 0.5$. Yet, this result does not quite coincide with our prediction. This is likely due to errors caused by the extrapolation to $\omega = 0$ or due to the precision in the calculated values for the energy of the Haldane gap as a function of Δ in [68]. Based on magnetization data as a function of the applied magnetic field, we could estimate the energy of the gap given the strength of the field at which the magnetization is not zero. But this is beyond the scope of this work.

For a spin-3/2 chain, Figure 6.7b, the behaviour of the spin-1/2 chain is recovered, as

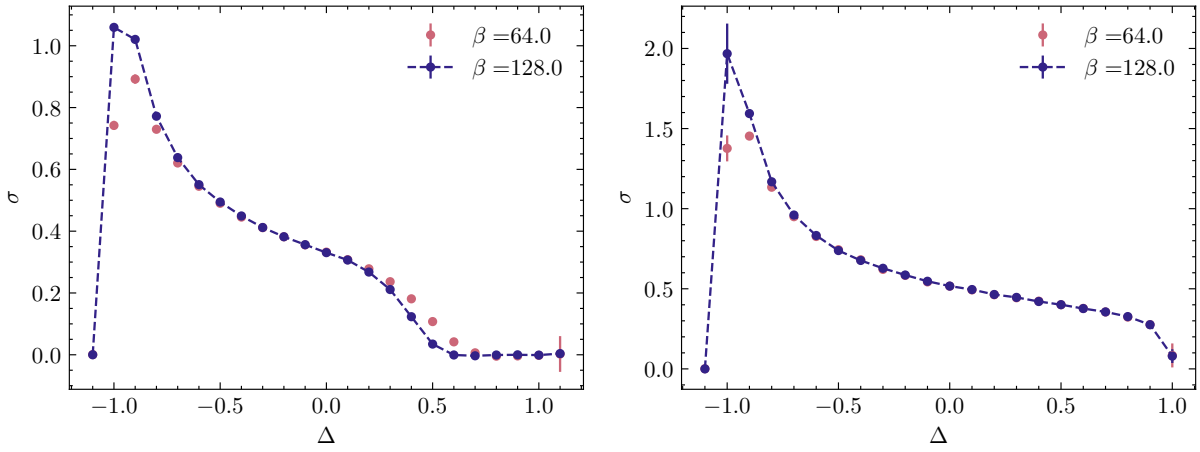

Figure 6.7: Spin conductivity as a function of the anisotropy parameter Δ for the **(a)** spin-1 and **(b)** spin-3/2 XXZ chains $L = 512$, with $h = 0$. The MC calculations were performed with 10^5 MCS and 25 bins. Statistical errors are sometimes smaller than the size of the symbols.

there is no gapped phase for $|\Delta| \leq 1$. Spin conductivity becomes larger as we approach ferromagnetic interactions. We can also see that there are traces of a divergence at the ferromagnetic Heisenberg point.

6.3.2 Adding Easy-Axis Anisotropy

Now we add an interaction with a crystal field resulting in the easy-axis anisotropy term as described in Equation (2.2). As this term is proportional to the spin operator in the z direction squared, its effects become interesting for spin numbers $S \geq 1$. Depending on the sign of D different spin projections will be energetically favoured, for example $S^z = 0$ for positive D and $S^z = \pm 1$ for negative D, for $S = 1$. The ground state phase space for the spin-1 chains was discussed in Chapter 2, Figure 2.2. The only gapless phases are the XY1 and XY2 phases. These phases exist for negative values of the anisotropy and easy-axis anisotropy parameters. Following [43], the XY1 phase is realized for $0 \leq \Delta \leq 1$ and for a wide range of D values. On the other hand, the XY2 phase is realized for a small range of anisotropy values $-0.1 \lesssim \Delta \lesssim 0$. At $\Delta = 0$, the transition between the XY1 and XY2 phase happens for $D \approx -2$. For positive Δ, we have the gapped Haldane phase. For spin-3/2 chains the Haldane phase is not present so the XY1 phase is extended to positive Δ values [44]. The XY2 phase is still present for a small range of negative Δ and D values. Our objective now is to investigate how the spin conductivity changes in the different phases raised by introducing an easy-axis anisotropy term.

Figure 6.8a shows the spin conductivity of a spin-1 XXZ chain as a function of the easy-axis anisotropy for some values of the anisotropy parameter. For $D \gtrsim 1$, the system

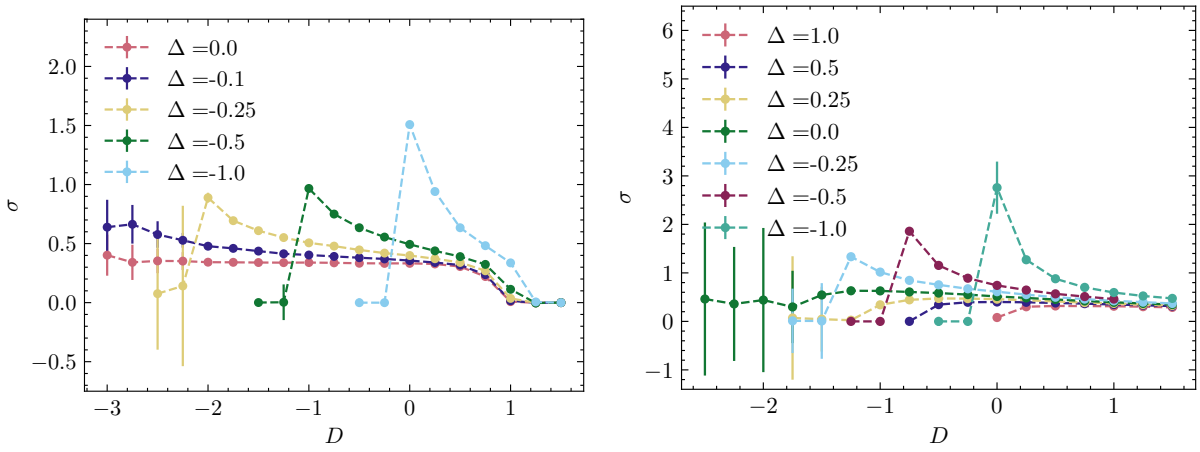

(a) **(b)**

Figure 6.8: Spin conductivity as a function of the easy-axis anisotropy D for the **(a)** spin-1 and **(b)** spin-3/2 for the XXZ chains with $L = 512$ at inverse temperature $\beta = 128$. Results for different values of Δ are presented. The MC calculations were performed with 10^5 MCS and 25 bins. Statistical errors are sometimes smaller than the size of the symbols.

is in the gapped large-D phase, so the spin conductivity vanishes. Conversely, when D is decreased, the conductivity increases and starts to depend on the value of Δ. As the anisotropy favours ferromagnetic interactions, the spin conductivity increases, resulting in a possible divergence at the ferromagnetic Heisenberg point, $\Delta = -1$. For $\Delta = -0.25$, -0.5, the spin conductivity increases until $D \approx -2$, -1, respectively. This is when the phase changes to the ferromagnetic phase. At his point the magnitude of the conductivity is about two times as large as for the $D = 0$ point. For the XY chain, the conductivity is unaffected by value the parameter D. When $\Delta = 0$, states with $S^z = 0$ are energetically favoured due to the vanishing interaction in the z directions. As so, adding an easy-axis anisotropy interaction results in a zero contribution to the energy. Therefore, states with $S^z = 0$ are still preferred and the conductivity remains unchanged. MC results for the XY2 phase, due to the larger error bars, are less conclusive. Nonetheless we can still see that the conductivity increases with decreasing D.

In Figure 6.8b we can see the spin conductivity for a spin-3/2 XXZ chain as a function of the easy-axis anisotropy for some values of Δ. For $\Delta \leq 0$, similar behaviour to spin-1 chains is observed. For $\Delta > 0$, the spin-3/2 XXZ chain has finite conductivity for D values in the XY1 phase. Furthermore, as D is increased, the conductivity becomes less dependent on the value of Δ. In this regime, states with $S^z = \pm 1/2$ are preferred, so the system is likely to exhibit similar behaviour to spin-1/2 chains. Without results for larger D values, it is difficult to take strong conclusions. By further extending the calculations for larger values of D, we could gauge a possible Δ dependency of the conductivity and compare with results for spin-1/2 XXZ chains.

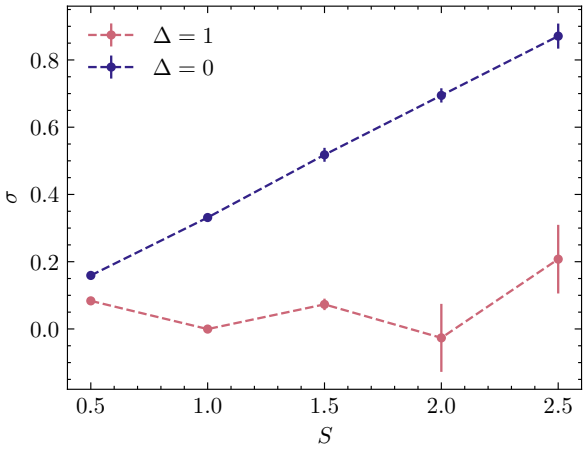

Figure 6.9: Dependence of the DC spin conductivity of spin-S XXZ chains on the spin number S. Results are presented for the Heisenberg ($\Delta = 1$) and XY ($\Delta = 0$) chains at the inverse temperature $\beta = 128$. The MC calculations were performed with 10^5 MCS and 25 bins. Statistical errors are sometimes smaller than the size of the symbols.

For both cases in Figure 6.8, results for the XY2 phase have larger standard deviations than results for other phases. This is due to an unoptimized sampling of the SSE configuration space by the Directed Loop algorithm in this regime. In the code used to compute the results, the vertex updates only change the state on the entrance legs by ± 1. Since in the XY2 phase states with $S^z = \pm S$ are preferred, vertex updates which change the entrance leg by $\pm 2S$ will lead to a more efficient sampling of the SSE configuration space, reducing the overhaul correlation between successive configurations each MCS. With this, results for the XY2 phase would probably have lower standard deviations, and more concrete conclusions could have been taken.

6.4 Dependence on the Spin Number S

As we have seen in Figures 6.6 and 6.7, as we increase the spin number S, the magnitude of the spin conductivity also increases. Figure 6.9 show the spin conductivity as a function of the spin number for the Heisenberg and XY chains. We see that due to the Haldane gap, the conductivity for the Heisenberg chain at integer spins are zero. For half-integer spin values and for the XY chain, the conductivity increases with S.

Now, we try to get an estimate of the value of the spin conductivity in the $S \to \infty$ limit, this is, in the classical spin limit. For this we can fit a polynomial to the spin conductivity values as a function of $1/S$, and extrapolate to $1/S = 0$. For the Heisenberg chain, this is not a straight forward procedure due to the zero values at integer spins. As this gap decreases exponentially for large S values [42], we ignore these values and perform the extrapolation for the conductivity values only at half-integer spins. Fitting

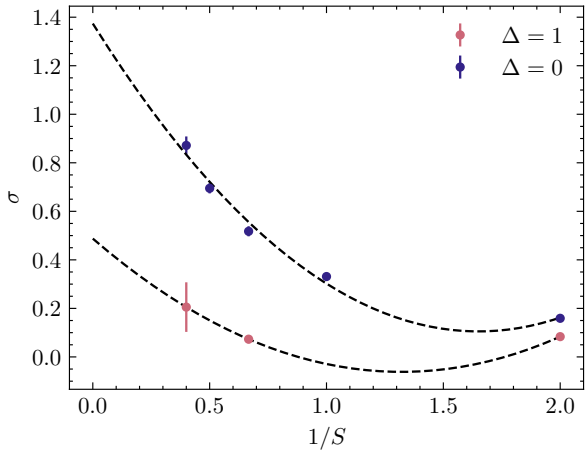

Figure 6.10: Spin conductivity of spin-S XXZ chains as a function of $1/S$, for half-integer S. Results are presented for the Heisenberg ($\Delta = 1$) and XY ($\Delta = 0$) chains at the inverse temperature $\beta = 128$. The black lines are second order polynomial fits to the MC calculated points.

a polynomial of degree 2, as shown in Figure 6.10, we obtain the following values for the conductivity in the classical spin limit: $\sigma = 1.37 \pm 0.06$ for the XY chain and $\sigma = 0.5 \pm 0.3$ for the Heisenberg chain.

Although the result for the XY chain is accurate, the one for the Heisenberg chain has a large standard deviation. This is also due to an unoptimized SSE sampling for chains with larger S by only considering vertex update types of ± 1, as descried in the last section. If other types of updates would have been considered, the extrapolation to the large S regime would have been more accurate. Nonetheless, our result agrees with results for the conductivity of classical spin systems. For example, [70] obtained $\sigma \approx 0.65$ for the classical isotropic Heisenberg antiferromagnet.

Chapter 7

Conclusion

The goal of this work was to develop a method, in the SSE framework, to efficiently sample transport coefficients, and to apply it to the computation of transport coefficients for spin-S XXZ chains, with $S = 1/2,\ 1,\ 3/2$, to find possible differences of transport in chains with larger spin number.

By introducing an imaginary time representation of the SSE configurations, were an imaginary time is randomly assigned to each Hamiltonian bond operator in the operator string, we were able to derive a new sampling routine to sample the kinetic coefficients. This method improves upon known approaches as it is more computationally efficient, i.e. scales linearly with the expansion order $\mathcal{O}(n)$, and does not require the calculation of any factorials or hypergeometric functions. This allows us to efficiently compute some of the kinetic coefficients at low temperatures and for large systems through the SSE method.

Calculations of the kinetic coefficients L_{SS}, L_{HH} and L_{SH} for small systems agree with ED results, proving our approach to be accurate. However, calculations for larger systems show large standard deviations in the estimated values of L_{HH} and L_{SH}. As a precise estimation of the kinetic coefficients is needed to reliably perform the extrapolation to $\omega = 0$, we decided to mostly focus our results on the DC spin conductivity σ, which is related to the coefficient L_{SS}.

Results for the spin conductivity of spin-1/2 XXZ chains agree well with both exact results from the JW transformation and results from Bosonization. Spin-1 chains, at low temperatures, show zero conductivity in the Haldane phase, but maintain the general behaviour of spin-1/2 chains for ferromagnetic interactions. The conductivity of spin-3/2 chains is similar to spin-1/2 chains. Generally the magnitude of the conductivity increases with the spin number S.

Adding an easy-axis anisotropy D term, certain spin projections are favoured for systems with $S \geq 1$. For negative D in the XY1 phase, the spin conductivity for both spin-1 and spin-3/2 chains increases as the interaction favours ferromagnetic alignment, whilst for positive D it decreases until it vanishes in the gapped large-D phase. Results

for the XY2 phase are somewhat inconclusive.

In the end, estimations for the spin conductivity in the large spin limit ($S \to \infty$) were obtained for the XY and Heisenberg chains. For the XY model we estimate the spin conductivity to be $\sigma = 1.37 \pm 0.06$, and for Heisenberg chain we estimate $\sigma = 0.5 \pm 0.3$, which shows good agreement with previous results [70]. For future work, it would prove interesting to verify the estimate for the spin conductivity in the $S \to \infty$ for the XY chain to a classical calculation.

Beyond the improvements mentioned in the results section, further improvements would include the development of a more computationally efficient way of implementing the sampling procedures for the other kinetic coefficients, such that accurate calculations of L_{HH} and L_{SH} will also be possible. With this, calculations for the heat conductivity and spin-Seebeck coefficient could become viable. In addition, for large S, one could try to use the coarse-grained loop algorithms approach by Harada and Kawashima [71], which might improve overall performance. One could also try to derive a formula to estimate the Drude weights [9] directly through SSE. This can prove useful in relating physics of non-integrable systems to those of integrable ones.

Appendix A

Equivalence of Equations (4.15) and (5.1)

In this Appendix, we show that Equations (4.15) and (5.1) are equivalent at $\omega = \omega_M$. First we start with the spectral representation, in terms of Hamiltonian eigenstates $H|n\rangle = E_n|n\rangle$, of the integral in Equation (4.15). Since $z = i\omega$, with $\omega \geq 0$, we have

$$I_1 = \int_0^\infty dt\ e^{-\omega t} \left\langle [A_x^i(t), A_y^j] \right\rangle$$

$$= \frac{1}{Z}\sum_n e^{-\beta E_n} \int_0^\infty dt\ e^{-\omega t} \left(\langle n| e^{iHt} A_x^i e^{-iHt} A_y^j |n\rangle - \langle n| A_y^j e^{iHt} A_x^i e^{-iHt} |n\rangle \right)$$

$$= \frac{1}{Z}\sum_{n,m} e^{-\beta E_n} \int_0^\infty dt\ e^{-\omega t} \left(\langle n| e^{iHt} A_x^i e^{-iHt} |m\rangle \langle m| A_y^j |n\rangle - \langle n| A_y^j |m\rangle \langle m| e^{iHt} A_x^i e^{-iHt} |n\rangle \right).$$

Interchanging $n \leftrightarrow m$ in the second term,

$$I_1 = \frac{1}{Z}\sum_{n,m} \int_0^\infty dt\ e^{-\omega t} \left(e^{-\beta E_n} - e^{-\beta E_m} \right) e^{i(E_n - E_m)t} \langle n| A_x^i |m\rangle \langle m| A_y^j |n\rangle$$

$$= \frac{1}{Z}\sum_{n,m} \underbrace{\langle n| A_x^i |m\rangle \langle m| A_y^j |n\rangle \left(e^{-\beta E_n} - e^{-\beta E_m} \right)}_{C_{nm}} \frac{1}{\omega - i(E_n - E_m)}.$$

Following a similar procedure for the integral in Equation (5.1), we arrive at

$$I_2 = \frac{1}{Z}\sum_{n,m} C_{nm} \frac{1}{i\omega_M + (E_n - E_m)}$$

Inserting the spectral representation of both integrals in Equations (4.15) and (5.1), we have

$$L_{ij}(\omega) = \omega \frac{1}{Z}\sum_{n,m} C_{nm}\, \mathrm{Im}\, \frac{1}{\omega - i(E_n - E_m)} = \omega \frac{1}{Z}\sum_{n,m} C_{nm} \frac{(E_n - E_m)}{\omega^2 + (E_n - E_m)^2},$$

$$L_{ij}(\omega_M) = \omega_M \frac{1}{Z}\sum_{n,m} C_{nm}\, \mathrm{Re}\, \frac{1}{i\omega_M + (E_n - E_m)} = \omega_M \frac{1}{Z}\sum_{n,m} C_{nm} \frac{(E_n - E_m)}{\omega_M^2 + (E_n - E_m)^2}.$$

So we have shown that Equations (4.15) and (5.1) are equivalent for $\omega = \omega_M$.

Appendix B

Proof of Integral Identities Used in Chapter 5

In this Appendix, we go through the proof for the four integral identities used in Chapter 5. These relate the combinatorial factors involved in calculating the kinetic coefficients in the series expansion formalism to a product of imaginary time integrals.

B.1 Identity for L_{SS}

From the series expansion of L_{SS} we get the following combinatorial factor

$$C_{kl}(\tau', \tau'') = \frac{(\beta - \tau'')^{n-k-l}(\tau'' - \tau')^l \tau'^k}{(n-k-l)!k!l!}\Theta(\tau'' - \tau').$$

We now show that this can be rewritten as

$$\int_0^\beta d\tau_n \dots \int_0^{\tau_2} d\tau_1 (\Theta(\tau''-\tau_{k+l})-\Theta(\tau''-\tau_{k+l+1}))(\Theta(\tau'-\tau_k)-\Theta(\tau'-\tau_{k+1}))\Theta(\tau''-\tau'). \quad \text{(B.1)}$$

We start by integrating until the integral of τ_k, which leads to

$$\int_0^\beta d\tau_n \dots \int_0^{\tau_{k+1}} d\tau_k \frac{\tau_k^{k-1}}{(k-1)!}(\Theta(\tau''-\tau_{k+l})-\Theta(\tau''-\tau_{k+l+1}))(\Theta(\tau'-\tau_k)-\Theta(\tau'-\tau_{k+1}))\Theta(\tau''-\tau').$$

Taking a closer look at the τ_k integral, we have

$$\underbrace{\int_0^{\tau_{k+1}} d\tau_k \frac{\tau_k^{k-1}}{(k-1)!}\Theta(\tau' - \tau_k)}_{\tau' \text{ can be } > \text{ or } < \text{ than } \tau_k} - \Theta(\tau' - \tau_{k+1}) \int_0^{\tau_{k+1}} d\tau_k \frac{\tau_k^{k-1}}{(k-1)!} =$$

$$\Theta(\tau_{k+1} - \tau') \int_0^{\tau'} d\tau_k \frac{\tau_k^{k-1}}{(k-1)!} + \Theta(\tau' - \tau_{k+1}) \int_0^{\tau_{k+1}} d\tau_k \frac{\tau_k^{k-1}}{(k-1)!}$$

$$-\Theta(\tau' - \tau_{k+1}) \int_0^{\tau_{k+1}} d\tau_k \frac{\tau_k^{k-1}}{(k-1)!} = \Theta(\tau_{k+1} - \tau') \frac{\tau'^k}{k!}.$$

Inserting this results in the original relation and integrating until the τ_{k+l} integral,

$$\frac{\tau'^k}{k!}\int_0^\beta d\tau_n \dots \int_0^{\tau_{k+2}} d\tau_{k+1}(\Theta(\tau''-\tau_{k+l})-\Theta(\tau''-\tau_{k+l+1}))\Theta(\tau_{k+1}-\tau')\Theta(\tau''-\tau') =$$
$$\frac{\tau'^k}{k!}\int_0^\beta d\tau_n \dots \int_0^{\tau_{k+l+1}} d\tau_{k+l}\frac{(\tau_{k+l}-\tau')^{l-1}}{(l-1)!}(\Theta(\tau''-\tau_{k+l})-\Theta(\tau''-\tau_{k+l+1}))\Theta(\tau_{k+l}-\tau')\Theta(\tau''-\tau').$$

Following the same procedure as for the τ_k integral, the τ_{k+l} integral yields

$$\int_0^{\tau_{k+l+1}} d\tau_{k+l}\frac{(\tau_{k+l}-\tau')^{l-1}}{(l-1)!}(\Theta(\tau''-\tau_{k+l})-\Theta(\tau''-\tau_{k+l+1}))\Theta(\tau_{k+l}-\tau') = \Theta(\tau_{k+l+1}-\tau'')\frac{(\tau''-\tau')^l}{l!}.$$

Inserting this back in to the identity and solving the rest of the integrals, we have

$$\frac{(\tau''-\tau')^l}{l!}\frac{\tau'^k}{k!}\Theta(\tau''-\tau')\int_0^\beta d\tau_n \dots \int_0^{\tau_{k+l+2}} d\tau_{k+l+1}\Theta(\tau_{k+l+1}-\tau'') =$$
$$\frac{(\beta-\tau'')^{n-k-l}(\tau''-\tau')^l\tau'^k}{(n-k-l)!k!l!}\Theta(\tau''-\tau') = C_{kl}(\tau',\tau'').$$

Just as we wanted to show, the combinatorial factor $C_{kl}(\tau',\tau'')$ can be written in terms of the integral identity in Equation (B.1).

B.2 Identity for L_{HH}

From the series expansion of L_{HH} we get the following combinatorial factor

$$C'_{kl}(\tau',\tau'') = \frac{(\beta-\tau'')^{n-2-k-l}(\tau''-\tau')^l\tau'^k}{(n-2-k-l)!k!l!}\Theta(\tau''-\tau').$$

We now show that this can be rewritten as

$$\int_0^\beta d\tau_n \dots \int_0^{\tau_2} d\tau_1\delta(\tau''-\tau_{k+l+2})\delta(\tau'-\tau_{k+1})\Theta(\tau''-\tau'). \tag{B.2}$$

We start by integrating until the τ_{k+1} integral. As a results, we have

$$\int_0^\beta d\tau_n \dots \int_0^{\tau_{k+2}} d\tau_{k+1}\frac{\tau_{k+1}^k}{k!}\delta(\tau''-\tau_{k+l+2})\delta(\tau'-\tau_{k+1})\Theta(\tau''-\tau') =$$
$$\frac{\tau'^k}{k!}\int_0^\beta d\tau_n \dots \int_0^{\tau_{k+3}} d\tau_{k+2}\Theta(\tau_{k+2}-\tau')\delta(\tau''-\tau_{k+l+2})\Theta(\tau''-\tau').$$

The Heaviside function was introduced as a result of setting τ' to τ_{k+1}. Then we require that $\tau_{k+2} > \tau'$. Integrating until the τ_{k+l+2} integral,

$$\frac{\tau'^k}{k!}\int_0^\beta d\tau_n \dots \int_0^{\tau_{k+l+3}} d\tau_{k+l+2}\frac{(\tau_{k+l+2}-\tau')^l}{l!}\Theta(\tau_{k+l+2}-\tau')\delta(\tau''-\tau_{k+l+2})\Theta(\tau''-\tau') =$$
$$\frac{(\tau''-\tau')^l}{l!}\frac{\tau'^k}{k!}\int_0^\beta d\tau_n \dots \int_0^{\tau_{k+l+4}} d\tau_{k+l+3}\Theta(\tau_{k+l+3}-\tau'')\Theta(\tau''-\tau').$$

Solving the rest of the integrals, we obtain

$$\frac{(\beta-\tau'')^{n-2-k-l}(\tau''-\tau')^l\tau'^k}{(n-2-k-l)!k!l!}\Theta(\tau''-\tau') = C'_{kl}(\tau',\tau''),$$

Just as we wanted to show.

B.3 Identity for L_{SH} and L_{HS}

From the series expansion of L_{SH} or L_{HS} we get the following combinatorial factor

$$C''_{kl}(\tau',\tau'') = \frac{(\beta-\tau'')^{n-1-k-l}(\tau''-\tau')^l\tau'^k}{(n-1-k-l)!k!l!}\Theta(\tau''-\tau').$$

We now show that this can be rewritten as either

$$\int_0^\beta d\tau_n \dots \int_0^{\tau_3} d\tau_2 \int_0^{\tau_2} d\tau_1 (\Theta(\tau''-\tau_{k+l+1}) - \Theta(\tau''-\tau_{k+l+2}))\delta(\tau'-\tau_{k+1})\Theta(\tau''-\tau'), \quad \text{(B.3)}$$

or

$$\int_0^\beta d\tau_n \dots \int_0^{\tau_3} d\tau_2 \int_0^{\tau_2} d\tau_1 \delta(\tau''-\tau_{k+l+1})(\Theta(\tau'-\tau_k) - \Theta(\tau'-\tau_{k+1}))\Theta(\tau''-\tau'). \quad \text{(B.4)}$$

In the last two sections we implicitly showed the procedures for integrating a delta function or a Heaviside step function. These can be applied to these identities as well. Since they are similar, we show the proof for the first one, Equation (B.3). We start by integrating until the τ_{k+1} integral,

$$\int_0^\beta d\tau_n \dots \int_0^{\tau_{k+2}} d\tau_{k+1} \frac{\tau_{k+1}^k}{k!}(\Theta(\tau''-\tau_{k+l+1}) - \Theta(\tau''-\tau_{k+l+2}))\delta(\tau'-\tau_{k+1})\Theta(\tau''-\tau') =$$
$$\frac{\tau'^k}{k!}\int_0^\beta d\tau_n \dots \int_0^{\tau_{k+3}} d\tau_{k+2}\Theta(\tau_{k+2}-\tau')(\Theta(\tau''-\tau_{k+l+1}) - \Theta(\tau''-\tau_{k+l+2}))\Theta(\tau''-\tau').$$

Integrating until the τ_{k+l+1} integral and applying the same procedure as in Section B.1, we get

$$\frac{(\tau''-\tau')^l}{(l)!}\frac{\tau'^k}{k!}\int_0^\beta d\tau_n \dots \int_0^{\tau_{k+l+3}} d\tau_{k+l+2}\Theta(\tau_{k+l+2}-\tau'')\Theta(\tau''-\tau').$$

Solving the rest of the integrals, we obtain

$$\frac{(\beta-\tau'')^{n-1-k-l}(\tau''-\tau')^l\tau'^k}{(n-1-k-l)!k!l!}\Theta(\tau''-\tau') = C''_{kl}(\tau',\tau'').$$

Just as we wanted to show.

Bibliography

[1] E. Ising, "Beitrag zur theorie des ferromagnetismus," *Zeitschrift für Physik*, vol. 31, no. 1, pp. 253–258, 1925.

[2] H. Bethe, "Zur theorie der metalle," *Zeitschrift für Physik*, vol. 71, no. 3, pp. 205–226, 1931.

[3] M. T. Hutchings, G. Shirane, R. J. Birgeneau, and S. L. Holt, "Spin dynamics in the one-dimensional antiferromagnet $(CD_3)_4$ nmncl$_3$," *Phys. Rev. B*, vol. 5, pp. 1999–2014, Mar 1972.

[4] L. Faddeev and L. Takhtajan, "What is the spin of a spin wave?," *Physics Letters A*, vol. 85, no. 6, pp. 375–377, 1981.

[5] F. Haldane, "Continuum dynamics of the 1-d heisenberg antiferromagnet: Identification with the o(3) nonlinear sigma model," *Physics Letters A*, vol. 93, no. 9, pp. 464–468, 1983.

[6] F. D. M. Haldane, "Nonlinear field theory of large-spin heisenberg antiferromagnets: Semiclassically quantized solitons of the one-dimensional easy-axis néel state," *Phys. Rev. Lett.*, vol. 50, pp. 1153–1156, Apr 1983.

[7] H. Castella, X. Zotos, and P. Prelovšek, "Integrability and ideal conductance at finite temperatures," *Phys. Rev. Lett.*, vol. 74, pp. 972–975, Feb 1995.

[8] X. Zotos and P. Prelovšek, "Evidence for ideal insulating or conducting state in a one-dimensional integrable system," *Phys. Rev. B*, vol. 53, pp. 983–986, Jan 1996.

[9] X. Zotos, F. Naef, and P. Prelovsek, "Transport and conservation laws," *Phys. Rev. B*, vol. 55, pp. 11029–11032, May 1997.

[10] J. V. Alvarez and C. Gros, "Low-temperature transport in heisenberg chains," *Phys. Rev. Lett.*, vol. 88, p. 077203, Feb 2002.

[11] B. Bertini, F. Heidrich-Meisner, C. Karrasch, T. Prosen, R. Steinigeweg, and M. Žnidarič, "Finite-temperature transport in one-dimensional quantum lattice models," *Rev. Mod. Phys.*, vol. 93, p. 025003, May 2021.

[12] C. Hess, "Heat conduction in low-dimensional quantum magnets," *The European Physical Journal Special Topics*, vol. 151, no. 1, pp. 73–83, 2007.

[13] C. Hess, "Heat transport of cuprate-based low-dimensional quantum magnets with strong exchange coupling," *Physics Reports*, vol. 811, pp. 1–38, 2019. Heat transport of cuprate-based low-dimensional quantum magnets with strong exchange coupling.

[14] A. V. Sologubenko, T. Lorenz, H. R. Ott, and A. Freimuth, "Thermal conductivity via magnetic excitations in spin-chain materials," *Journal of Low Temperature Physics*, vol. 147, no. 3, pp. 387–403, 2007.

[15] S. Sanvito, O. Heinonen, V. A. Dediu, and N. Rizzo, *Novel Materials and Devices for Spintronics*. Cambridge University Press, 2014.

[16] Y. Imry, *Introduction to Mesoscopic Physics*. Oxford University Press, 2008.

[17] W. Apel and T. M. Rice, "Combined effect of disorder and interaction on the conductance of a one-dimensional fermion system," *Phys. Rev. B*, vol. 26, pp. 7063–7065, Dec 1982.

[18] C. L. Kane and M. P. A. Fisher, "Transport in a one-channel luttinger liquid," *Phys. Rev. Lett.*, vol. 68, pp. 1220–1223, Feb 1992.

[19] C. L. Kane and M. P. A. Fisher, "Transmission through barriers and resonant tunneling in an interacting one-dimensional electron gas," *Phys. Rev. B*, vol. 46, pp. 15233–15262, Dec 1992.

[20] A. W. Sandvik and J. Kurkijärvi, "Quantum monte carlo simulation method for spin systems," *Phys. Rev. B*, vol. 43, pp. 5950–5961, Mar 1991.

[21] O. F. Syljuåsen and A. W. Sandvik, "Quantum monte carlo with directed loops," *Phys. Rev. E*, vol. 66, p. 046701, Oct 2002.

[22] K. Louis and C. Gros, "Quantum monte carlo simulation for the conductance of one-dimensional quantum spin systems," *Phys. Rev. B*, vol. 68, p. 184424, Nov 2003.

[23] O. F. Syljuåsen, "Length-dependent conductance of a spin-incoherent hubbard chain: Monte carlo calculations," *Phys. Rev. Lett.*, vol. 98, p. 166401, Apr 2007.

[24] K. Louis and C. Gros, "Diverging magnetothermal response in the one-dimensional heisenberg chain," *Phys. Rev. B*, vol. 67, p. 224410, Jun 2003.

[25] J. V. Alvarez and C. Gros, "Conductivity of quantum spin chains: A quantum monte carlo approach," *Phys. Rev. B*, vol. 66, p. 094403, Sep 2002.

[26] F. Heidrich-Meisner, A. Honecker, D. C. Cabra, and W. Brenig, "Zero-frequency transport properties of one-dimensional spin-$\frac{1}{2}$ systems," *Phys. Rev. B*, vol. 68, p. 134436, Oct 2003.

[27] D. Heidarian and S. Sorella, "Finite drude weight for one-dimensional low-temperature conductors," *Phys. Rev. B*, vol. 75, p. 241104, Jun 2007.

[28] F. Heidrich-Meisner, A. Honecker, D. C. Cabra, and W. Brenig, "Thermal conductivity of anisotropic and frustrated spin-$\frac{1}{2}$ chains," *Phys. Rev. B*, vol. 66, p. 140406, Oct 2002.

[29] F. Heidrich-Meisner, A. Honecker, and W. Brenig, "Thermal transport of the xxz chain in a magnetic field," *Phys. Rev. B*, vol. 71, p. 184415, May 2005.

[30] S. Furukawa, D. Ikeda, and K. Sakai, "Thermomagnetic power and figure of merit for spin-1/2 heisenberg chain," *Journal of the Physical Society of Japan*, vol. 74, no. 12, pp. 3241–3247, 2005.

[31] J. Karadamoglou and X. Zotos, "Diffusive transport in spin-1 chains at high temperatures," *Phys. Rev. Lett.*, vol. 93, p. 177203, Oct 2004.

[32] J. Richter, N. Casper, W. Brenig, and R. Steinigeweg, "Magnetization dynamics in clean and disordered spin-1 xxz chains," *Phys. Rev. B*, vol. 100, p. 144423, Oct 2019.

[33] M. Dupont and J. E. Moore, "Universal spin dynamics in infinite-temperature one-dimensional quantum magnets," *Phys. Rev. B*, vol. 101, p. 121106, Mar 2020.

[34] A. Auerbach, *Interacting Electrons and Quantum Magnetism*. Springer New York, NY, 1994.

[35] W. Heisenberg, "Zur theorie des ferromagnetismus," *Zeitschrift für Physik*, vol. 49, pp. 619–636, 1928.

[36] J. M. Kosterlitz and D. J. Thouless, "Ordering, metastability and phase transitions in two-dimensional systems," *Journal of Physics C: Solid State Physics*, vol. 6, p. 1181, apr 1973.

[37] N. D. Mermin and H. Wagner, "Absence of ferromagnetism or antiferromagnetism in one- or two-dimensional isotropic heisenberg models," *Phys. Rev. Lett.*, vol. 17, pp. 1133–1136, Nov 1966.

[38] P. Jordan and E. Wigner, "Über das paulische äquivalenzverbot," *Zeitschrift für Physik*, vol. 47, no. 9, pp. 631–651, 1928.

[39] E. Lieb, T. Schultz, and D. Mattis, "Two soluble models of an antiferromagnetic chain," *Annals of Physics*, vol. 16, no. 3, pp. 407–466, 1961.

[40] H. Mikeska and A. Kolezhuk, *One-Dimensional Magnetism*, vol. 645, pp. 1–83. 06 2004.

[41] M. den Nijs and K. Rommelse, "Preroughening transitions in crystal surfaces and valence-bond phases in quantum spin chains," *Phys. Rev. B*, vol. 40, pp. 4709–4734, Sep 1989.

[42] I. Affleck, "Quantum spin chains and the haldane gap," *Journal of Physics: Condensed Matter*, vol. 1, p. 3047, may 1989.

[43] W. Chen, K. Hida, and B. C. Sanctuary, "Ground-state phase diagram of $s = 1$ XXZ chains with uniaxial single-ion-type anisotropy," *Phys. Rev. B*, vol. 67, p. 104401, Mar 2003.

[44] H. J. Schulz, "Phase diagrams and correlation exponents for quantum spin chains of arbitrary spin quantum number," *Phys. Rev. B*, vol. 34, pp. 6372–6385, Nov 1986.

[45] H. Kadowaki, K. Ubukoshi, and K. Hirakawa, "Neutron scattering study of successive phase transitions in triangular lattice antiferromagnet csnicl3," *Journal of the Physical Society of Japan*, vol. 56, no. 2, pp. 751–756, 1987.

[46] U. Schollwöck, O. Golinelli, and T. Jolicœur, "S=2 antiferromagnetic quantum spin chain," *Phys. Rev. B*, vol. 54, pp. 4038–4051, Aug 1996.

[47] U. Schollwöck and T. Jolicoeur, "Haldane gap and hidden order in the s = 2 antiferromagnetic quantum spin chain," *Europhysics Letters*, vol. 30, p. 493, jun 1995.

[48] K. Joel, D. Kollmar, and L. F. Santos, "An introduction to the spectrum, symmetries, and dynamics of spin-1/2 heisenberg chains," *American Journal of Physics*, vol. 81, no. 6, pp. 450–457, 2013.

[49] D. C. Handscomb, "The monte carlo method in quantum statistical mechanics," *Mathematical Proceedings of the Cambridge Philosophical Society*, vol. 58, no. 4, p. 594–598, 1962.

[50] D. C. Handscomb, "A monte carlo method applied to the heisenberg ferromagnet," *Mathematical Proceedings of the Cambridge Philosophical Society*, vol. 60, no. 1, p. 115–122, 1964.

[51] N. Metropolis, A. W. Rosenbluth, M. N. Rosenbluth, A. H. Teller, and E. Teller, "Equation of state calculations by fast computing machines," *The Journal of Chemical Physics*, vol. 21, no. 6, pp. 1087–1092, 1953.

[52] D. H. Lee, J. D. Joannopoulos, and J. W. Negele, "Monte carlo solution of antiferromagnetic quantum heisenberg spin systems," *Phys. Rev. B*, vol. 30, pp. 1599–1602, Aug 1984.

[53] M. Suzuki, S. Miyashita, and A. Kuroda, "Monte Carlo Simulation of Quantum Spin Systems. I," *Progress of Theoretical Physics*, vol. 58, pp. 1377–1387, 11 1977.

[54] O. F. Syljuåsen, "Directed loop updates for quantum lattice models," *Phys. Rev. E*, vol. 67, p. 046701, Apr 2003.

[55] E. Y. Loh, J. E. Gubernatis, R. T. Scalettar, S. R. White, D. J. Scalapino, and R. L. Sugar, "Sign problem in the numerical simulation of many-electron systems," *Phys. Rev. B*, vol. 41, pp. 9301–9307, May 1990.

[56] A. W. Sandvik, "A generalization of handscomb's quantum monte carlo scheme-application to the 1d hubbard model," *Journal of Physics A: Mathematical and General*, vol. 25, pp. 3667–3682, jul 1992.

[57] A. W. Sandvik, "Finite-size scaling of the ground-state parameters of the two-dimensional heisenberg model," *Phys. Rev. B*, vol. 56, pp. 11678–11690, Nov 1997.

[58] A. W. Sandvik, "Stochastic series expansion method with operator-loop update," *Phys. Rev. B*, vol. 59, pp. R14157–R14160, Jun 1999.

[59] G. T. B. M. E. J. Newman, *Monte Carlo Methods in Statistical Physics*. Clarendon Press, 04 1999.

[60] S. Eggert, I. Affleck, and M. Takahashi, "Susceptibility of the spin 1/2 heisenberg antiferromagnetic chain," *Phys. Rev. Lett.*, vol. 73, pp. 332–335, Jul 1994.

[61] N. Pottier, *Nonequilibrium Statistical Physics: Linear Irreversible Processes*. Oxford Graduate Texts, OUP Oxford, 2010.

[62] F. Heidrich-Meisner, A. Honecker, and W. Brenig, "Thermal transport of the xxz chain in a magnetic field," *Phys. Rev. B*, vol. 71, p. 184415, May 2005.

[63] P. L. Hauge, "Thermal transport in the spin-1/2 antiferromagnetic xxz model," Master's thesis, University of Oslo, 2022.

[64] A. N. Kirillov and N. Y. Reshetikhin, "Exact solution of the integrable xxz heisenberg model with arbitrary spin. i. the ground state and the excitation spectrum," *Journal of Physics A: Mathematical and General*, vol. 20, p. 1565, apr 1987.

[65] E. Süli and D. F. Mayers, *An Introduction to Numerical Analysis*. Cambridge University Press, 2014.

[66] T. Giamarchi, *Quantum Physics in One Dimension*. International Series of Monographs on Physics, Clarendon Press, 2004.

[67] C. J. De Leone and G. T. Zimanyi, "Schwinger-boson theory of the quantum xxz model," *Phys. Rev. B*, vol. 49, pp. 1131–1136, Jan 1994.

[68] C. Yu and J.-W. Lee, "Closing of the haldane gap in a spin-1 xxz chain," *Journal of the Korean Physical Society*, vol. 79, no. 9, pp. 841–845, 2021.

[69] S. R. White and D. A. Huse, "Numerical renormalization-group study of low-lying eigenstates of the antiferromagnetic s=1 heisenberg chain," *Phys. Rev. B*, vol. 48, pp. 3844–3852, Aug 1993.

[70] B. Jenčič and P. Prelovšek, "Spin and thermal conductivity in a classical disordered spin chain," *Phys. Rev. B*, vol. 92, p. 134305, Oct 2015.

[71] K. Harada and N. Kawashima, "Coarse-grained loop algorithms for monte carlo simulation of quantum spin systems," *Phys. Rev. E*, vol. 66, p. 056705, Nov 2002.